CRANFIELD INSTITUTE OF TECHNOLOGY

DEPARTMENT OF MATERIALS

Ph.D. THESIS

Academic Year 1972-73

M. DAVIES

The high temperature oxidation and corrosion of irons and steels

Supervisor: R. C. Hurst

September, 1973

SUMMARY

This research has been concerned with the oxidation and corrosion of iron and mild steels, with particular reference to the importance of the mechanical properties of the surface oxides formed. A vibration technique has been used as the basic means of investigation, complemented by hot stage microscopy, thermobalance, microscopy, etc., where applicable. It has been found that the oxides formed on iron and steel become partially detached at the scale/metal interface continually during growth. This form of damage has been found to have a profound effect on the dynamic modulus of the oxides, and on its behaviour under thermal shock or corrosive conditions. A particular EN2 steel has been found to be largely resistant to sodium chloride and sodium sulphate corrosion when preoxidised. This enhanced corrosion resistance has been attributed to the presence of a thin adherent oxide layer on the metal surface, whose adherence is due to the concentration of nickel in that region during oxidation.

The vibration apparatus and specimens have been modified to enable tensile loading during oxidation such that the strains, that a surface oxide is able to withstand before cracking, may be measured. It has been found that the strains to fracture increases with increasing temperature. The application of the vibration technique, in this role as a crack detection system, has been shown to be very satisfactory.

CONTENTS

CHAPTER 3

3. THE INFLUENCE OF STRESS ON THE OXIDATION OF STEEL

CHAPTER 4

4. THE EFFECTS OF CONTAMINANTS ON HIGH TEMPERATURE OXIDATION

CHAPTER 5

5. DISCUSSION AND CONCLUSIONS

FIGURES

NOTATION

Q = activation energy

R = gas constant

k = oxidation rate constant

f_o = natural resonant frequency

Δf = change in resonant frequency

m_o = mass of unoxidised bar

m = total mass of oxidised bar

$\Delta = \dfrac{m - m_o}{m_o}$

a = specimen radius

l = specimen length

E_1 = metal dynamic modulus

E_2 = oxide dynamic modulus

ρ_1 = metal density

ρ_2 = oxide density

M_1 = metal molecular weight

M_2 = oxide molecular weight

δ = damping

Q^{-1} = internal friction

α_m = coefficient of thermal expansion of metal

α_o = coefficient of thermal expansion of oxide

CHAPTER 1

1. INTRODUCTION

1.1. Oxidation kinetics of irons and steel

The oxidation of metals and alloys has been the subject of extensive research over many years, consequently no attempt will be made here to fully review even the literature apertaining to the oxidation of ferrous materials. This section of the introduction will merely attempt to present a general survey of the literature relating to the kinetics of the oxidation of iron and steels.

Oxidation is rarely, if ever, carried out under equilibrium conditions, nevertheless thermodynamic data can be of some value in understanding the reactions occuring during oxidation, and, more particularly, during corrosion. Thermodynamic data will predict whether a given oxide may or may not be formed under specific temperature and pressure conditions. Although, for example, FeO is thermodynamically unstable below 570°C (1) but has been found to form at temperatures well below 570°C (2)(3), and may be retained at room temperature in oxide layers formed at high temperatures. The iron - oxygen phase diagram is shown in Fig.1.1. (1). Thermodynamic data is unable to predict whether an oxide will be formed in any given time and, in the practical situation, the kinetics of the oxidation process are of greater interest. The rate of oxidation, under given conditions, may be dependent on the rate of reaction at one of the phase boundaries, but is usually controlled by the rate of movement of reactants through the oxide film. Under such conditions the increase in weight of an oxidising specimen may be said to vary with time according to one, or a combination of several, well defined relationships. After the initial, thin film stage, iron and mild steels oxidise in a manner approximating to a parabolic relationship at temperatures above 200° - 300°C, and the change in weight, Δm, varies with time t as:-

$$(\Delta m)^2 = k.t.$$

where k is the rate constant, which varies with temperature in a manner governed by an Arrhenius type of equation:-

$$k = Ae^{-Q/RT}$$

A = constant
Q = activation energy
R = gas constant

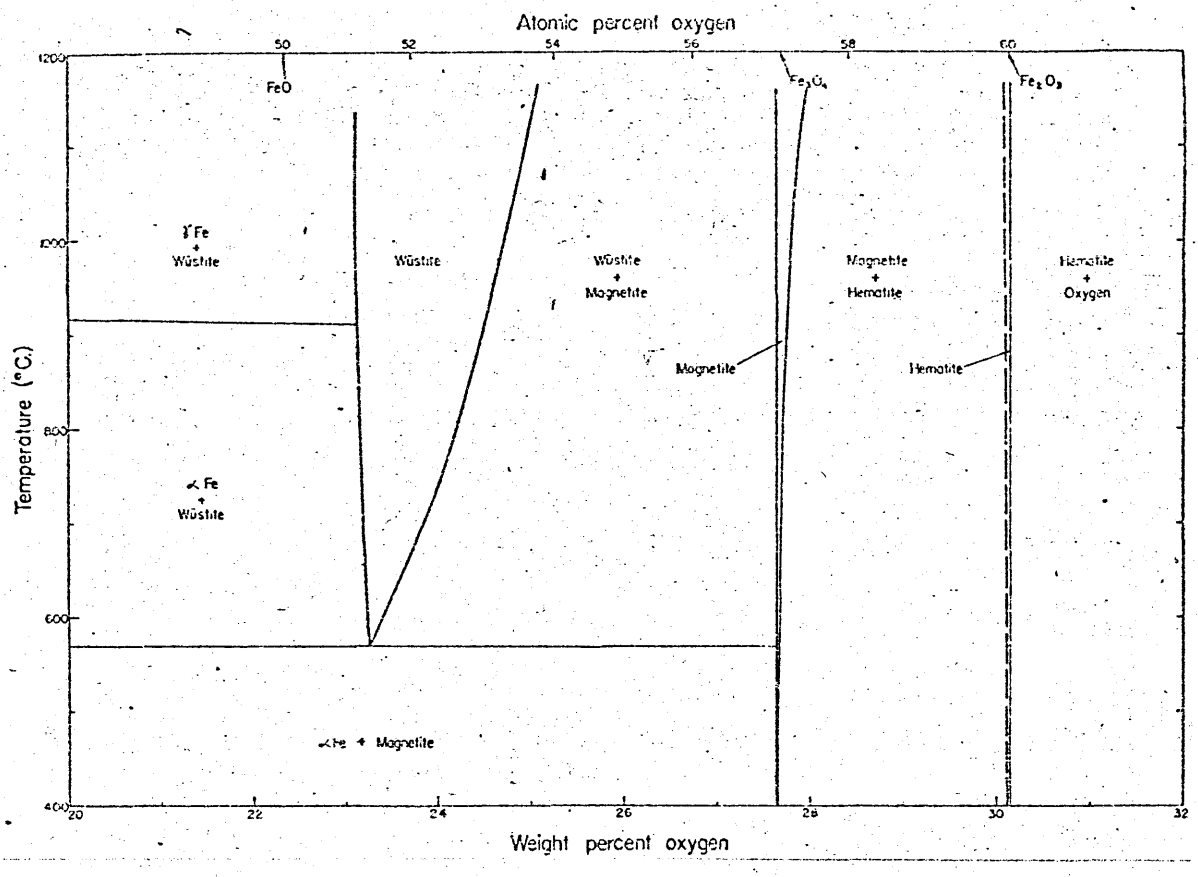

Fig.1.1. Iron - Oxygen phase diagram.

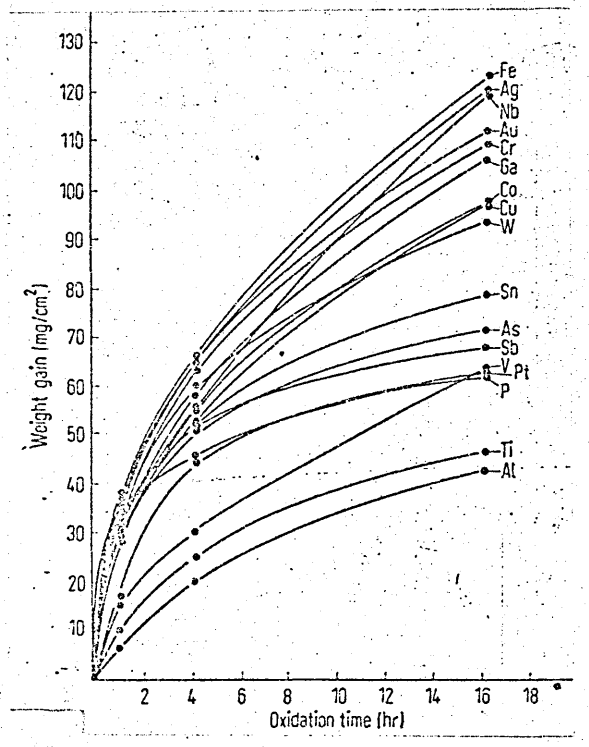

Fig.1.2. Weight gain for oxidation of carbon-free alloys at 930°C.

For pure iron, oxidised in air in the temperature range 497°-903°C, the following values have been determined (4) :-

$$k = 0.37e^{-33000/RT}$$

Several authors, (5)(1), have reported discontinuities in the plot of $\ln k$ against 1/T. Two such inflections have been attributed to the iron phase change at 910°C (6), and the magnetic transformation at 760°C (6). Davies, Simnad and Birchenall (1) disagree with this interpretation and attribute the higher temperature discontinuity, which they place at about 800°C, to the appearance of a finite quantity of Fe_2O_3, and the lower temperature one, at about 600°C, to the presence of FeO as a stable component of the scale.

The mechanism by which the metal and/or oxygen are transported through the scale has been the subject of much conjecture. The usually accepted model, resulting from the work of Wagner (7) (8) (9), assumes that the scale is either a semiconductor or an ionic conductor. Diffusion across the scale requires a concentration gradient which means that the composition of the oxide must vary from the stoichiometric composition. In the case of FeO, the lattice is metal deficient and termed a p-type semiconductor, in which the cations are the only mobile species. Fe_3O_4 is also metal deficient but has a smaller range of composition than FeO, although in Fe_3O_4 the anion is said to diffuse as well as the cation (1). Fe_2O_3 is an n-type semiconductor deficient in oxygen and the anion is the only mobile species (1). On iron all three oxides are formed at temperatures above 570°C (10), when heated in air at normal pressures.

Holmes (11) presents self diffusion coefficients, which are the coefficients for the relevant anion and cation species diffusing in any given oxide, as a function of 1/T. This data should enable the rate of oxide growth to be calculated for given conditions, but for this approach to be applied to a practical oxidation process several factors have to be considered. For example, it is necessary to know the type and composition of the oxide produced, and which oxide layer is rate controlling in multi-layer oxides. Also the self diffusion coefficients must be determined under conditions appropriate to the state existing during oxidation i.e. at the same oxygen partial pressure for cationic diffusion, and oxides in equilibrium with the metal for anionic diffusion.

For example, examination of this data suggests that the rate of oxidation of Fe to Fe_2O_3 (by anion or cation

diffusion) might be expected to be slower than the rate of oxidation of Cr to Cr_2O_3 (by anion or cation diffusion), but this is known to be untrue. The explanation for this is said to be due to the possibility of Fe_2O_3 showing much larger departures from stoichiometry (11). Davies et al (1) report that the relative proportions of the three oxides vary with temperature, whilst Paidassi (10), reports virtually constant proportions of 95% FeO, 4% Fe_3O_4 and 1% Fe_2O_3, over the temperature range 700° - 1250°C. Paidassi however notes that these constant results are only applicable to scales that remain strongly adherent to the metal, since the presence of a discontinuity at the interface modifies the constitution of the scale.

Thus, there are inherent difficulties in approaching the subject of oxidation by studying kinetics alone. Benard (12) has listed some of the reasons why the growth rate of an oxide growing under normal conditions cannot be specified with any great accuracy, and hence is likely to be non-reproducible. These are:-

(a) the process of transfer across an interface which has a rate approximately independent of time, is coexisting with the diffusion process which has a rate decreasing with time, and this combination can lead to discontinuities in growth rate.
(b) changes in oxide/metal adherence which may produce changes in the rate of transfer of reactants across the interface and therefore affect rate of oxidation.
(c) variations in the chemical composition of the oxide film which modify the diffusion conditions.
(d) recrystallisation of the oxide.

Lawless (13) discussed other factors which can provide problems in kinetic studies. He suggests that purity of both the metal and the atmosphere are extremely important since, for example, very small concentrations of a contaminant, such as H_2S, in the oxidising atmosphere can have a profound effect on the rate of oxidation. The effect of small quantities (less than 0·5%) of alloying elements on the rate of oxidation of pure iron has been demonstrated, for example, by German and Maxwell (14). Some of their kinetic results are shown in Fig.1.2..The effect of using a polycrystalline sample, with the unknown factors of grain size, grain boundaries, orientation, etc., was also discussed,(13) and results on single crystals, where crystallographic orientation has a large effect on the rate of oxidation, were quoted. Also, differences in kinetic results obtained by different researchers may often be attributable to differences in specimen geometry, size or surface preparation.

If, however, all the conditions that may be standardised are controlled there is still a basic variability in kinetic results, obtained under apparently identical conditions. This may be largely due to the seemingly random nature of oxide cracking and changes in adherence, which greatly influence the rate of oxide growth. The study of oxidation therefore requires information concerning the mechanical properties of oxides, their adherence to the metal, and the effects of stresses and contaminants on these factors.

1.2. The effects of contaminants

The effect of corrosive contaminants on high temperature oxidation has been the subject of much research. Materials and conditions used in boilers and turbines have been particularly of industrial interest. The three main contaminants encountered in such engineering applications are vanadium compounds, sulphur (including sulphates and sulphur oxides), and chlorides. The influence of these contaminants will be discussed separately, although, of course, a combination of these contaminants is likely to be present in a number of practical situations. For example, the main reason for the interest in the high temperature corrosion resistance of gas turbine materials is that the increased efficiency of operation, that would ensue from increasing the working temperature, cannot be realised due to costs and delays resulting from corrosive attack by sulphate, vanadium and chloride.

1.2.1. Vanadium compounds.

This particular aspect of the corrosion problem has, to some extent, been by-passed at the present time in that fuels with high vanadium content are not currently being used in gas turbines. Most gas turbines are now run on low vanadium distillate fuels. However, there is a financial inducement to use the higher vanadium fuels in industrial turbines, and this financial pressure is likely to increase with time. The effects of contamination with vanadium on high temperature oxidation is therefore worthy of study.

Hancock (15), has reviewed the subject of high temperature corrosion and quotes Wickerts (16), work which shows that oxidation under fuel deposit, rich in the vanadium oxides, increases with increasing temperature, whereas attack by sulphate goes through a maximum at about 700°C. Three mechanisms (17) appear to be possible to explain the type of corrosive attack produced.

(a) the vanadium compound acts as an oxygen carrier.

(b) the vanadium compound dissolves the oxide scale.
(c) vanadium enters the oxide scale, increasing the defect concentration and allowing accelerated attack.
Other workers (18)(19) have shown that of these mechanisms (a) and (b) appear reasonable whilst (c) receives little support. It was also shown that accelerated attack only occurs when a liquid phase is present (18).

Small, Strawson and Lewis (19), consider that the most aggressive of the sodium/vanadium oxide mixtures is 1.1.5. sodium vanadyl vanadate ($Na_2O.V_2O_4.5V_2O_5$), which is frequently found in boiler deposits. They used a crucible test method in which 25/20 Cr/Ni steel specimens were heated in mixtures of corrodents, for various times, and then removed for weighing and examination. These tests showed that the corrosive attack by sodium vanadyl vanadate was the same whether sulphates were present or not. The proposed mechanism of sodium vanadyl vanadate acting as an oxygen carrier seems to best explain their results. This mechanism receives further support since the rate of corrosion is found to decrease drastically when nitrogen is used above the melt (20), and Panthony (21) has also shown that corrosion in vanadium melts depends upon oxygen diffusion through the melt.

Fairman (22) carried out crucible tests on mild steel in mixtures of 90% V_2O_5, 10% Na_2SO_4 for 24 hours at 850°C. He found a reduction in metal thickness of 26% below the liquid level, 48% at the interface and 18% above the interface. From this he deduced that the vanadium acted by transferring oxygen atoms or ions to the metal surface. Fairman also concluded that the most satisfactory explanation for the corrosive effect of vanadium is that V_2O_5 acts as a catalyst, and also increases the defect concentration of the scale.

Reid (23) has also reviewed the subject of corrosion and deposition in boilers and gas turbines. He finds that there is general agreement that sodium vanadate can be more aggressive than vanadium oxides alone. On 25/20 Cr/Ni stainless steel in a simulated gas turbine combustor $Na_2O.3V_2O_5$ was found to be the most corrosive of all components in the Na_2SO_4-V_2O_5 system. There also seems to be general agreement that the presence of a liquid phase is necessary for serious corrosive attack to occur.

1.2.2. Sulphur

(a) Sulphur containing gases.

Under oxidising conditions, sulphur in the fuel burns to produce SO_2 and/or SO_3, whilst under reducing conditions hydrogen sulphide or sulphur vapour may be formed.

Ross (24) has shown that corrosion occurs when mild steel is exposed to an otherwise inert atmosphere containing 0·02% sulphur dioxide at 600°C, and that the scale shows alternative layers of sulphide and oxide. Ross explains this phenomenon of alternate oxidation and sulphidation, in terms of relative rates of transfer of sulphur vapour (produced by oxidation of the iron by SO_2) to the gas stream, and transfer of SO_2 to the scale to produce further oxidation.

Preece (25) found that when mild steel was exposed to an atmosphere containing SO_2, (at temperatures above 900°C), a molten oxide-sulphate complex was formed at the metal/scale interface which penetrated into the grain boundaries. Below 900°C the sulphide was distributed as discrete particles throughout the scale. Excess oxygen in the furnace atmosphere was found to prevent the formation of sulphides but, of course, increased the rate of oxidation in all cases except where the SO_2 content was high (i.e. more than 0·1%).

Edstrom (26) considering the oxidation of stainless steels, also reported the absence of attack in an oxidising atmosphere containing sulphur, but found an increased rate of scaling and the formation of sulphides when sulphur was present in a reducing atmosphere.

Flatley and Birks (27) exposed samples of pure Fe to atmospheres of argon containing various quantities of SO_2, and found that for all SO_2 concentrations an initially linear rate of attack was followed by a parabolic rate, when cationic diffusion became rate controlling. They quote the three eutectics present in the Fe-O-S system viz;

Fe - FeS - FeO at 925°C
FeS - FeO at 940°C
Fe - FeS at 988°C

and say that these low melting point eutectics produce serious attack, strongly adherent scales, and, as a consequence, poor surface quality.

Corey and co-workers (28) demonstrated that direct reaction between iron oxides and sulphur oxides, only occured when there was more than 0·5% SO_3 by volume in the gas and hence the corrosive attack must normally proceed through other chemical mechanisms, such as by the formation of complex sulphates.

(b) Sulphates.

Sodium and potassium sulphate frequently occur in deposits from oil and coal fired boiler installations. It has been shown (29) that below 750°C, in air, the effect of sodium and potassium sulphate contamination does not produce excessive corrosion on either ferritic or austenitic steels. It was postulated by Simons, Browning and Liebhafsky (30) that reducing conditions

are necessary to trigger off the sulphate attack, and that these conditions may arise by several mechanisms viz;

(1) If the atmosphere becomes locally reducing.
(2) If carbon is present in the gas or alloy.
(3) If chloride is present in the atmosphere.

They considered that an accelerated sulphate attack, seen in some crucible tests on Type 310 stainless steels was due to active sulphur species produced by the reduction of sulphates by the metal surface. This active sulphur could then form a low melting point metal/metal sulphide which could readily penetrate the scale and metal.

This accelerated attack needs to be triggered and it was demonstrated that this triggering could be provided by an applied e.m.f., or alternatively by chemical means, for example, by providing alternate oxidising and reducing conditions. Dravnieks (31) again mentioned the possibility of chlorides providing this triggering effect.

The need for reducing conditions was substantiated by Sykes and Shirley (32) who found that stainless steels in contact with pure sodium sulphate for 500 hours in static air at 700° to 750°C produced only a slight increase in the rate of oxidation. Imperfect gas combustion led to very severe attack on some stainless steels in contact with pure sodium sulphate. Sulphur in the gas stream did not markedly increase the rate of attack, but the combination of sulphur in the gas stream and the presence of pure sodium sulphate gave serious acceleration of attack, more so on some steels than on others.

Conversely Rahmel (33) examining the corrosion of austenitic stainless steels, found that sodium sulphate was hardly aggressive even in atmospheres containing SO_3, but increased the corrosiveness of deposits containing potassium sulphate. He also found that a considerable decrease in corrosion resulted from the addition of $CaSO_4$ and $MgSO_4$ to potassium sulphate, even in atmospheres containing an unusually high proportion of SO_3. It is worth noting that the atmosphere used was an oxidising one consisting of air water vapour plus the sulphur oxide additions, which would seem to support the proposed need for the presence of reducing conditions to produce sulphate attack.

The overall reaction suggested for sulphate attack has been represented (15) as :-

$$SO_2 + \tfrac{1}{2}O_2 \xrightarrow[\text{Catalyst}]{Fe_2O_3} SO_3$$

$$SO_3 + (Na,K)_2SO_4 \longrightarrow (Na,K)_2S_2O_7 \text{ (liquid)}$$

$$3(Na,K)_2S_2O_7\text{(liquid)} + Fe_2O_3 \longrightarrow 2(Na,K)_3Fe(SO_4)_3$$

sodium or potassium pyrosulphate — alkali iron trisulphate

It is therefore said that SO_3 is required, and that the pyrosulphate is the active species forming the alkali iron trisulphate as the product.

The maximum temperature of stability of sodium and potassium pryosulphates is in the order of 800° and 590°C respectively, (depending on the SO_3 concentration). Wickert (16) showed that attack by sodium sulphate/SO_3 on a 16%Cr, 17%Ni, 3%W steel had a maximum rate between 600°-750°C, which seems to support the pyrosulphate mechanism.

Other researchers have proposed mechanisms which do not require the initial formation of the pyrosulphate. For example, Corey and his associates (28) suggested that rapid oxidation of the metal occurs after the protective oxide scale has been destroyed by chemical reaction with alkali sulphates and SO_3 to form the alkali iron trisulphate. The reactions proposed were:-

$$3(Na,K)SO_4 + Fe_2O_3 + 3SO_3 \longrightarrow 2(Na,K)_3Fe(SO_4)_3$$

They demonstrated that at concentrations of SO_3 as low as 250ppm the trisulphate was formed by reaction with Fe_2O_3 and the alkali sulphates at 538°C.

These researchers also demonstrated the presence of small amounts of pyrosulphates in the furnace wall deposits and agreed that molten pyrosulphates reacted rapidly with Fe_2O_3. However, they also demonstrated that the pyrosulphate decomposed at around 316°C and the alkali iron trisulphate at around 593°C.

Cain and Nelson (34) were able to produce considerable amounts of alkali iron trisulphate by exposing a mixture of K_2SO_4, Na_2SO_4 and Fe_2O_3 to a synthetic flue gas (containing 3.6% O_2 and 0.25% SO_2) for 30 hours at about 600°C. They agreed with Corey et al (28) in saying that the alkali iron trisulphate was formed by reaction between Fe_2O_3, $(Na,K)SO_4$ and SO_3. Cain and Nelson however said that these molten complex trisulphates then migrate to the metal surface where the reaction was then represented as:-

$$10Fe + 2K_3Fe(SO_4)_3 \rightleftharpoons 3Fe_3O_4 + 3FeS + 3K_2SO_3$$

so that the essential corrosive reaction was:-

$$3Fe + SO_4^{2-} \longrightarrow Fe_3O_4 + S^{2-}$$

They found that the temperature range for rapid liquid phase attack by complex sulphates was bounded by:-
(a) The melting point of the mixture of complex alkali sulphates present, and
(b) Their thermal stability limit.
This temperature range was said to be 552° - $704^{\circ}C$.

A similar view is held by Simons et al (30) and also by Adams and Raask (35) who did not detect any sulphur or sulphides in the deposit or metal and hence concluded that the only part of the reaction to be completed was the first, viz:-

$$3SO_3 + 2Fe \longrightarrow Fe_2O_3 + 3SO_2$$

They (35) said that the SO_3 could diffuse inwards, and the SO_2 could diffuse outwards through cracks and pores in the scale.

From a study of thermodynamics of various reactions that might occur in boiler gases and deposits, Boll and Patel (36) concluded that the pyrosulphate - complex iron sulphate corrosion mechanism cannot operate above $620^{\circ}C$ because the corrosion product $Na_3Fe(SO_4)_3$ cannot form. Therefore severe corrosion that occurs above this temperature (37) must be due to the fact that the stability limit for $K_3Fe(SO_4)_3$ is some $100^{\circ}C$ higher than that of the sodium iron trisulphate, or due to some other mechanism. If a different mechanism is not operating then this supports Rahmel's (38) view of the importance of the potassium salt, and the ratio of potassium to sodium in deposits would strongly influence the degree of corrosion.

A recent review of this subject by Stringer (38) included thermodynamic data and equilibrium constants for various reactions that might be occuring between metals and sulphur species in gas turbines. Stringer stated that this data showed that no sulphides will be stable in a turbine atmosphere and hence some method for enhancing sulphur activity must be postulated to explain the sulphides found in practice.

Goebel, Petit and Goward (39) also used a thermodynamic approach to corrosive attack by sulphates. They viewed Na_2SO_4 as having both a basic and acidic component Na_2O or O^{2-}, and SO_3 respectively. They postulate removal of sulphur from the Na_2SO_4 to form

sulphides with the metal, which would then cause an increase in the activity of the Na_2O to an extent that destructive reaction between the Na_2O and the oxide scale could occur. It is not clear however to what extent the reaction between sulphur and the metal is responsible for corrosive attack and metal loss. In nuclear reactors the liquid sodium, used for cooling, is found to produce serious attack of the stainless steel cladding at 480°-540°C if 20ppm oxygen is present (40). This shows that sodium oxide can be an active steel corrodent even without the presence of SO_3 or an oxide scale, but this could well be some attack of the chromium present.

All proposed mechanisms require the presence of SO_3 in the atmosphere. It is generally agreed that SO_3 can be produced from SO_2 present in the atmosphere by the catalytic action of Fe_2O_3, for example, Harlow (41) found that when gases containing SO_2 are passed over heated Fe_2O_3, SO_3 is produced. Subsequently, SO_3 either combines with the Fe_2O_3 catalyst to form iron sulphate, or passes forward in the flue gases. Which of these two alternatives occurs depends on the temperature of the catalyst surface and the concentration of SO_2 in the gases. Crossley (42), referring to Harlow's results, said that in the presence of a suitable catalyst, and at temperatures of about 590°C, the probability of SO_3 formation will depend on the presence of sufficient quantities of oxygen. If SO_3 is formed it will only be free to enter into the flue gases if there is an insignificant amount of sodium or potassium salts present for combination.

Thus there is a great deal of debate concerning the exact mechanism of attack of steels by sulphate, particularly with regard to the part played by the pyrosulphate, and to whether the important reaction involves the metal surface or the iron oxide.

1.2.3. Chloride.

Most of the literature concerning chlorine and chlorides attempts to assess the effects of these species on the high temperature corrosion by sulphates. It is generally agreed that the presence of chlorides with sulphates produces a greater attack than sulphate alone. For example, in Sykes and Shirley's (32) results steels which were completely resistant to attack by pure sodium sulphate at 750°C, were severely corroded, accompanied by exfoliation of the scale, when 0.3% sodium chloride was added to the sulphate.

Crossley (42) reported that although corrosion by trisulphate tends to decrease at temperatures above

635°C, corrosion does occur at temperatures higher than this expected critical temperature when chlorides are present, and Crossley quoted Edwards, Jackson and Howes' (43), results to support this.

Greenert (44) tested a variety of ferrous alloys by coating them with a mixture of 90% Na_2SO_4, 10% NaCl and heating them in either nitrogen or oxygen. He found that corrosion did not occur below about 850°C, but was rapid above this threshold temperature. Corrosion was found to be greater in nitrogen than in oxygen atmospheres, which is consistent with the mechanism of sulphate attack being lessened by the presence of oxygen in the atmosphere. In a neutral atmosphere the chloride can presumably trigger the sulphate attack more easily.

Pickering, Beck and Fontana (45) studied the corrosion of 18-8 stainless steel in oxygen and dry sodium chloride at temperatures of 593°-760°C. Attack is more severe in steel containing 0.08%C than lower carbon or stabilised steels. The mechanism postulated is the reaction between $Cr_{23}C_6$ and the sodium chloride and oxygen. Since these carbides are confined to the grain boundaries in the austenitic steels then rapid intergranular corrosion occurs. Sodium bromide and sodium fluoride acted in a similar way, showing both a uniform surface attack and the rapid intergranular attack.

Alexander (29), suggested that chloride reacts with Cr_2O_3 in austenitic stainless steel to produce the volatile chromic chloride, which could explain why very little chloride is detected in deposits after reaction. She suggests the reaction:-

$$24KCl + 10Cr_2O_3 + 9O_2 = 12K_2CrO_4 + 8CrCl_3$$

The apparent catalytic effect of chlorides on the attack by sulphates can be explained if the chloride removes protective Cr_2O_3 layer allowing attack of the iron by the sulphate ion.

$$3Fe + SO_4^{2-} = Fe_3O_4 + S^{2-}$$

She found that 10%NaCl/90%Na_2SO_4 was slightly less corrosive that NaCl or KCl alone, and appreciably more corrosive than Na_2SO_4 alone for exposure times of less than 200 hours on 2¼% Cr, 1%Mo alloy, at about 600°C.

The importance of microstructure is shown for both ferritic and austenitic steels in determining the type of attack suffered by super heater tubes at temperatures up to about 700°C. Toft and Marsden (46), in agreement with Pickering et al (45), showed that preferential attack is associated with the presence of chromium carbides. Corrosion in industrial boilers of high

chromium steels, (either austenitic or ferritic), under aggressive atmospheres was said to be initiated by removal of the chromic oxide film, the mode of subsequent attack of the chromium depleted metal depending on the distribution of the chromium carbides, and the rate of attack depending on the composition of the matrix.

Marsden (47) reported the effect of chromium and nickel content on corrosion in the gas stream of power station superheaters. With low sulphur coals the resistance to corrosion increased with chromium content up to 25%, when resistance was quite adequate for superheater applications. Similar trials in oil fired boilers, where conditions were more aggressive, showed a greater scatter of results, but this was thought to be due to the effects of nickel. The deleterious effects of nickel could be seen from results in coal fired boilers in which steel containing 26% Cr and no Ni were more corrosion resistant than those containing more than 35% Cr and some Ni, presumably due to the formation of a low melting point nickel sulphide.

DeCrescente and Bornstein (48) considered the reactions:-

$$2NaCl\ (g) + SO_2\ (g) + \tfrac{1}{2}O_2 + H_2O\ (g) = Na_2SO_4\ (g) + 2HCl\ (g)$$

and

$$2NaCl\ (g) + SO_3\ (g) + H_2O\ (g) = Na_2SO_4\ (g) + 2HCl\ (g)$$

The equilibrium constants for these reactions were large in the temperature range 427° - 1024°C, indicating virtually complete conversion of the chloride to the sulphate. Tschinkel (49) has also considered these reactions, and has pointed out that at 1125°C sodium hydroxide replaces sodium chloride as the stable compound:-

$$NaCl\ (g) + H_2O\ (g) = NaOH\ (g) + HCl\ (g)$$

So that the equation,

$$2NaOH\ (g) + SO_3\ (g) = Na_2SO_4\ (g) + H_2O\ (g)$$

must also be considered. Some combination of these reactions would cause sodium chloride to disappear, particularly at temperatures of 1025° - 1630°C.

Cutler et al (50) suggest that when chemical equilibrium is reached, the reaction producing the combustion residue is:-

$$2NaCl + H_2O + SO_3 = Na_2SO_4 + 2HCl$$

Stringer (38) reports that mixtures of $NaCl/Na_2SO_4$ are more aggressive than Na_2SO_4 alone, and that NaCl alone may increase the rate of oxidation. Thermodynamic considerations suggest that in the presence of sulphur, all NaCl should be converted to Na_2SO_4. However, the reaction time available in a turbine for example, may be insufficient for equilibrium to be reached, and it is then possible that chloride particles may deposit on the metal surface.(51). If blade cooling is employed the temperature gradient will establish a concentration gradient for the dissolved metal ions through the molten deposit layer, which will favour continuous dissolution of the protective oxide. Thermodynamic data suggests that iron and chromium oxides will be much less soluble in molten sulphates than cobalt and nickel oxides, under conditions occuring in gas turbines. Cutler and Grant (51) also postulated the possible formation of the metal chloride as a separate phase having an appreciable vapour pressure, therefore formation and evaporation of the metal chloride will lead to loss of the protective oxide.

Examination of the information concerning the effects of mixtures of sulphates and chlorides show that all of the chloride should be converted to sulphate, but this does not explain the accelerated attack produced when chloride is added to sulphate, or the fact that chloride alone produces severe corrosion. The production of a volatile chloride compound seems to best explain the reported behaviour of chloride attack.

1.3. The stresses produced during oxide growth.

The effects of stress and mechanical properties have been reviewed recently, for example, by Stringer (52) and Hancock and Hurst (53), where the sources of stresses in oxide films are discussed as :-

(a) Pilling - Bedworth ratio (PBR)

The Pilling - Bedworth ratio is the ratio of the volume of oxide to the volume of metal from which it was formed. When this ratio is other than unity, stresses must be produced in the oxide scale due to coherency strains at the interface. This mechanism assumes that only the anion is mobile, since if the metal ions are the diffusing species then the oxidation process is occuring at a free surface and should be stress free. Fe/FeO has a low PBR (approximately 1·7) and is characterised by continuous oxide cracking during oxidation (54), and although this may be partly induced by compositional changes in the oxide, or specimen geometry, it demonstrates the limitations in relating PBR to the magnitude of the stress in the oxide.

The maintenance of a protective scale will still be governed by the ability of the oxide to plastically deform and accomodate growth stresses, whatever the magnitude of the volume ratio.

(b) Epitaxy

Since the lattice of the metal and the oxide are normally appreciably different and the oxide nucleates and grows on the metal surface, stresses will be produced due to this epitaxy. In the case of the oxides growing on iron the following lattice characteristics are known (53):-

	Lattice parameter c.	Structure.
Fe	2·86	b.c.c.
FeO	4·3	f.c.c.

Any epitaxial stress produced will be a maximum at the interface and reducing to zero at the free surface. It is probably more correct to consider the cation sublattice in the oxide, rather than the bulk lattice constants, but the stresses produced in the sublattice are extemely difficult to predict. Also, these epitaxial stresses will only be effective over a short distance and will only be of real importance for thin film growth at low temperatures or pressures.

(c) Recrystallisation stresses

It has been suggested (55) that any recrystallisation occuring in the oxide could lead to the production of stresses in that area, but it seems equally likely that such recrystallisation could act as a stress relief mechanism (52).

(d) Compositional changes

If there are compositional changes in either the metal or the oxide in the region of the interface during oxidation, then stresses may be produced. This could well be important in the oxidation of Fe where the three oxides are usually present and are able to exist over a wide stoichiometry range. For example, Howes and Richardson (56) suggest that the tensile stresses produced during the early stages of oxidation of Fe-Cr alloys are due to changes in the amount of iron present in the scale during growth.

Phase changes in the substrate may also impose stresses on the growing oxide film, due to the accompanying volume changes.

(e) Vacancy generation

Metals, such as iron, that oxidise by outward diffusion of cations produce vacancies at the metal/oxide interface. Some of these vacancies will undoubtedly precipitate at interface sinks, and will have a profound effect on adherence. Others will be injected into the metal setting up a defect gradient

which Jaenicke et al (55) suggest will produce stresses near the interface. Vacancies in the metal phase will usually assist with creep and thereby act to aid stress relief processes, unless the extent of creep in the metal exceeds the creep capability of the oxide perhaps leading to oxide damage.

(f) Microstresses

Douglass (57) discusses the importance of micro-stresses produced in the oxide scale at local heterogenities. The grain boundaries in an oxide oxidise more rapidly than the oxide grains, so that at any given time the grain boundary develops an oxide that is thicker than the average oxide thickness. Since the stress depends to some extent on the oxide thickness, stresses will be induced in the region of an oxide grain boundary which may be sufficient to crack the scale locally.

Similarly differences in oxide thickness may exist between adjacent grains as a result of different orientations, since it is well known that the rate of oxidation varies on different crystallographic planes, (14)(58).

Another source of microstress might arise from segregation of an alloying element or impurities at grain boundaries affecting oxidation rate locally.

It is also possible that oxygen can diffuse through cracks, pores, or down grain boundaries in the oxide even when unable to diffuse through the oxide lattice. This may lead to the formation of further oxide within the bulk scale layer producing compressive stresses.

Specimen geometry may also produce stresses in the oxide and influence the distribution of stress, but this aspect will be discussed in a later part of this introduction.

(g) Thermally induced stress

The stresses discussed so far can be produced isothermally. In the practical situation the stresses produced by temperature fluctuations are likely to be of more significance than the growth induced stresses because they may be much greater, and because engineering components do not normally operate isothermally. Some stresses will be produced because of the thermal gradient existing across the section during heating or cooling, but differences in expansion coefficients of oxide and metal will be of greater importance. Tylecote (59) has tabulated the relative expansion coefficients for various metals and their oxides, those pertaining to iron are:-

	Coefficient $x10^{-6}$	Temperature range ^{o}C
Fe	15•3	0 - 900
FeO	12•2	100 - 1000
Fe_2O_3	14•9	20 - 900

On the unlikely assumption that there is no plastic deformation, Tylecote (59) also calculated the compressive stresses due to differential thermal contraction during cooling as below. These calculations also assume a rather low value for the oxide modulus of $1•3 \times 10^{-3}$ tons/in^2.

		Cooling temp. range ^{o}C	Compressive stress tons/in^2
Fe	FeO	900	3•63
Fe	FeO	1000	-0•65

In summary, it is clear that during oxidation there are many sources of stress which can only be relieved by deformation or fracture of the scale, and/or by detachment of the scale from the metal. In order to assess what effect stresses will have on an oxide it is necessary to know the mechanical properties of theooxide, and its adherence to the metal surface.

1.4. Mechanical properties of oxides

It is possible to increase the oxidation resistance of a metal by adding elements that will slow down the rate of diffusion of the reactants. If, however, the alloy oxide so formed either cracks or does not remain adherent to the metal surface, then the reduction in diffusion rate will not be effective in reducing overall oxidation rate, since the oxidising gas can have ready access to fresh metal surface.

Engineering components operating at high temperatures, are often subjected to thermal cycles, superimposed stress, stresses due to geometry, etc., and any oxide formed is required to remain protective to prevent severe loss of section. A knowledge of the mechanical properties of oxides, particylarly during growth, will be essential in devising methods of limiting cracking and loss of adhesion.

Most methods used for determining oxide mechanical properties involve the preparation of bulk oxide samples either by the complete oxidation of metal samples, or by the sintering of powdered oxide. Several authors (53)(57) have questioned the validity of using results obtained from bulk oxides in assessing the behaviour of growing oxide films. For example, Douglass (60)states that there

is probably no true coherency between the metal and the oxide so that it is expected that misfit dislocations will be created. In the case of dislocations forming in the oxide, glissile slip dislocations will move away from the interface as the oxide grows and become sessile growth dislocations. The stresses will be highest next to the interface and are relieved somewhat as misfit dislocations are formed, thus the residual stress will equal the stress necessary to nucleate dislocations. This stress can be quite different to the yield stress of the bulk oxide. A further source of differences in behaviour is that the porosity is unlikely to be the same in both the bulk oxide and in oxides during growth.

In spite of these difficulties, oxide mechanical properties measured on bulk oxides can be used to give some indication of the manner in which oxides can plastically deform under the influence of the induced stresses.

There is much conjecture concerning the mechanisms operating when oxides plastically deform, and it seems likely that more than one mechanism may act at any time. The relative contribution of each mechanism depending principally on temperature and on the particular oxide system.

Douglass (60) discusses three posibilities that give rise to high temperature plasticity:-

(a) Grain boundary sliding. If no deformation takes place within the grains then the strains resulting from grain sliding must be accomodated at triple points. Unless localised folding occurs this should lead to nucleation of cracks at the triple point, or grain boundary migration would occur. In FeO, growing on pure iron, single columnar crystals form and therefore there are no triple points, deformation being accommodated by grains protruding from the surface.

(b) Herring-Nabarro or diffusion creep. This is a mechanism involving self diffusion, that permits deformation of polycrystalline grains under the influence of a shear stress by a flow of material away from boundaries where there is a normal pressure, and towards those where there is a normal tension. A high strain rate is favoured by a small grain size.

(c) Dislocation climb. Large numbers of vacancies exist in growing oxides which should permit easy climb of misfit dislocations after they are nucleated.

Exfoliation should not be expected for metals that oxidise to form highly defective oxides. Unfortunately, oxidation rate also increases with increasing vacancy concentration, and, as Birchenall (61) states, the fastest growing oxides are generally the most plastic, whereas the slower growing ones are brittle.

Stringer (52) states that in general it will not be possible for oxides to deform by crystallographic slip alone.

He discusses many possible mechanisms of plastic flow in oxides and concludes that the degree of plasticity theoretically possible for growing oxide scales is much greater than that observed in bulk oxides, e.g. at least an order of magnitude higher at the same temperature. The strain rates are such that any plastic deformation probably takes place by creep, the most likely mechanisms being dislocation climb, grain boundary sliding and Herring-Nabarro creep. If there is large scale plastic flow, dislocation climb processes of one sort or another are largely responsible. In an earlier review (62), Stringer points out that although oxides are supposed to deform plastically only at very high temperatures, extensive deformation normally being observed at high temperatures in excess of 0·85Tm, signs of considerable plastic deformation are frequently observed in oxides formed on metals at lower temperatures. However this could be due to departures from stoichiometry.

Clauer et al (63) reviewing the effects of non-stoichiometry on the creep of oxides, say that whilst the introduction of lattice defects usually strengthens crystals at low temperatures, at high temperatures they decrease strength. These authors also quoted the results of Ilschner et al (64) who found that single crystals of FeO were more plastic than polycrystalline samples, with creep rates ten times that of polycrystals under the same test conditions.

The mechanical properties determined will obviously depend on the stress system imposed during testing, so that application of test results to the growing oxide condition will have to take account of this. Vagnard (65) showed that in compressive tests on FeO appreciable plastic deformation was obtained at 600° - 700°C, whilst under tensile loading no plastic ductility was observed. At 800°C the tensile test gave only 3% strain whereas compressive testing resulted in strain greater than 40%. The results of ductility at the various temperatures under different stress systems is shown in Fig. 1.3. He also showed that the rate of straining was important in that again at 800°C strains greater than 12% are possible under tensile creep conditions.

The overall mechanical properties of a composite oxide during growth will depend on the composition of the oxide since the various oxides have markedly different mechanical properties.

MacKenzie and Birchenall (66) showed that the higher oxides of iron have higher strengths than FeO, but have negligible ductility.

Tylecote (59) completely oxidised specimens of pure iron and commercial iron, and, after allowing for the porosity present, obtained the results shown in Table 1.

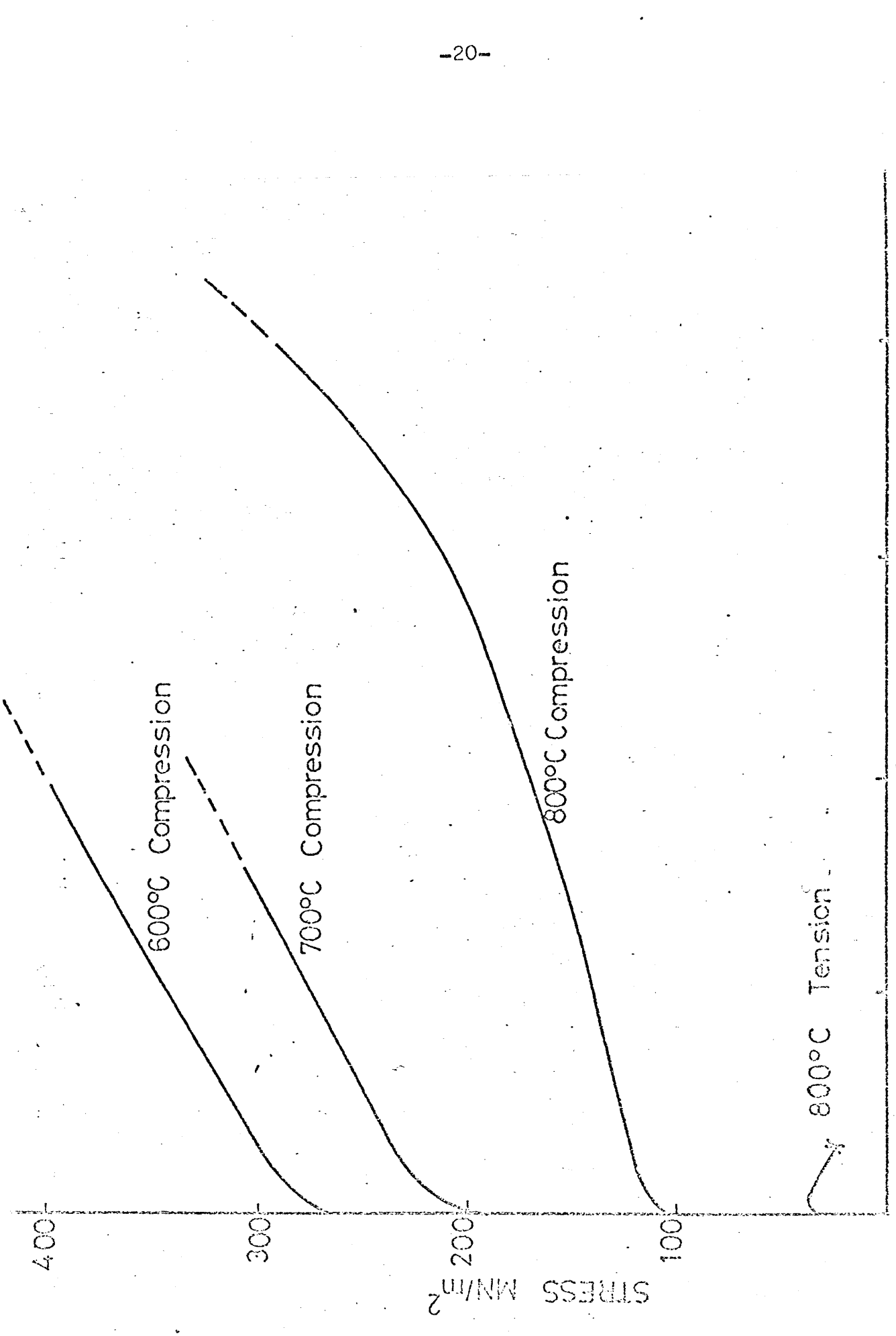

Fig. 1.3. Tension and compression tests on FeO (ref. 65)

Table 1.

Oxide	Test Temperature °C.	U.T.S. lb/in^2	Rate of Loading
Fe_2O_3	900	1000	Fast
Fe_2O_3	1150	5000	Fast
FeO (0·02%Mn)	500	1100	Fast
"	700	1100	Fast
"	1000	400	Fast
"	500	1700	Slow
"	700	2600	Slow
"	1000	400	Slow

Appleby and Tylecote (67) also obtained mechanical properties of Fe_2O_3 on compacted and sintered Fe_2O_3 powder using compression tests in the temperature range 20° - 920°C. They found that fracture and yield stress coincided i.e. there was no plastic ductility at any temperature within this range.

Hulley and Rolls (68) completely oxidised specimens of 0·1wt.% carbon steel in a modified Hounsfield tensometer machine and found yield stress values of around 1600lb/in^2 and UTS of around 3000lb/in^2 for FeO and Fe_3O_4 scales at 1000°C. A yield stress of around 1500lb/in^2 and UTS of around 2500lb/in^2 for magnetite and hematite scales at 1100°C were found. They compared these values with those obtained by Tylecote of UTS around 1000lb/in^2 at test temperatures between 1100° and 1200°C. Hulley and Rolls found the elastic strains of 0·016in/in at 1000° and 1100°C, and plastic strains of 0·051in/in at 1000°C and zero at 1100°C for the porous scales.

Holmes and Pascoe (69) discussing fracure strains in oxides, report the conflicting strains in published literature of between 0·05% and 50%. They quote data on the fracture strains of iron oxide as:-

Oxide	Test Temperature	Stress system	Fracture strain
Fe_3O_4 (on iron)	300°C	Tension	0·05 - 0·08%
Fe_2O_3 (bulk)	990°C	Compression	50%
"	1000°C	Tension	21%

Bruce and Hancock (54) were able to calculate the adherence of the oxide film by subjecting thermobalance specimens to thermal shocks, and also specimens in a vibration rig, to be described in detail in a later section. The onset of oxide failure due to the thermal shock was detected by observing the subsequent oxidation behaviour. It was found that oxide/metal adhesion increased with increasing temperature of oxidation. The plasticity of the surface oxides was estimated by noting the difference between the strains produced by thermal shocks in these experiments, and the values of elastic strain to failure determined previously by Tylecote (59). These results are shown in Fig. 1.4. and indicate that at 500°C the plastic strain possible appears to be between 1×10^{-4} and 2×10^{-4}, whereas strains of between 7×10^{-4} and 10×10^{-4} appear possible at 800°C for oxides on iron.

Ward, Hockenhull and Hancock (70) investigated the effects of tensile cyclic stressing on the oxidation of mild steel at 500°C and 570°C. They found an oxide fracture strain under these conditions of between 0·027% and 0·051%.

Grosskreutz and McNeil (71) devised an analytical method for relating the crack spacing in an oxide to the strain in the substrate. They conclude that if substrate slip is possible the criteria for oxide fracture are that the interface adhesive stress must be too large for the coating to sustain the necessary stress for oxide peeling. The thinner the film the more likely is fracture to occur.

There have therefore been many attempts to determine oxide mechanical properties, usually under far from ideal conditions, and the results obtained are not generally applicable to the practical situation of growing surface oxides.

1.5. Adherence

If the stresses produced in an oxide film are high, stress relief may occur either by ffacture of the oxide if the metal/oxide adherence is high, or by plastic deformation perhaps leading to blistering of the film (with possible oxide fracture), if adherence is poor.

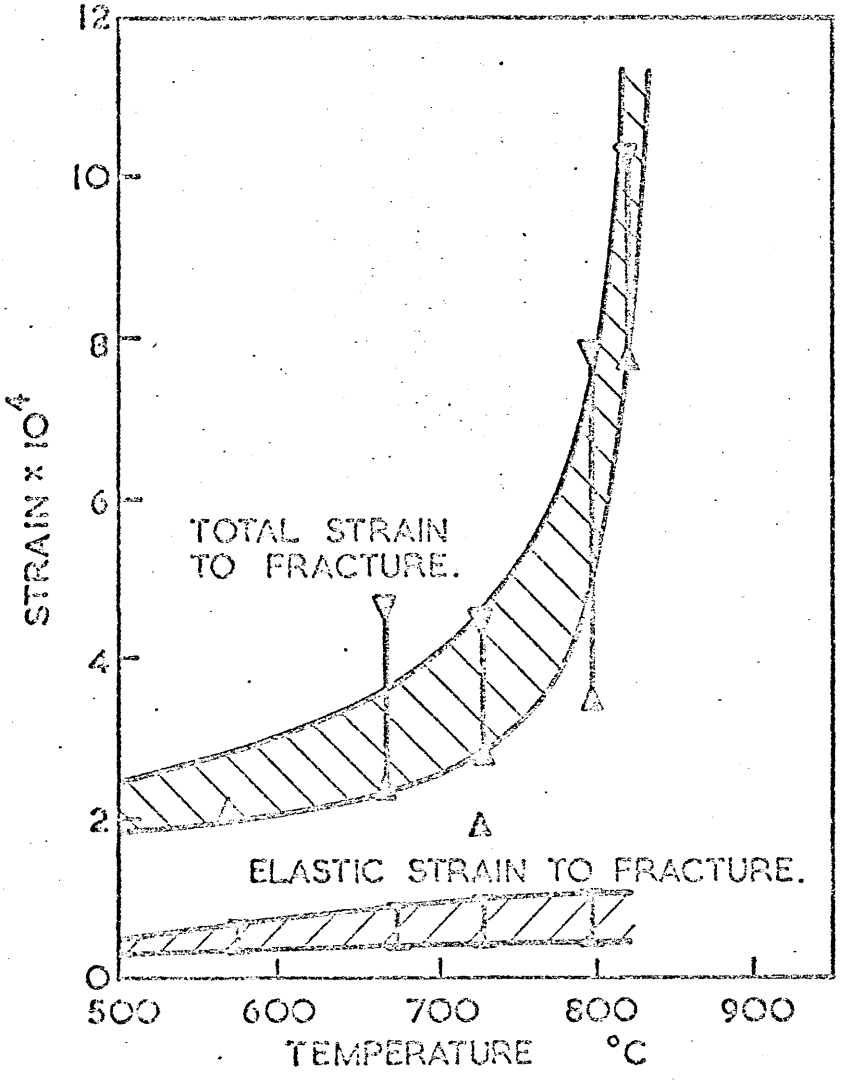

Fig. 1.4. Strains due to thermal shock accommodated by the oxide on mild steel prior to failure. (ref. 54)

There is the further possible means of stress relief through plastic deformation of the substrate, but this is usually only of importance during the oxidation of thin sections.

Tylecote (59)(72) reviewed the available information on adherence, and also published the results of some practical measurements of adhesive and cohesive strengths of oxides. He proposed that scales formed at 1000°C might well be more adherent than scales of the same thickness formed at 900°C, due to the superimposition of the tensile stress produced by the transformation. Paidassi (73) examining the oxides formed on iron found that to produce adherent films the specimens had to be electropolished prior to oxidation, since surface roughness was thought to produce high stresses due to oxide filling the surface grooves or valleys. In some circumstances an irregular interface will assist with oxide adherence, particularly where inward diffusion of oxygen and grain boundary penetration occurs.

On a flat surface, where edge effects are absent, it is extremely unlikely that an oxide film will inherit a stress normal to the interface, but in most practical situations, where edge effects are present stresses normal to the interface are produced. Thick oxides do not easily exfoliate due to their inherent mechanical stability, whereas thin films are more likely to become non-adherent, e.g. when thermally cycled. The converse of this is true for alloys for use at high temperatures in that adherence seems to decrease with increase in thickness (72). Hulley and Rolls (68) found a similar effect of scale thickness on adhesion, except in that they observed an optimum scale thickness above which adhesion decreased, (this was almost certainly a function of their specimen size and geometry). They measured adhesive strengths of oxides on a 0·2% carbon steel by allowing an oxide joint to be produced between two halves of a sectioned Hounsfield tensometer specimen, in a Hounsfield machine. The force required to detach the oxide from one half was then determined. They found that scale formed after 4½ hours at 1000°C showed stronger adhesion (about 940 lb/in.^{2}), than thicker or thinner scales. The authors concluded that the thinner scales contained growth defects that had not yet healed, and that scales thicker than the optimum value had lower adhesion because of the condensation of vacancies at one of the interfaces. The effect of increased temperature was to decrease the adhesive strength, e.g. a scale formed after oxidation at 850°C for 3 hours had an adhesive strength of about 1050 lb/in^2, compared with a strength of 870 lb/in^2 after 3 hours oxidation at 1000°C.

This trend appears to contradict the findings of Bruce and Hancock (54) that the adhesive strengths, measured by response of oxidised specimens to thermal shocks in a thermobalance, or in a vibration apparatus, increased with increased temperature in the range 570° - 800°C. Bruce and Hancock attributed the increased adhesion either to the changing interface conditions, or to increased oxide plasticity at the higher temperature. The obvious difference between these two pieces of research is that in the case of Hulley and Rolls' (68) work the $\alpha - \gamma$ phase transformation would occur within the temperature range of their tests, and the transformation of the metal beneath the oxide could quite likely affect the adherence.

Engell and Wever (74) examined the adherence of films on iron, and postulated a Kirkendall type effect due to preferential diffusion of either cation or anion. If the cation diffusion is dominant, as with iron, either voids should be formed at the interface or the oxide should be porous. Engell and Wever reported that they rarely found gaps between the metal and wustite formed at 600° - 850°C, and the oxide was dense and free from pores. They demonstrated that the adherence observed was due to plastic flow of the oxide in the region of the interface.

The relative plasticity of the three oxides of iron has a marked influence on the adherence of the multi-oxide layer to the metal, so that changes in oxidation atmosphere that change the proportions of the three oxides in the scale also strongly influence the adhesive properties.

MacKenzie and Birchenall (66) oxidised iron parallelepipeds to completion in pure oxygen and in hydrogen/water vapour mixtures at temperatures from 800° - 1050°C. The specimens oxidised in pure oxygen, i.e. comprising all three oxides, contained rectangular box-like cavities, the size and regularity of the cavity decreasing with increasing temperature of oxidation. The specimens oxidised in the H_2/H_2O mixture i.e. producing wustite only, contained no such central cavity, although some porosity was observed. They suggested that the magnetite and haemetite layers, having limited ductility, were able to restrain the more plastic wustite from following the interface inwards during oxidation and maintaining adherence. Creep curves were presented for the three oxides illustrating their relative plasticities. The authors say that the observed differences in behaviour were to be expected because of the differences in oxide structure, and therefore in the number of glide directions. However, this does not seem to be the complete explanation, since deformation of oxides by crystallographic slip alone is not possible at normal temperatures (52).

Tuck and Barlow (75) examined the effect of reheating atmosphere on scale adhesion on steel. They distinguished between four different types of scale structures and designated them:- (a) coherent, (b) layered, (c) porous, and (d) transverse cracked. They found that layered structures were most adherent and that the structure of the scale produced was not influenced by the fuels used or the oxygen content of the atmosphere, except in the case of nickel bearing steels where decreasing oxygen favoured a layer structure. In the nickel bearing steel, nickel was found to concentrate in the oxide near the metal/oxide interface. This nickel entanglement was only found to give good adhesion when associated with a layer type scale structure.

Juenker, Meussner and Birchenall (76) examined adherence and cavity formation on pure iron oxidised in oxygen. They classified the adherence phenomena into three arbitrary categories:-

(a) Incomplete separation of scale from the iron base with oxidation proceeding at the remaining adherent regions.

(b) Complete separation of the iron and scale followed by continuing iron and oxygen transportation as evidenced by progressive depletion of the free iron supply. This is on the lines of the Pfeil type loose core scale (77).

(c) The peeling off of a thin layer of adherent scale as the oxide separates from the iron. This consists of a localised rupture within the scale layer near, and parallel to, the metal surface leaving on the iron an adherent coating which joins elsewhere to the main oxide body.

A possible fourth category suggested, but not discussed by these authors, is the deep rupture of the oxide permitting free access of oxygen to the metal surface.

Griffiths (78) examined the effect of atmosphere on adherence and blistering of oxides on steels many years ago. He found that the scale formed on steel in pure oxygen was non-adherent, not blistered and uniform. When more than 50% CO_2 was present in a CO_2/O_2, or 30% N_2 in an N_2/O_2 mixture, then blistering occured in the temperature range 850° - 1000°C. The presence of steam in the air was found to prevent blistering but to form a non-adherent scale, the lower the temperature of oxidation the greater had to be the content of steam to prevent blistering. Griffiths postulated the need for an inert gas to keep blisters expanded, i.e. in pure oxygen blisters produced by growth stresses would collapse since the oxygen inside them would immediately be consumed in oxidising freshly exposed metal surfaces.

The action of steam in preventing blistering was explained in terms of a slowing down in the rate at which the specimen reached the oxidation temperature, thereby producing a more gradual and uniform growth.

Tuck, Odgers and Sachs (79) also investigated the effects of steam, (added to pure oxygen), on pure iron at 950°C. They found that scale adhesion was improved in the presence of steam, and found that samples admitted directly to steam/air atmospheres at temperature, blistered badly compared to those that were allowed to attain furnace temperature in argon before the oxidising gas was admitted. They account for the action of steam on blistering and adhesion by suggesting that the creep or plastic flow necessary to maintain scale/metal contact is enhanced by the presence of hydrogen.

The process of iron oxidation involves the injection of vacancies into the metal at the interface, and this can have a large effect on the adherence of the film. These vacancies can coalesce at the interface or at some suitable site within the metal to form pores. If the specimen is thin, Dunnington, Beck and Fontana (80) showed that lack of adhesion on one side of the specimen produces a suitable site at the other side of the specimen for the condensation of vacancies. In this way, oxide on one side of thin specimens remains adherent whilst the oxide on the other side of the specimen continues to be separated from the metal. Cracks in this separated oxide during growth give access of air to the metal surface, forming a series of thin separated films all transformed to the higher oxides. With thicker specimens this interaction between both sides of the specimen is not possible so that the two phenomena occur side by side, i.e. void formation and adherent oxidation. The result for the larger specimen, in a broken mass of oxide particles resting on a retreating metal surface.

Further evidence for this increase in adherence in the presence of a suitable vacancy sink, was obtained by Tylecote and Mitchell (81). They drilled a series of longitudinal holes in iron plates, sealed the ends of the holes, and oxidised the specimens at 700°, 800° and 950°C for 22 hours. They found that the scales, particularly on the specimens oxidised at 800°C contained cavities and were firm and adherent, whilst the scales on the control specimens without the drilled holes were completely non-adherent on one side, and showed intermittent contact on the other side of the specimen.

Bruce and Hancock (82) studied the effects of specimen geometry on the growth and mechanical stability of iron oxides. They showed that on cylindrical specimens of small radius, non-adherent, porous scales are formed, and that if the oxide mechanical properties

are known then the oxide thickness at which loss of adhesion will commence may be predicted for any specimen diameter at a given temperature.

Hancock and Hurst (53) have discussed the interaction between specimen geometry and stress generation during oxidation in the four categories of anionic and cationic diffusion for both convex and concave surfaces. Where growth is by cationic diffusion, (as is largely the case when iron is oxidised), they conclude that stress relief on a convex surface occurs either by shear fracture of the scale if adherence is good, or by detachment leading to oxide buckling and possible local tensile failure of the oxide film. In cationic oxidation on a concave surface the initial compressive stresses are relieved as the metal retreats. Further oxidation leads to detachment of the oxide layer if adhesion is poor. If adhesive forces are high, further oxidation will produce tensile stresses in the oxide leading to radial cracking. The influence of vacancy ingestion into the metal would reduce the recession of the metal during oxidation and merely delay the onset of failure. The effect of the superimposition of a cooling cycle on such an oxide will be to increase the compressive stress and increase the risk of failure on a convex surface, and reduce the possibility of decohesion and failure on a concave surface.

Romanski (83) discusses the effects of the specimen surface area to mass ratio on the kinetics of oxidation and sulphidation. He shows that in the study of rapid reaction processes, allowances must be made for the rapid reduction of the metal core dimensions unless great care is taken in the selection of experimental conditions and geometrical factors. Suitable area mass ratio may be chosen such that the oxidation rate is independent of geometry factors, and it was found in this work that large flat discs were the optimum specimen shape, and that cylindrical specimens with diameter were the least suitable. However the criteria for choosing specimen shape for experiments should be that the shape is suitable to simulate the practical situation.

A method for investigating the effects of small additions of alloying elements on the adherence of oxide scales on iron, was devised by Peters and Engell (84). In this method the adhesion was determined by glueing the oxide, on an oxidised specimen, to a soiled base and measuring the force required to detach the oxide from its' metal base at ambient temperature. Specimens containing about 0·04wt.% of various alloying additions were tested in this way. More recently German and Maxwell (14) have used a modification of this test

to investigate the effects on adhesion of additions of 0·1wt.% for Ag, Au, Cr, Nb, P and Pt, 0·2wt.% for Be, 0·35wt.% for Ge, and 0·5wt.% for Al, As, Co, Ga, Sb, Sn, Ti, V and W, and a range of iron-carbon alloys with from 0·25wt.% C to 0·95wt.% C. Other elements in each alloy was below 0·01wt.%, and were mostly less than 0·002wt.%, B.I.S.R.A. "AH" pure iron was used as a standard of comparison. Those alloying elements with a high negative free energy of oxide formation, relative to FeO, were generally found to segregate in the oxide layer near to the oxide/metal interface. Those with a lower free energy of oxide formation were generally found to segregate in the metal phase near the interface. Formation of a mixed oxide usually led to a loss of scale by spalling during cooling, or to very weakly adherent bulk scales. In either case a thin, very strongly adherent, layer remained on the metal surface, and consisted mainly of the spinel or other mixed oxide (Al, Be, Ti, V). The Cr and W alloys produced an adherent scale that fractured at about half the load needed for pure iron. The scales on the more noble metal alloys were generally as adherent as those on pure iron. Alloys containing As, P, Sb, or carbon produced weakly adherent swollen scales, usually with a very thin adherent layer on the metal surface. Unfortunately, apart from the scale removal load of 3·8 - 2·8 Kgf/mm^2 quoted for scales 40 - 120 m on pure iron, very little other quantitative data is given to indicate the order of the effect.

The recent review by Wright (85) of the oxidation of iron -, nickel -, and cobalt - based alloys, discusses the effects of alloying additions on the adherence of oxide films. The tendency for the scale to spall on Fe - Cr alloys increases with increasing chromium content (86). Apparently, the scales develop tensile stresses in the early stages (56), and compressive in the later stages (87). In the higher chromium alloys the mechanical properties and the physical nature of both the scale and the alloy/oxide interface, play a larger role in the oxidation behaviour than previously thought. Although nickel enters the scale on Fe - Ni - Cr alloys only in small amounts, it plays an important role in dictating the nature, composition and possibly mechanical properties of the protective scale, the incidence and severity of its subsequent failure, and its healing characteristics.

Much recent work has been directed towards determining the effects on adherence of rare earth additions. For example Tien and Rand (88) found that 0·2wt.% of either yttrium or scandium to Fe - 25Cr - 4Al produced a tenaciously adherent scale and an absence of voids at the interface. This compares with the spalling

of non-adherent Al_2O_3 films on a similar alloy, but without the yttrium or scandium additions. The alloying additions were said by these researchers to work by forming complexes with vacancies or by providing internal oxide boundaries for the condensation of vacancies.

The many suggested explanations for the mechanism by which rare earth additions increase oxide adhesion and reduce oxidation rate, were discussed in the review by Wright (85). The decline in oxidation rate might be explained by the formation of a rate controlling layer at the scale base, although such a layer has not yet been detected. Doping of the protective layer by the trace elements leading to reduced ion transport or modification of oxide mechanical properties and thus improving adhesion has been suggested but remains speculative. It has also been proposed that intermetallic particles can act as keys to anchor the scale to the alloy surface. There is thus little agreement regarding the mechanism of the effects of rare earth additions, and it seems likely that no single mechanism will be responsible for all the effects noted, in the various alloy systems at all temperatures. What is generally agreed, however, is that these rare earth addtitions provide improved oxidation resistance, sometimes a reduced oxidation rate, refinement of the alloy grain size, a general retention of the small grain size at temperature, a fine grained oxide, and sometimes a reduction in the extent of the transient oxidation period.

Several methods have been used to attempt to measure the strength of the adhesive bond existing between a metal and its oxide. The method of Hulley and Rolls (68) in which an oxide joint was allowed to form between two halves of a tensometer test piece, has already been mentioned. Bateman and Rolls (89) developed a hot bend technique in which the extent of oxide/metal adhesion was measured in terms of the ratio of weight of scale displaced by the bend, to the weight of scale formed. Pure iron gave an index value of 0·96 - 1·0 which was much higher than the values obtained on Fe - Al alloys (up to 0·2% Al), tested in the same temperature range.

Arnold and Rolls (90) investigated scale deformation on some iron based alloys using a three point bend test at temperature, and adhesion using a test in which an oxide weld, was allowed to form between two specimens with a configuration similar to a fillet weld. The tensile force required to fracture the scale or detach the scale was then measured. The method used is shown diagrammatically in Fig. 1.5.. They found that at 1000°C a fracture stress of 2·87 MN/m^2 was required for

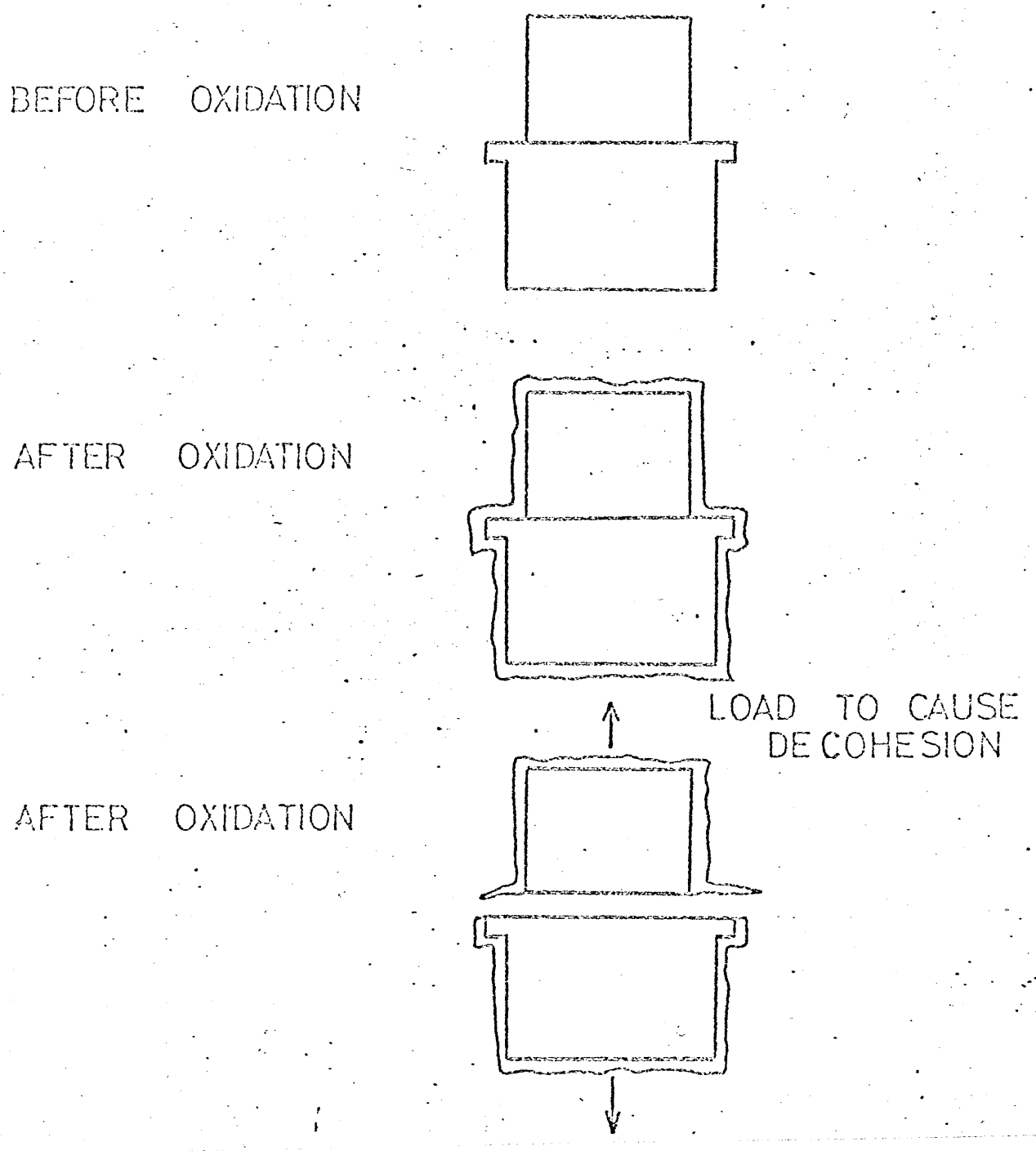

Fig. 1.5. Method of measuring oxide/metal adhesion. (ref 90)

Fe - Cr - Mo alloy and of 3·39 MN/m^2 for an Fe - Ni - Mo alloy. Fracture occured within the scale near the scale/metal interface and therefore the cohesive rather than adhesive strength was being measured. The fact that the fracture was within the scale layer was explained in terms of the adherence of the inner scale layer which was enriched with alloy elements.

Peters and Engell (84) measured the adhesive forces between oxide and mild steel by gluing the oxide to a solid base and measuring the force required to detach it, but the values are all measured at room temperature and are therefore of limited use.

A method used by Nicholson (91) allows a fine stainless steel guaze to become embedded in a growing oxide scale. After a suitable period of oxidation the force required to detach the guaze and the surrounding oxide can be determined. If the scale fractures at the interface adhesion is measured, and if the fracture occurs within the scale then cohesion is measured by this test. The major problem with this type of test is that the mesh is almost certain to interfere with the oxidation process.

A recent survey (92) of methods available for investigating oxide mechanical properties and scale/metal adhesion concluded that a vibration technique developed by Hancock and Bruce (54) was the only method available for studying both of these phenomena on the oxide during growth.

1.6. Vibration technique

The inherent problems in studying oxide mechanical properties when using bulk oxides at elevated temperatures or surface oxides at room temperature led to the development of the vibration technique. This technique involves the suspension of a rod of metal from a pair of mechanical vibrators and monitoring the change in resonant frequency of the rod as it oxidises. Rayleigh (93) showed that the characteristic frequency of the first mode of vibration (f_o) is related to the specimen dimensions, and to the dynamic modulus (E) of the metal by the following equation:-

$$f_o^2 = \frac{(4{\cdot}73)^4 \, E \, a^4}{16 \, \pi \, l^3 \, m_o} \qquad (1)$$

where a, l, m_o are the radius, length and mass of the rod.

If the rod is oxidised, then the metal with its oxide film approximates to a composite cylinder. If the radius of the composite cylinder is b, and the radius of the inher metal core is c, then the frequency of the

first mode of vibration (f) of the composite cylinder is given by:-

$$f^2 = \frac{(4{\cdot}73)^4}{16\ \pi\ l^3\ m} \quad (E_1\ c^4 + E_2\ (b^4 - c^4)\ ) \qquad (2)$$

where m = total mass of composite bar
E_1 = metal modulus
E_2 = oxide modulus

It is extremely difficult to determine these changing dimensions during oxidation, but the natural resonant frequency can be related to the mass gain, which can be determined continuously using a thermobalance. This relationship is:-

$$\frac{f^2 - f_o^2}{f_o^2} = \Delta \left[\frac{2\ \beta\ M_1}{M_2 - M_1} - \frac{M_2 + M_1}{M_2 - M_1}\right] +$$

$$\frac{\Delta^2}{1+\Delta} \left[\frac{M_2\ \rho_1}{M_1\ \rho_2} + \frac{M_2^2}{M_1^2} - \frac{2\beta M_2}{M_1}\right] \left[\frac{M_1}{M_2 - M_1}\right]^2 \qquad (3)$$

Δ is defined by $m = m_o\ (1 + \Delta)$
f = the natural frequency of the oxidising rod
f_o = the natural frequency of the original, unoxidised rod at the same temperature
M_1, ρ_1, E_1 are atomic weight, density and dynamic modulus of the metal
M_2, ρ_2, E_2 are atomic weight, density and dynamic modulus of the oxide

and $$\beta = \frac{E_2\ \rho_1\ M_2}{E_1\ \rho_2\ M_1} \qquad (4)$$

It has been shown (94) that this equation can be reduced to:-

$$\frac{f^2 - f_o^2}{f_o^2} = \Delta \left[\frac{2\ \beta\ M_1}{M_2 - M_1} - \frac{M_2 + M_1}{M_2 - M_1}\right] \qquad (5)$$

This method is able to follow the rate of oxidation of a metal, and can also sensitively detect cracks or blisters occuring in the oxide, since such growth defects are indicated by discontinuities in the frequency response.

This technique was used by Bruce (94) to examine the oxidation of Armco iron, mild steel and pure nickel. The results obtained showed that the oxide on iron was cracking continuously during growth, and that the cracking was less at higher temperatures. The frequency response of nickel during oxidation was shown to be smooth and regular with no discontinuities, since oxide cracking did not occur. Values of dynamic modulus for the surface oxide on iron were determined during growth using this method in the temperature range 570° - 800°C. The modulus value for the oxide on nickel were obtained in a similar manner, but adhesion and plasticity values could not be determined, since even quenching in water from 1000°C did not lead to visible damage of the scale.

Since the original work by Bruce and Hancock (54) the apparatus has been refined and improved, and has been used to examine the oxidation of nickel based superalloys, (95)(96), which of course oxidise at a very slow rate.

The apparatus is now also sensitive enough to detect oxide cracking during cooling, and does not have to rely on the increased oxidation rate upon reheating as an indication that the oxide has fractured, which can easily be determined in a thermobalance.

CHAPTER 2

2. OXIDATION OF IRONS AND STEELS

2.1. Vibration technique - Experimental

2.1.1. Material.

The principal material used in this investigation was an EN2C type steel, with pure iron and other steels used for comparison purposes. The analyses of these materials is shown in Table 2. The EN2 steel as received was in the form of ½" diameter bars in 12' lengths all produced from the same cast of metal. The transverse microstructure consisted of grains of ferrite, (with an average grain count of 120 grains/sq.in), interspersed with colonies of fine pearlite. The longitudinal section revealed the directionality due to the rolling, and also the recrystallisation that would be expected for a steel correctly hot rolled. A number of specimens from several different bars were examined metallographically and were found to have a consistant structure.

The mechanical properties of the as received steel were tested using both Instron and 50 ton Dennison testing machines, and the following average results were obtained:-

U.T.S. = 93,300 psi ($\mp$ 2,650 psi)

% extension = 41·4% ($\mp$ 1·4%)

Reduction of area = 57·4% ($\mp$ 5%)

The hardness value was uniform across the cross section at a value of 214 VHN ($\mp$ 14), except for a very thin decarburised region at the bar surface, where the hardness fell to about 160 VHN.

These mechanical properties were very high for material of this specification, so samples were tested for preferred orientation using a back reflection X-ray technique. No preferred orientation was found to be present, either at the bar surface, or after the removal of the surface layer by machining. These high mechanical properties were thought to be due to the combination of an optimum chemical analysis and processing conditions, since after annealing at 950°C for one hour the properties were as to be expected in such a steel, and the annealed material had an average UTS of 55,700 psi, and a uniform hardness of 112 VHN.

The microstructure was identical whether the steel was annealed in argon, nitrogen, hydrogen, or under vacuum, but annealing in vacuum was the only method that did not produce any detectable surface oxide. Vacuum annealing was therefore used for all specimens in this investigation. The microstructure after annealing was very little changed from that of the as received

Table 2

Element	EN2 Steel	Mild Steel	Armco Iron	Johnson Matthey Specpure
Carbon	0·11%	0·04%	0·038%	-
Silicon	0·21%	0·04%	-	1 p.p.m.
Sulphur	0·023%	0·072%	0·009%	-
Phosphorus	0·009%	0·015%	0·01%	-
Manganese	0·44%	0·32%	0·075%	1 p.p.m.
Nickel	0·20%	0·02%	Trace	-
Chromium	0·02%	0·01%	-	less than 1 p.p.m.
Molybdenum	0·03%	0·06%	-	-
Aluminium	0·04%	0·07%	-	less than 1 p.p.m.

material, except that the grain count was reduced to an average of 100 grains/sq.in. by annealing.

2.1.2. Specimens.

The $\frac{1}{2}$" diameter bar was centreless ground, to a nominal diameter of 0·2". This method of preparation proved to be an excellent method of obtaining specimens of uniform and reproducible dimensions and surface finish. This diameter was uniform in any given specimen, and only varied between 0·1997" and 0·1998" for all the specimens prepared.

As it is well known that the surface finish may have a large effect on the oxidation process, several methods of surface preparation were investigated. These included polishing the as ground specimens with various grades of emery paper, electro-polishing using different electrolytes and current conditions, and a combination of these techniques. It was found that electro-polishing did not produce a uniform, reproducible surface finish, particularly for the long specimens required for the vibration work. The main problem was the prevention of surface pitting which usually occured in isolated areas. Emery polishing did not produce an acceptably uniform surface finish either, and it also tended to diminish the dimensional accuracy produced by the centreless grinding operation.

It was decided therefore that although the ground surface was comparatively rough, it was extremely uniform and consistent. Surface roughness measurements of a number of specimens using the Taylor Hobson Talysurf equipment confirmed this uniformity, and gave results of centreline average of 10 ∓ 2 μ". This surface roughness was apparently unchanged by annealing.

2.1.3. Vibration apparatus.

The vibration technique and theory were briefly described in the Introduction. Several modifications have been made to the original equipment, principally to the electronic components. The basic apparatus used in this investigation is shown schematically ih Fig.2.1. and photographically in Figs.2.2. and 2.3..

The equipment shown in Fig. 2.3. is fitted with the necessary vacuum pumps to enable the furnace and vibrator box to be evacuated. The electronic system is shown diagrammatically in Fig. 2.4., and consists essentially of a signal generator or oscillator which supplies a disrete frequency signal to a 30 Ω Goodman vibrator, via a transformer or resistor which provides a suitable impedance for the oscillator. One end of the specimen is suspended from this vibrator by asbestos string, and is vibrated by the signal transmitted through the suspension string. The other end of the specimen is similarly suspended from another vibrator

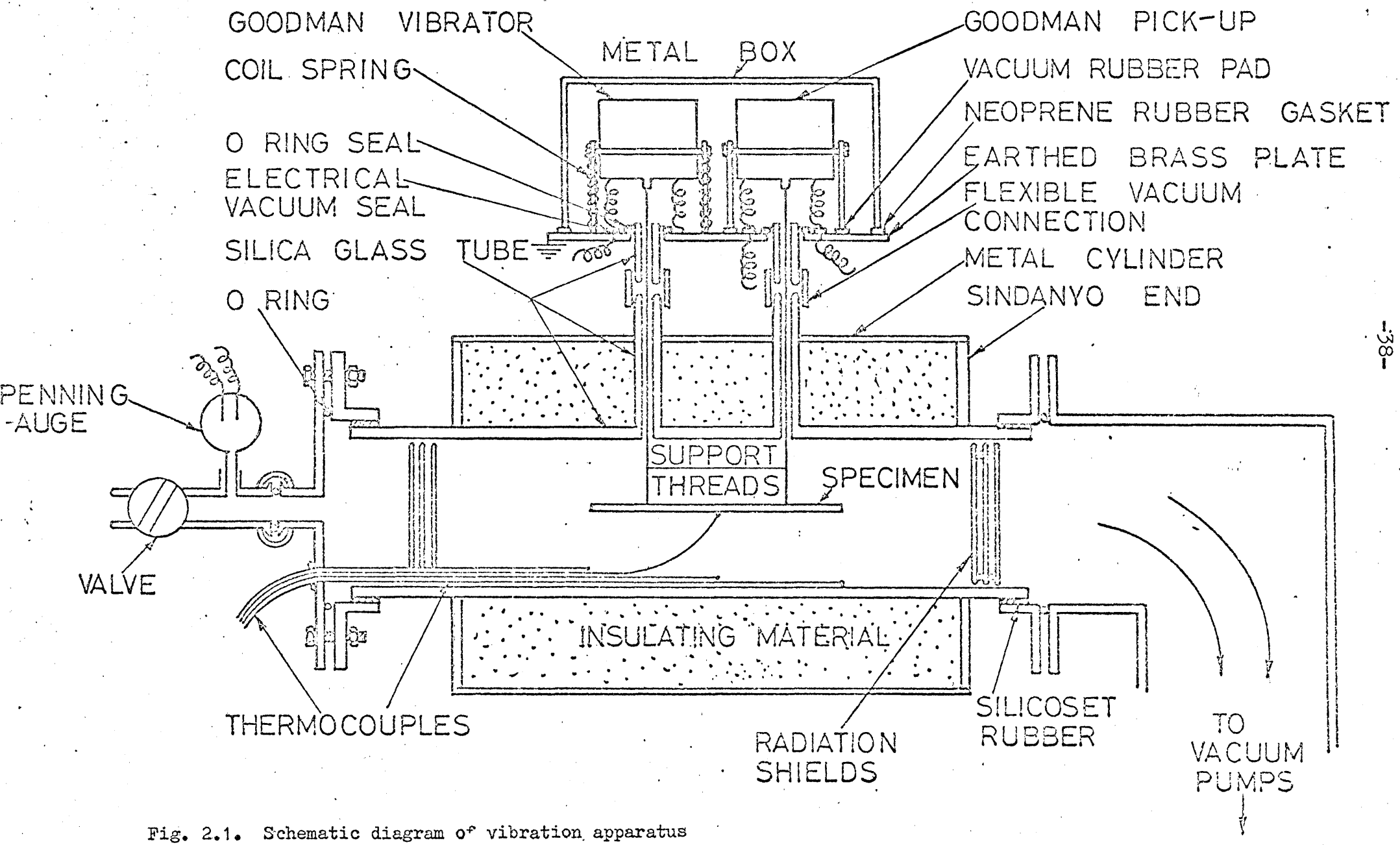

Fig. 2.1. Schematic diagram of vibration apparatus

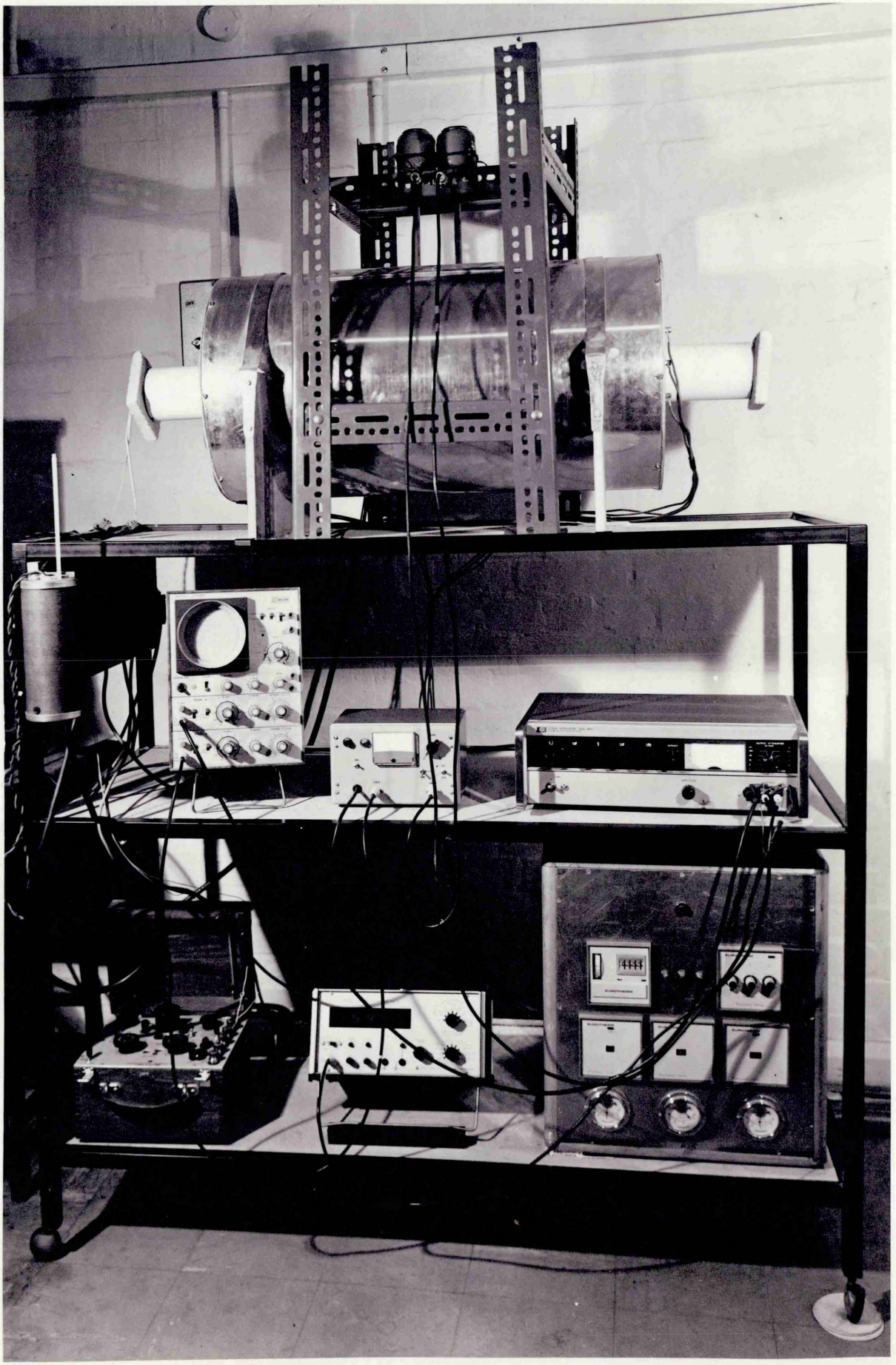

Fig. 2.2. General view of vibration apparatus.

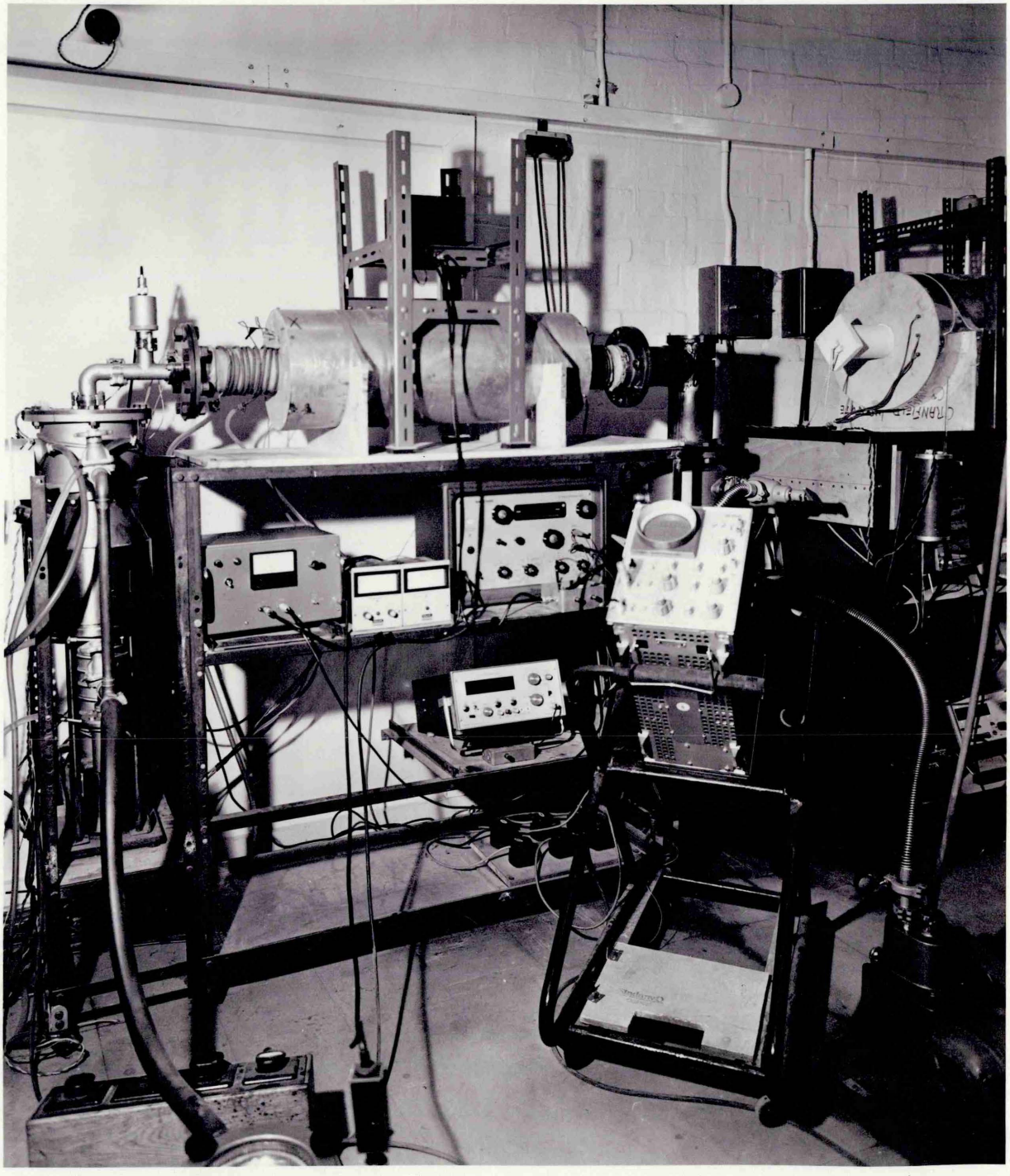

Fig. 2.3. General view of vibration apparatus fitted with vacuum system.

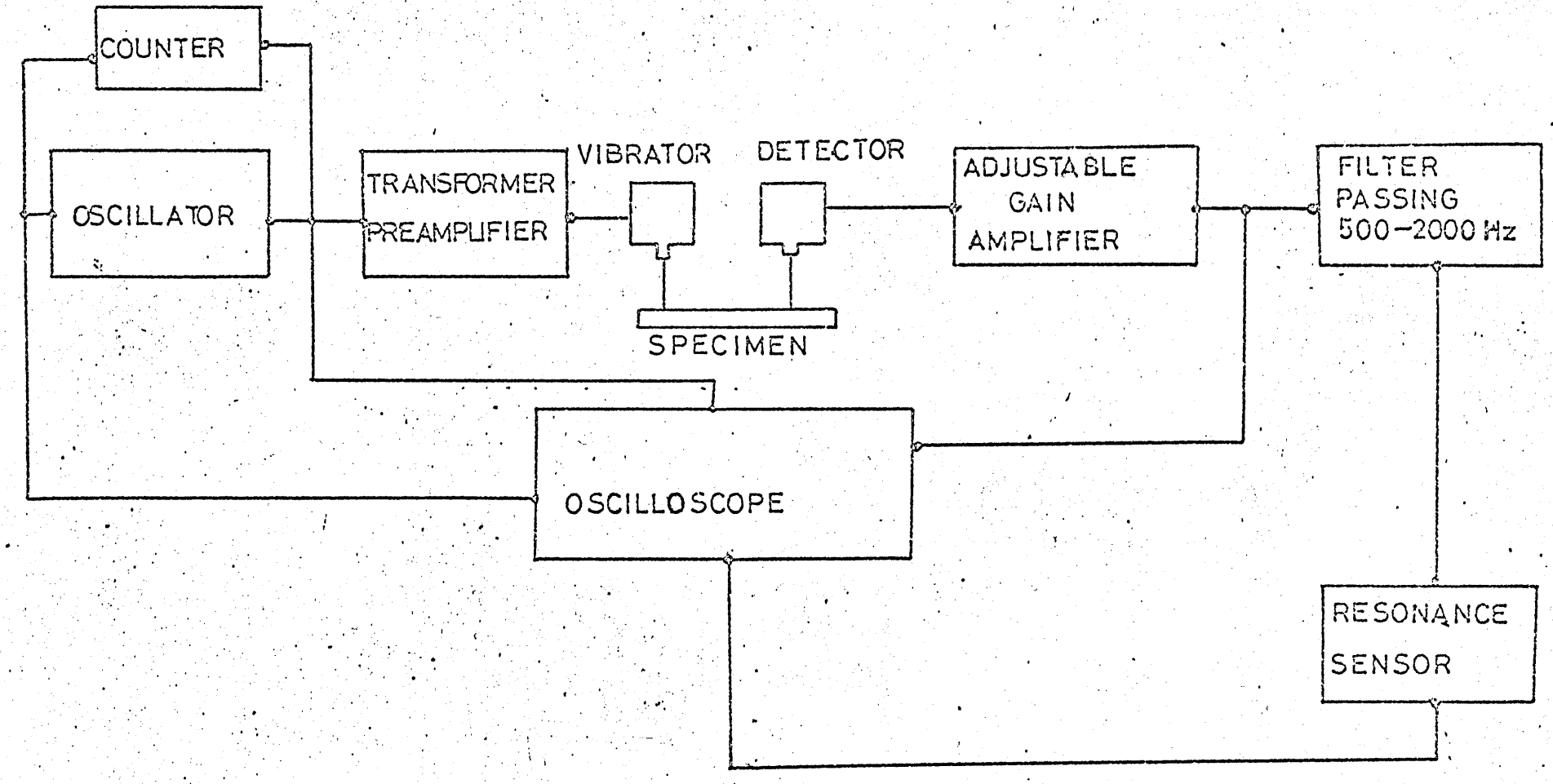

Fig. 2.4. Circuit diagram of vibration apparatus

which acts as the signal pick-up. The suspension of the specimen from the vibrators is shown in Fig. 2.5.. This signal is then amplified and passed through a high band-pass filter with a range of 500 - 2000 Hz. The output signal from the filter could be monitored on both an oscilloscope screen and on a milliammeter. A counter/timer to accurately measure the input frequency completes the electronic circuitry. The method of obtaining the resonant frequency is to adjust the input frequency until the output signal amplitude is a maximum. This maximum occurs when the specimen is at resonance, and the frequency applied may be noted from the counter/timer.

The vibration furnace is Kanthal wound in three separately controlled heating zones 6", 10" and 6" in length respectively. The furnace temperature feedback to the 15amp Eurotherm controller is from a chromel/alumel thermocouple located on the bottom of the furnace tube in the centre of the furnace, Specimen temperature could be measured using a potentiometer and a Pt/Pt 10% Rh. thermocouple positioned within about $\frac{1}{4}$" of the end of the specimen. The temperature distribution over the specimen length was first determined by attaching glass fibre coated thermocouples to either end and the centre of the specimen, and heating the furnace through the working temperature range. The furnace heating zones were adjusted so that the temperature variation along the specimen length was less than $\frac{1}{2}^{o}$C over the entire testing temperature range.

2.1.4. Adiabatic and isothermal modulus.

When a material is compressed heat is released and the temperature of the material rises causing an increase in volume and a decrease in modulus. This is termed the thermo-elastic effect, and is the reason for obtaining different values for modulus with fast or slow strain rates. Different values are also obtained using dynamic or static methods of modulus determination. Bruce (94) examined these effects and showed that the volume expansion term in the thermo-elastic effect had a negligible effect on modulus, and that the change in modulus due to the compression gave values that were 0·16% higher than the modulus value determined in static tests.

2.1.5. Damping measurements.

In order to investigate the damping capacity of the EN2 steel, it was first necessary to determine whether or not the damping was dependant on the amplitude of the applied vibration. This factor was of great importance since in most cases where the internal friction is amplitude dependant, it is found that the

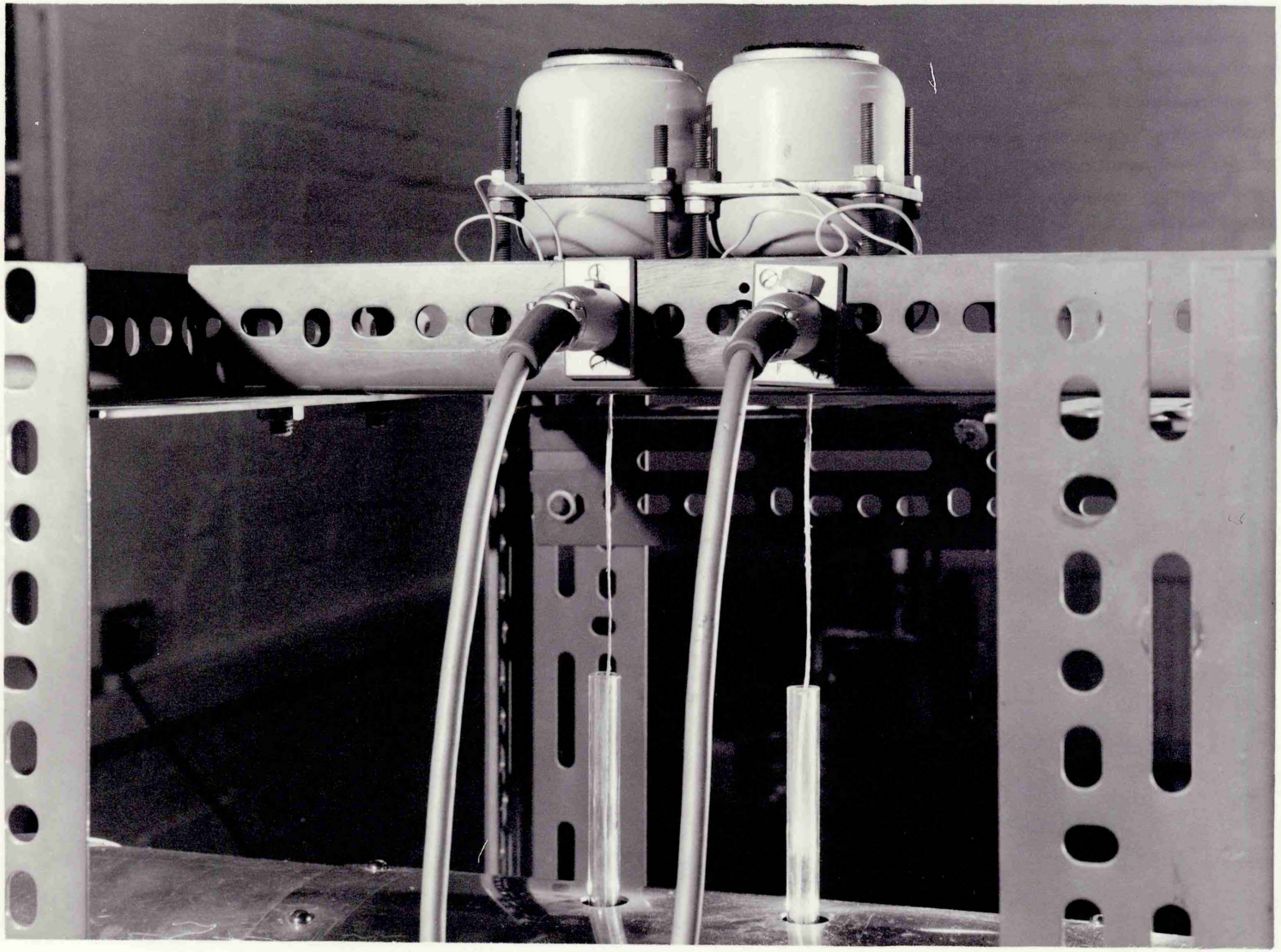

Fig. 2.5. Close up of vibrators showing furnace side arms and asbestos suspension strings

dynamic modulus also varies with amplitude (97).

With this EN2 steel it was found that the values of damping and resonant frequency did not alter when the input amplitude was varied progressively from 1 volt to 10 volts, using a signal generator that was customarily employed at an output amplitude of 3 volts. therefore, within the range of input amplitudes to be used in this investigation, the dynamic modulus and damping were found to be independant of input signal amplitude.

A measure of the damping or internal friction of the material was obtained by determining the frequency band width, Δf, at half the amplitude of the natural resonant frequency, f, and applying the formula:-

$$\text{Damping } \delta = 1{\cdot}814 \frac{\Delta f}{f}$$

In a similar manner the internal friction Q^{-1}, could have been calculated from:-

$$Q^{-1} = \frac{0{\cdot}5773}{f} \Delta f$$

hence $Q = \delta$ approximately

The values of damping at room temperature were of the order of 2×10^{-3}, and were similar for both the as received, and annealed specimens. This was to be expected, since damping capacity in iron is said to recover rapidly at room temperature (97). The effect of evacuating the furnace chamber was to approximately halve the measured damping, due presumably to the removal of air damping effects.

If the specimen was far from the horizontal position the damping was greatly increased, e.g. with the specimen at 45° to the horizontal the damping was increased by about four times. Even at this large angle the natural resonant frequency was unchanged from that obtained with the specimen in the horizontal position.

The damping of the specimen was measured in vacuo at various temperatures during heating. The change in damping with temperature is shown in Fig. 2.6., which represents the average of several reproducible experiments. The maximum damping was observed at about $650^{\circ}C$, and consequently the natural resonant frequency peak was very broad in this temperature region. This form of damping increase with rise in temperature is in accord with the findings of other researchers on steels (94)(98).

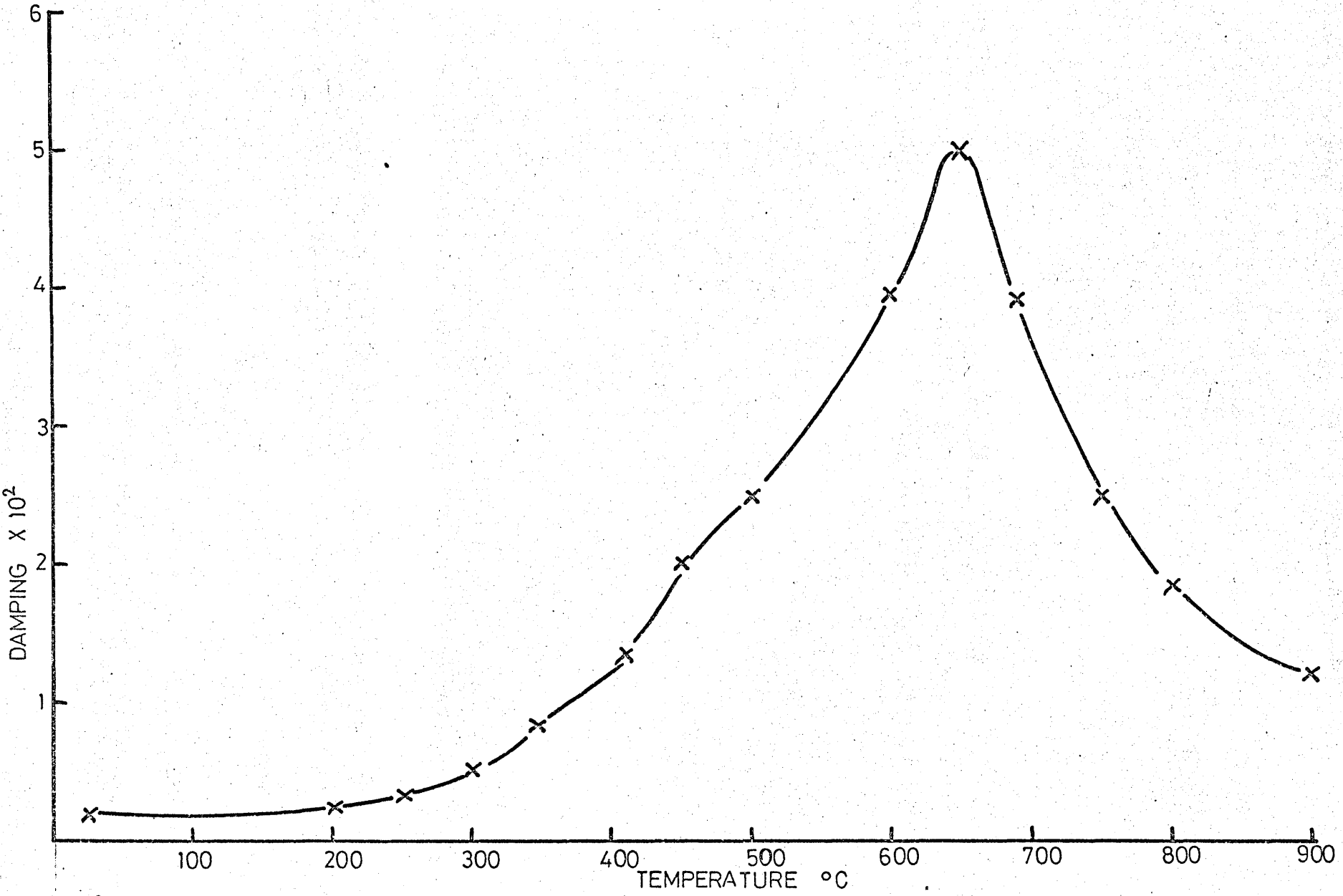

FIG. 2·6 CHANGE IN DAMPING WITH TEMPERATURE

2.1.6. Effects of suspension positions.

The distance between the suspension points on the specimen was effectively fixed, since the furnaces being used had permanently positioned glass tubes for the suspension strings to pass through, Fig. 2.5.. However, both strings could be moved along the specimen while still maintaining the required distance between the suspension points. Experiments were carried out to determine the effects of suspension position on the resonant frequency, and on the specimen damping. Measurements were made of the amplitude of the signal transmitted through the specimen for a given input amplitude, and of the damping, for various suspension positions along the specimen length. Typical results are shown in Fig. 2.7.

The true resonant frequency is obtained when suspension is near the specimen nodes and damping is a minimum (99), and the nodes for a 6" long cylindrical specimen are situated 1·4148" from either end. The nodal position was calculated using the formula 0·2358 L (93).

It was found that the value of resonant frequency measured for the various suspension positions varied by ∓6 cycles, from the true resonant frequency measured near the nodes. However, the amplitude near the nodes is very low, and is zero when suspension is actually at the nodes. Fig. 2.7. shows a maximum amplitude of pickup signal with the drive suspension point at approximately $\frac{3}{4}$" from one end of the specimen, and the resonant frequency measured with this suspension differed from the true reonant frequency by about 1 cycle. This error in measuring resonance is not really a problem since the change of resonant frequency, Δf, is of prime interst in studying oxidation using this method.

There were several distinct advantages in choosing a suspension position that would produce the largest output signal from any given amplitude. Firstly, less amplification of the output signal is required and therefore any electrical interference is also amplified to a smaller extent, giving a clearer signal for monitoring. Also, by increasing the amplitude of the natural resonant frequency in the transverse mode effectively reduces the possibility of exciting other modes of vibration, e.g. torsion, which might otherwise produce secondary resonant peaks.

All tests were therefore carried out using a suspension configuration of the input suspension string positioned $\frac{3}{4}$" from the specimen end, and the pick-up suspension point $2\frac{3}{4}$" away from this first string.

2.1.7. Effect of annealing and vacuum.

The natural resonant frequency of the specimens as

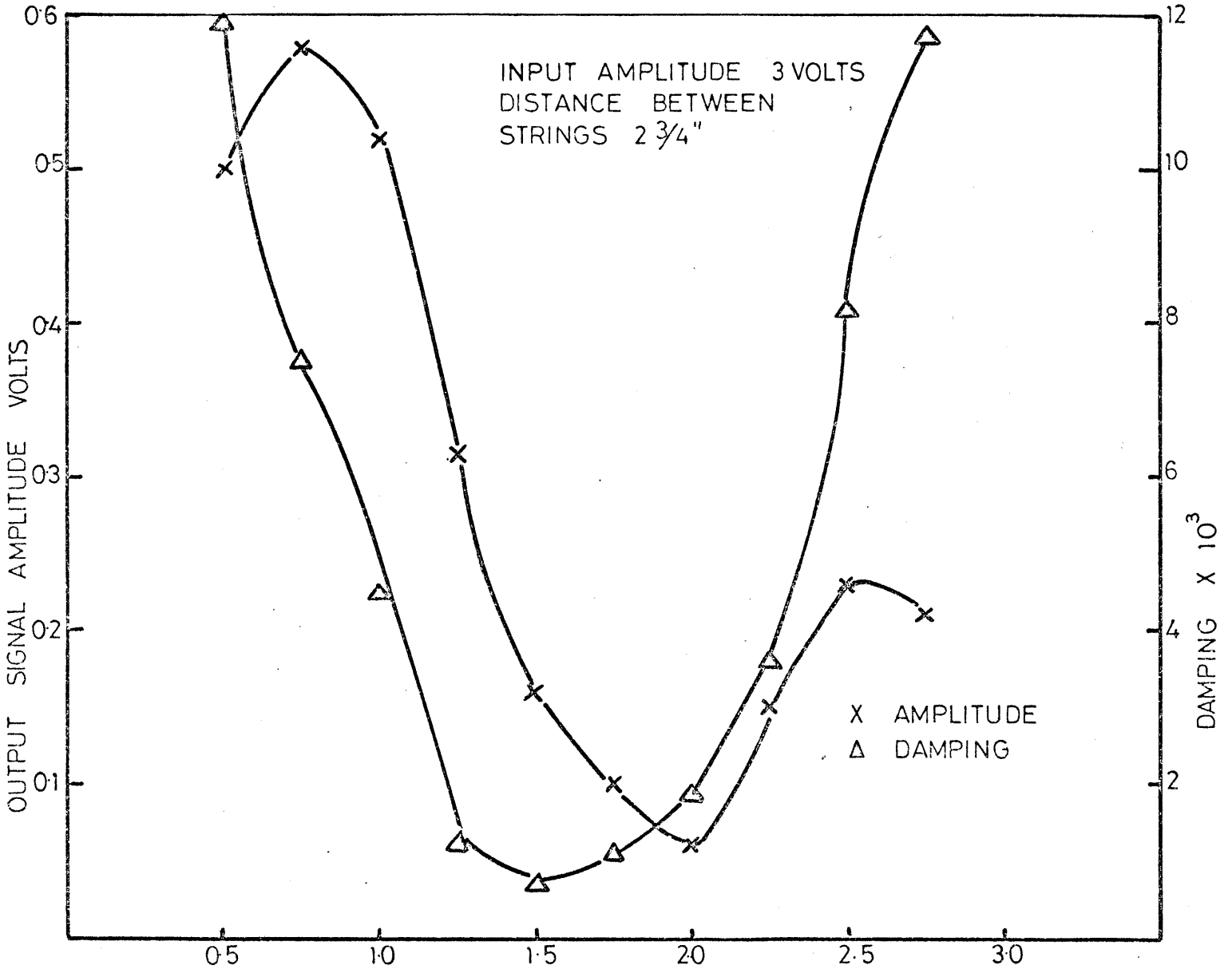

FIG. 2·7 SHOWING EFFECT OF SUSPENSION POSITION ON AMPLITUDE AND DAMPING

received was 997·7 ∓ 2Hz. After vacuum annealing at 950°C for one hour the room temperature natural resonant frequency became 1006·3 ∓ 3Hz. Since modulus is virtually structure insensitive, but varies with crystal orientation, this change must presumably be due to an alteration in any preferred orientation present. These frequency measurements were made in air at room temperature. The effect of evacuating the vibration rig on the natural resonant frequency was to increase it by an average of approximately 2Hz at a vacuum of 1×10^{-4} Torr. The ultimate vacuum attainable in this equipment was of the order of 10^{-6} Torr, and it was found that as long as the vacuum was never allowed to become worse than 8×10^{-5} Torr during heating, no detectable oxide was formed on this steel at temperatures up to 950°C.

No change in resonant frequency or specimen mass was detected on holding an oxidised specimen overnight in vacuum at 750°C, indicating that holding in a vacuum had no effect on the oxide or the metal.

2.1.8. Strains in the specimen due to the imposed vibration.

The form of the transverse mode of vibration is such that the maximum strains in the specimen occur at its centre. The strains at the specimen centre were measured by cementing two 600 Ω strain guages on opposite sides of a specimen and feeding the signals from them to a type PT1200 Phillips direct reading measuring bridge. The three different signal generators that were to be used were all tested in this manner, at a range of output amplitudes up to their maxima. It was found that the maximum strain that could be induced at the specimen centre by any of these signal generators was 6×10^{-5}, and the strain induced with the output at the level normally used was in the order of 1×10^{-5}.

2.1.9. Spurious frequencies.

One of the main experimental problems in operating this equipment was due to the detection of resonant frequencies, other than that of the specimen. These were particularly troublesome at elevated temperatures since the specimen damping increased to an extent such that the amplitude of the specimen at resonance was of a similar order to the amplitude of the other resonant frequencies. The source of at least some of these spurious frequencies was determined, and some attempts were made to reduce or eliminate them.

As has been mentioned previously, with the specimen suspended symmetrically near its nodes and vibrated in a transverse mode, other modes of vibration were also excited. Mounting the specimen assymetrically such that

the amplitude of the transverse mode was increased, largely removed this problem.

If any coupling occured between the two vibrators, other than through the specimen, then strong resonant frequencies could be produced, i.e. from the resonance of the vibrators themselves. Both vibrators were insulated from the support frame work by thick rubber pads, and all electrical connections to them were also well insulated to try to prevent any pick-up through common earth connections.

It was also found that if a specimen was bent, then the resonant frequency was altered and the new amplitude and frequency depended on the orientation of the bend in relationship to the input wave motion, e.g. a 7° bend from the horizontal at the centre of the specimen reduced the resonant frequencies by 3 cycles (approx. 0·3%) if the bend was orientated in the plane of the suspension string, and also by about 3 cycles if the bend was at right angles to the suspension plane, but reducing the amplitude of the output signal by about 5 times. With a 17° bend orientated in the plane of the suspension strings a drop in resonant frequency of about 17 cycles was found with a similar amplitude, with the bend at right angles to the suspension plane two very low amplitude resonant frequencies were found at approximately 20 cycles and 65 cycles below the original straight specimen resonant frequency. For this reason all specimens were checked for flatness before testing and were found to be satisfactorily straight, and were not found to bend during testing, for example by creep.

These measures removed the majority of the spurious resonant frequencies, but some remained for which it hasnot been possible to either identify the source or to suggest a method of elimination. The majority of the remaining frequencies did not alter with time at temperature, or alter substantially with temperature so were presumably some function of resonance of the system. The position of these frequencies were noted for each vibration rig used and were thereafter not considered. Also, the true resonant frequency of the specimen could be accurately predicted for any given temperature so any frequencies outside this range could also be ignored. This left the problems of the very few frequencies that were altered by either temperature or time at constant temperature, and the occasional fixed frequency of a similar value to that of the specimen resonant peak at temperature. These two remaining problems were largely overcome by experience, and by the discarding of the few tests that were in any way made doubtful by these difficulties.

2.1.10. Computer analysis.

Partly as an attempt to eliminate the problems of

spurious frequencies, and partly to investigate the possibility of automating the technique, a method of collecting experimental data on tape and computer analysis of the data was attempted. The method used was by feeding "white noise", in the frequency range either 20 - 20000 Hz or 512 - 1024 Hz to the input vibrator, filtering the output signal with a high band pass filter at 500 Hz, and feeding both signals to a multitrack tape recorder during an otherwise normal heating and oxidation run. The final tape was then fed through a computer which checked for cross correlation between input and output frequencies. Particularly with the smaller frequency range input some strong evidence of correlation was obtained, but more than one frequency showed such correlation. In fact during some of the analyses correlated peaks in multiples of 50 cycles right across the frequency range were detected, suggesting resonant pick-up from some electrical supply circuit. This work looks promising and is continuing, but much more refinement is required before it can usefully be employed.

2.2. Vibration technique results

Initially EN2 specimens were heated in air to temperatures varying from 500° - 900°C and held for various times up to 100 hours. The change in natural resonant frequency during isothermal oxidation was monitored. Some examples of these initial experiments are shown in Fig. 2.8.. From these preliminary experiments, it was clear that at all temperatures below 900°C there were discontinuities in the frequency response, particularly in the early stages. It was decided that the greatest amount of information concerning oxide mechanical properties, cracking, etc., would be obtained if exposure times were limited to 25 hours, since a greater number of specimens could then be tested.

All the specimens subsequently tested were cleaned, vacuum annealed as described previously, then heated in vacuum to the test temperature. Once test temperature had been attained by the specimen, air was admitted, and the change of resonant frequency during oxidation was monitored.

If the test temperature altered during the test, usually to a maximum of 1° or 2°C, then a correction was made to the resonant frequency to allow for this. The correction applied was to determine the change in frequency/°C over the last 50°C of the heating cycle and if the test temperature increased during test a suitable addition was made to the resonant frequency according to the °C rise. Typically the correction was

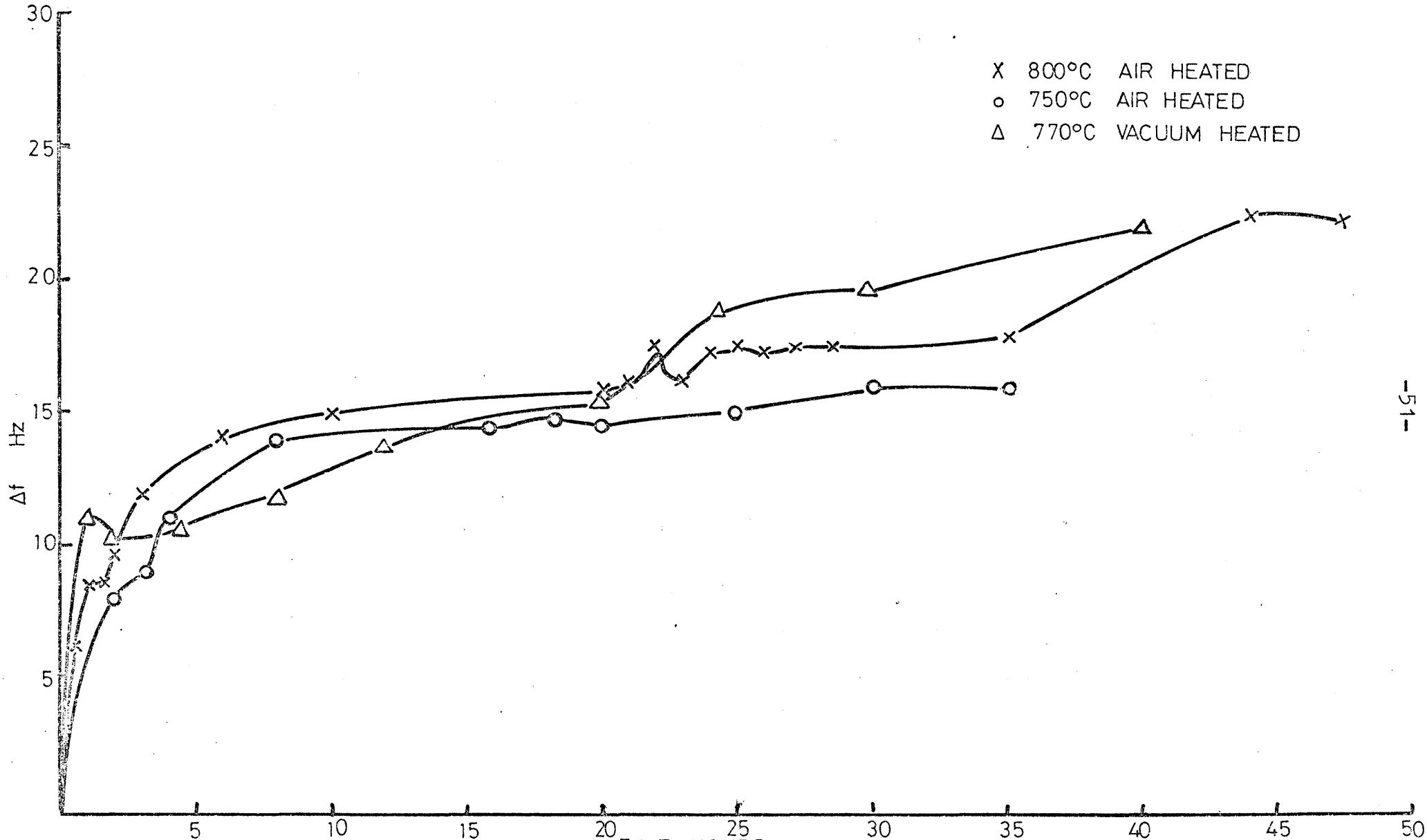

FIG. 2·8 CHANGE IN NATURAL RESONANT FREQUENCY WITH TIME ISOTHERMALLY

of the order of 0·8 - 1 cycle/°C. The only other correction required was in the higher temperature tests in which the rate of frequency change in the initial stages (first 5 - 15 mins.), was too rapid to follow, and the starting frequency was obtained by interpolation.

These measured isothermal changes are plotted against time and shown in Figs. 2.9. - 2.13.

Tests at 600°C, Fig. 2.9., show some degree of discontinuity of change in frequency with time, over approximately the first five hours of oxidation. After that time the curve is reasonably smooth showing no such sudden drops or gains in frequency. These discontinuities in the frequency curve are similar to those reported in the work by Bruce (94), and were thought by him to be due either to decohesion or to cracking of the oxide.

Similar discontinuities in Δ f response were found at 700°C, Fig. 2.10., particularly over the first two hours. The results at 750°C and 800°C are shown in Figs. 2.11. and 2.12..

It can be seen that at these two temperatures the irregularities in the frequency curve continue during the complete oxidation period indicating apparently continuous oxide damage for this period.

At 900°C, Fig. 2.13., the frequency change was much more smooth and uniform. Also the agreement in response between duplicate specimens was much better than at the lower temperatures.

The likely explanation for the behaviour observed at the various temperatures is as follows:-

(a) at 600° and 700°C the first formed film is being subjected to the growth and geomtrical stresses discussed previously, and is being damaged by these stresses because of the limted plasticity of the oxide at these lower temperatures. After a few hours the rate of growth of the oxide slows down considerably, and therefore the rate of stress increase reduces, leading to a reduction in the amount of oxide damage occuring and giving a relatively smooth increase in frequency with time.

(b) at about 800°C the Fe_2O_3 is said to become a stable oxide in the scale (1) and such changes in the scale composition are presumably having a disruptive effect on the oxide formed in the 750° and 800°C tests.

(c) at 900°C the oxide plasticity is presumably high enough, especially now that the scale is largely FeO, to deform under the action of the growth stresses, rather than crack or become non-adherent.

The macroscopic appearance of the oxide scales formed at all the lower test temperatures, indicated blistering in both the longitudinal and transverse direction, the 900°C tests showed largely uniform

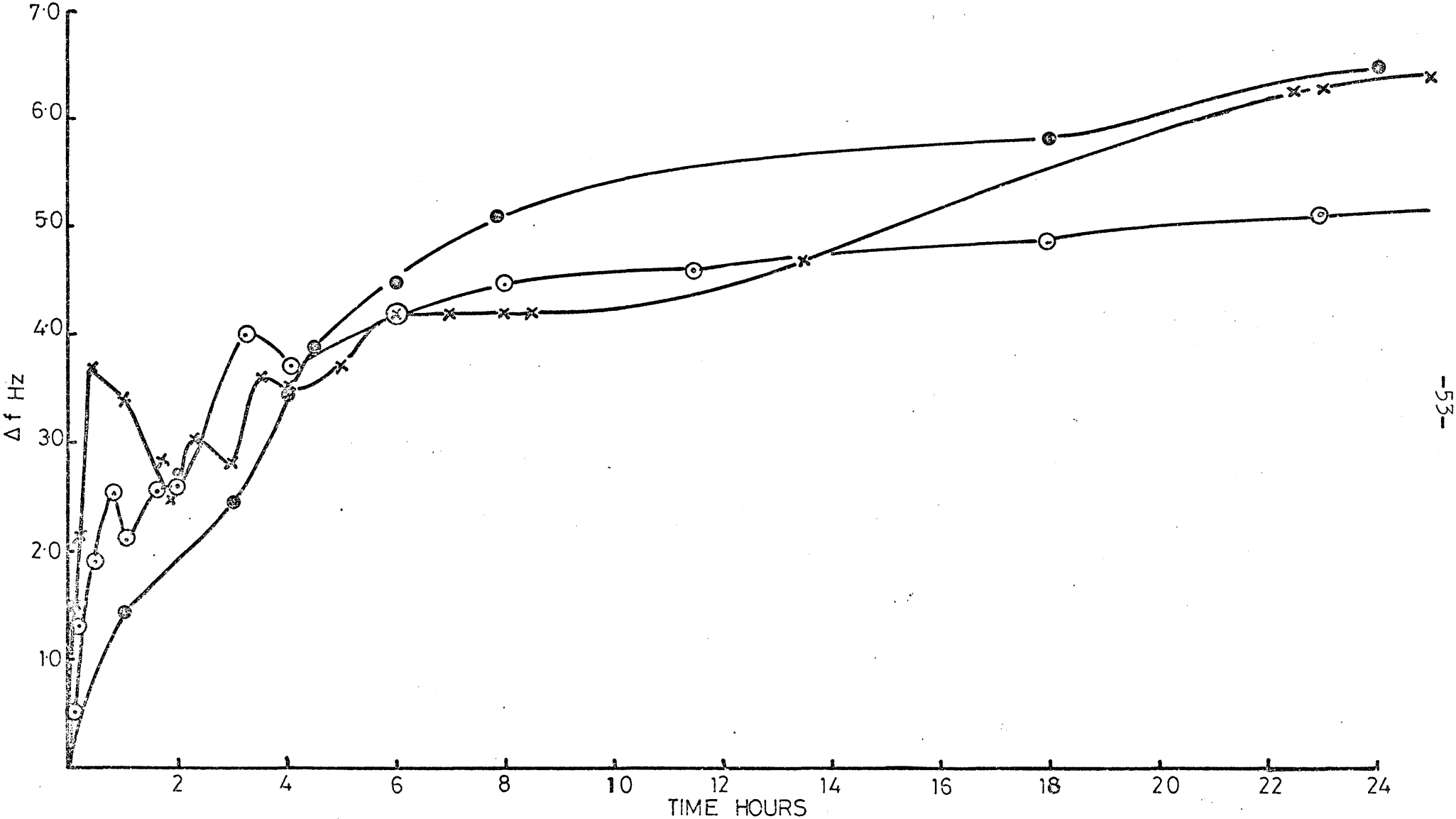

FIG. 2·9. ISOTHERMAL CHANGE IN NATURAL RESONANT FREQUENCY AT 600°C

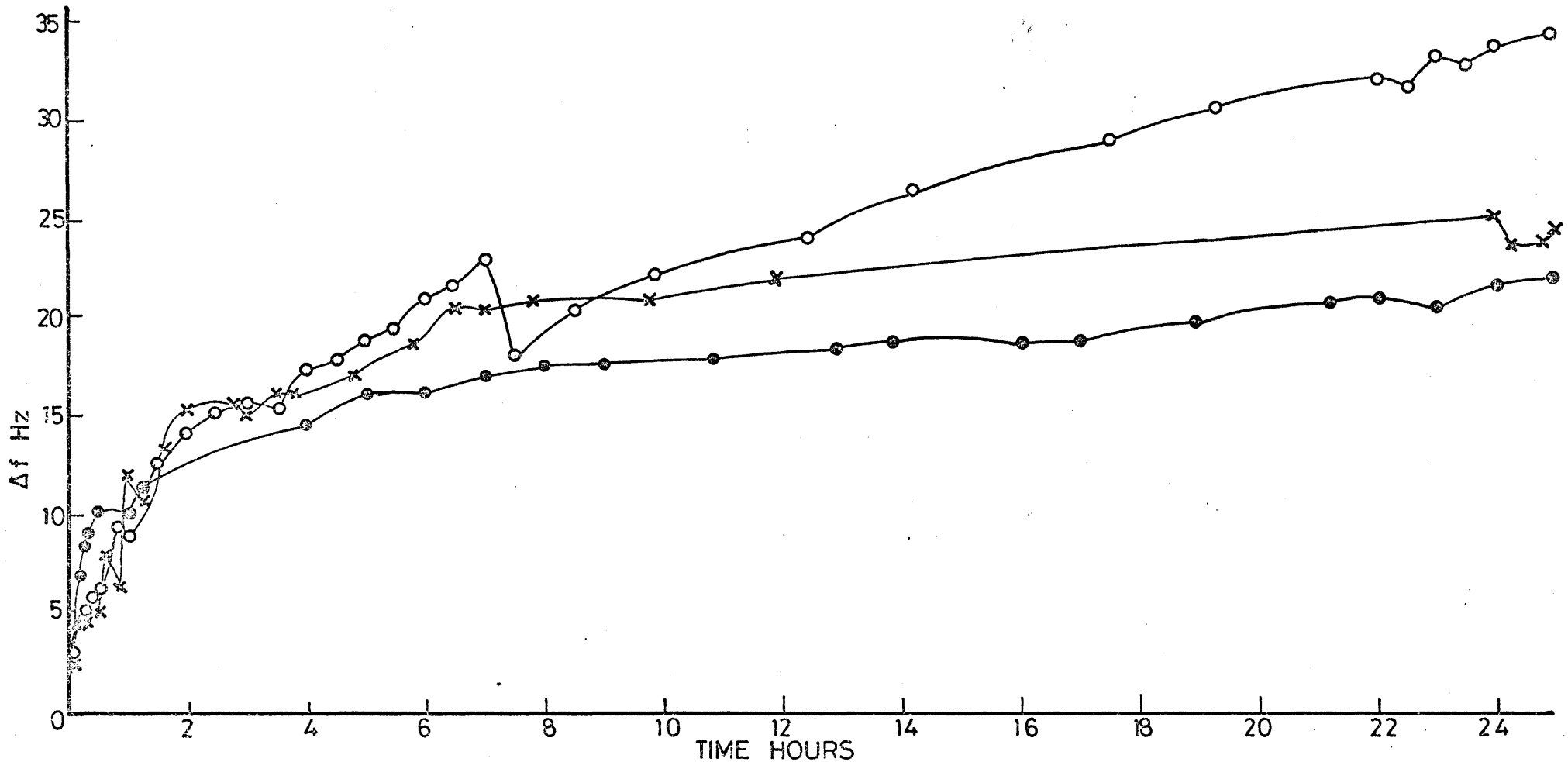

FIG. 2·10 ISOTHERMAL CHANGE IN NATURAL RESONANT FREQUENCY AT 700°C

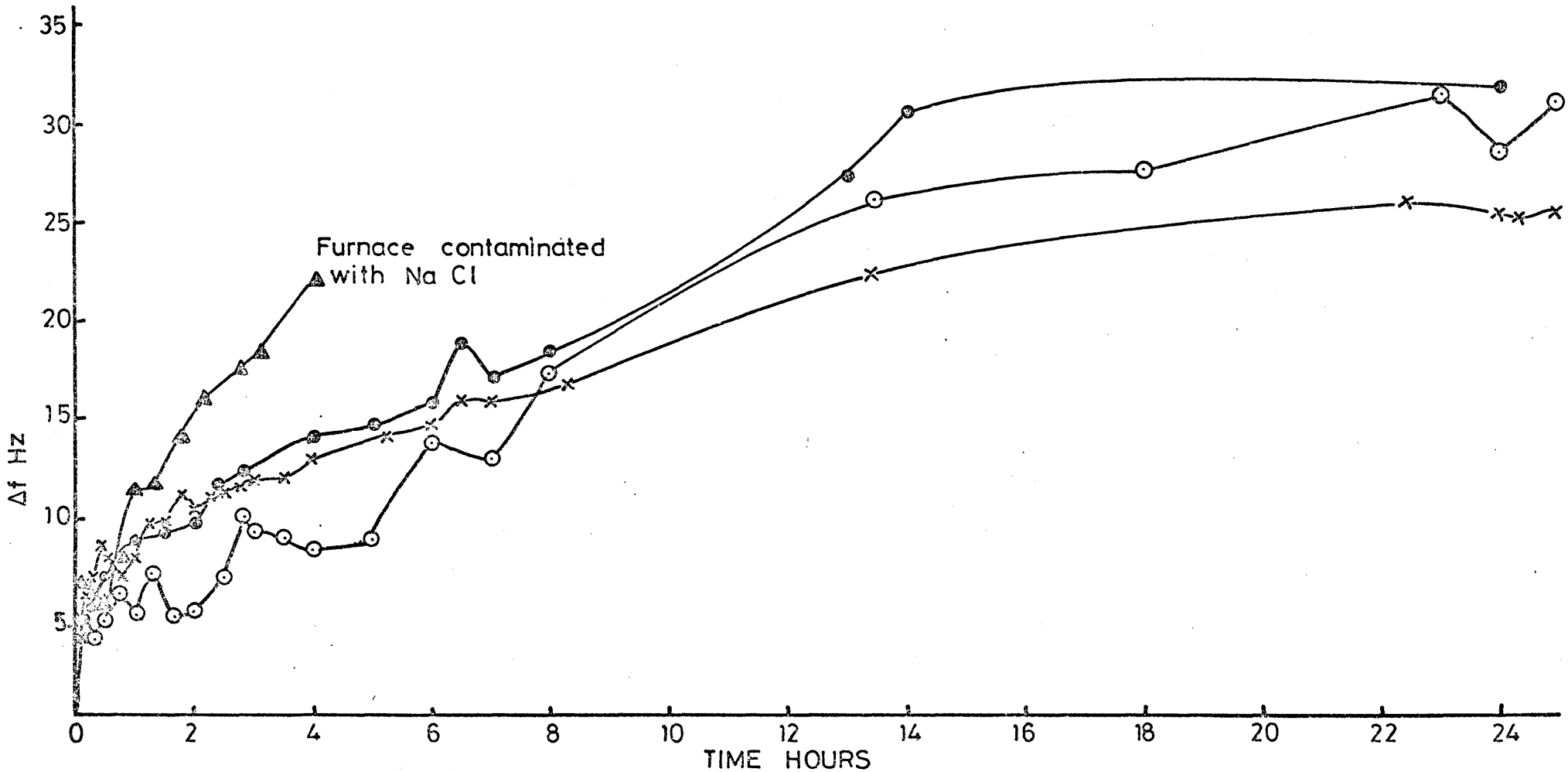

FIG 2.11 ISOTHERMAL CHANGE IN NATURAL RESONANT FREQUENCY AT 750° C

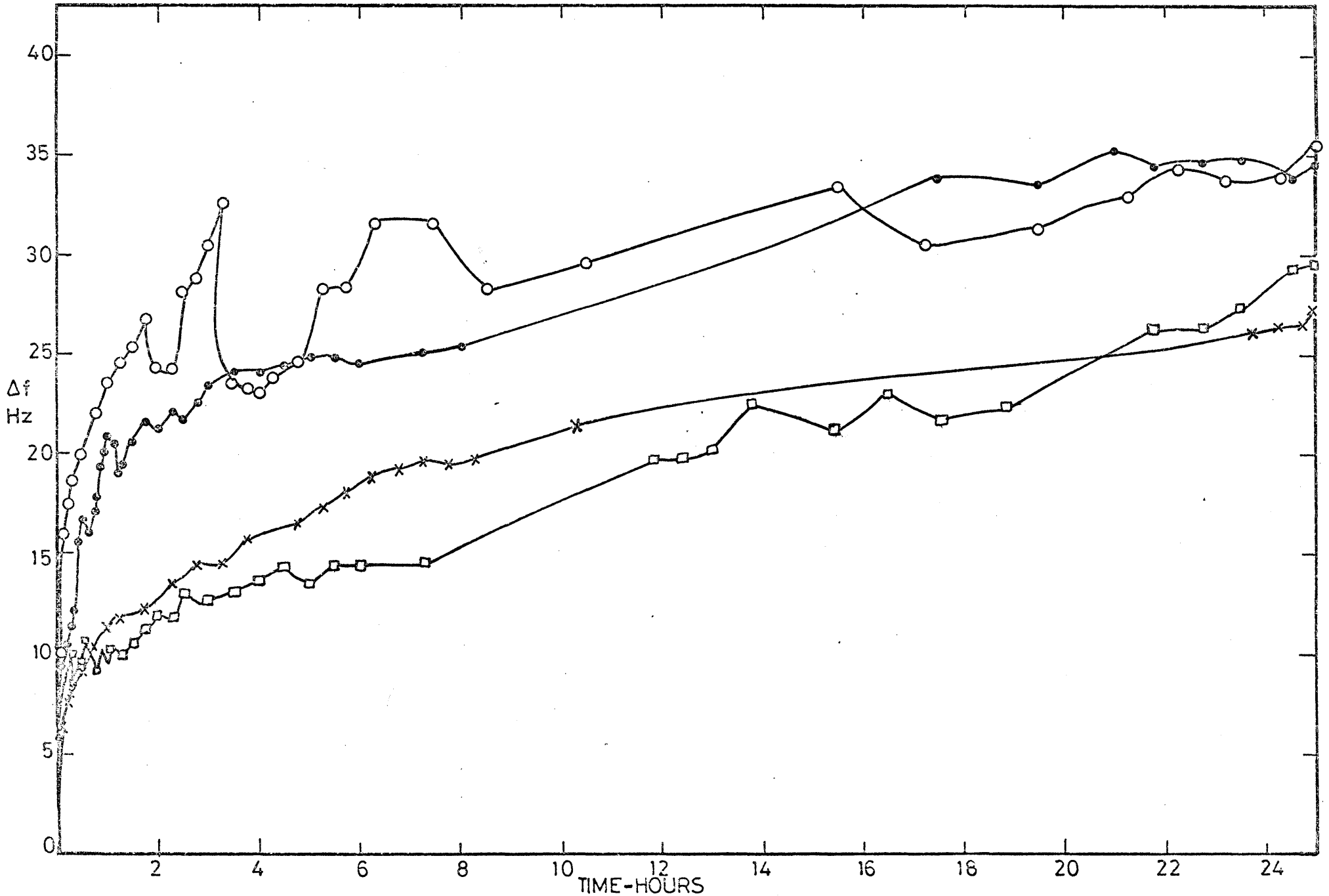

FIG. 2-12 ISOTHERMAL CHANGE IN NATURAL RESONANT FREQUENCY AT 800°C

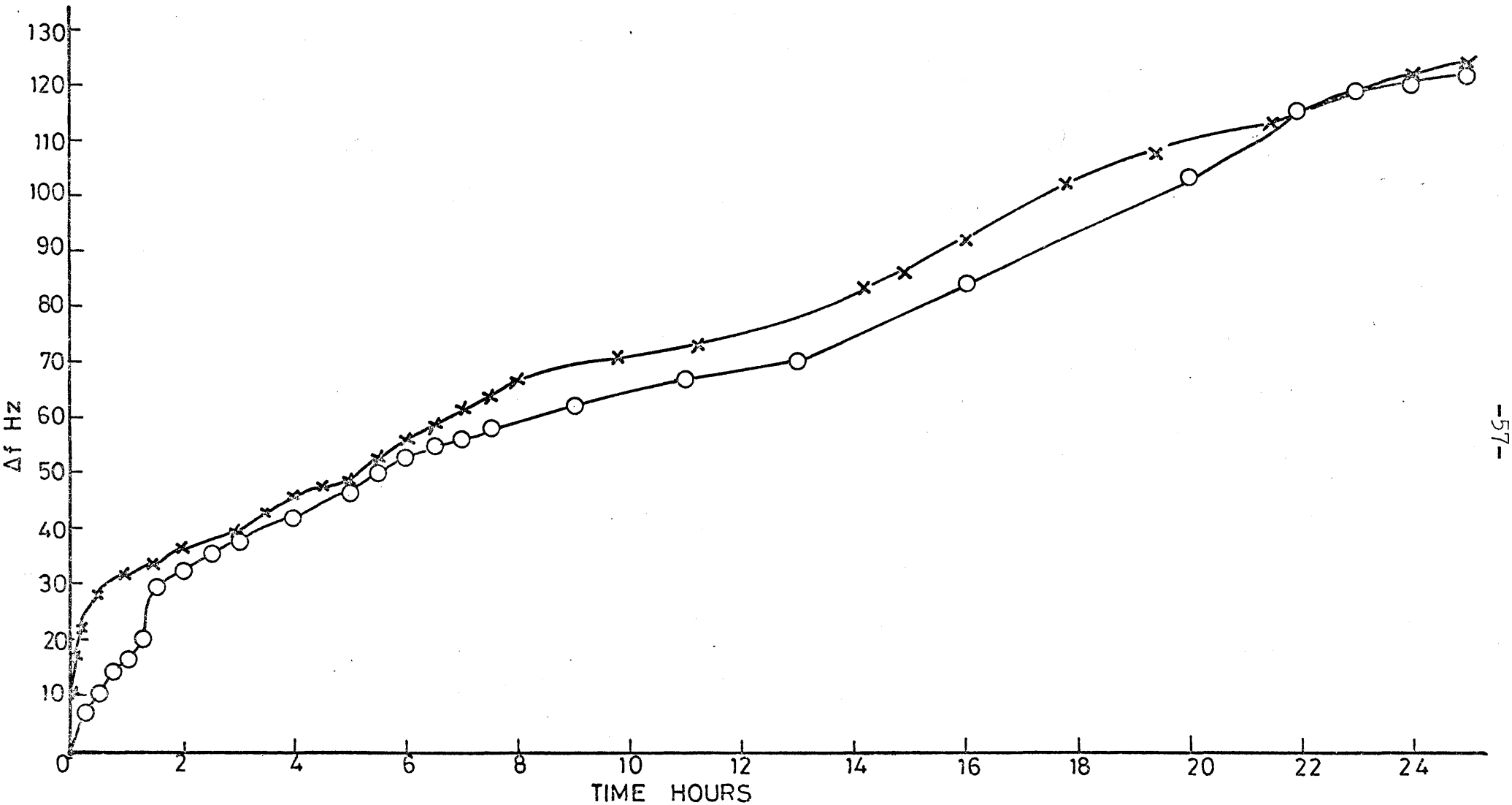

FIG. 2-13 ISOTHERMAL CHANGE IN NATURAL RESONANT FREQUENCY AT 900°C

smooth oxides. However, these specimens were viewed at room temperature and are therefore not necessarily relevant to the isothermal oxidation behaviour. Both the macroscopic and microscopic examination of the oxides at room temperature will be discussed in detail in a later section

2.3. Thermobalance experiments

In order to correlate the natural resonant frequency changes to the kinetics of the oxidation process, mass gains with time over the temperature range of testing were required. These mass gains were determined using two standard Stanton HT-D thermobalances. Preliminary experiments with these thermobalances indicated a tendency for the measured mass to vary with changes in ambient temperature. For this reason all tests were carried out with the thermobalances located in a room whose temperature was controlled at a temperature in excess of the highest ambient temperature, i.e. at 26°C.

The operation of these thermobalances was standard and as described in the manufacturers handbooks, and will not be detailed here. The specimen temperature was measured using a Pt, Pt/Rh thermocouple sited directly beneath the platform supporting the crucible holding the specimen. Buoyancy determinations were made using both an empty crucible and also a crucible containing alumina powder of the same mass as the average specimen used. The procedure used in the determination of the oxidation mass gains was such that the buoyancy correction was not in fact applied, but was merely used to check the accuracy of the method employed. The measured, weighed specimen in the weighed crucible was placed on the balance platform and the mass was matched by weights placed on the balance pan. The thermobalance furnace was heated to the test temperature and allowed to equilibrate, and was then lowered over the specimen. The mass gain record showed an immediate decrease in weight, due to buoyancy, followed by an increase when the crucible and specimen attained test temperature. This change in direction of the mass gain curve was taken as the starting point for the mass gains recorded, and they showed good agreement both with results obtained using bouyancy corrections and with the total mass gain of the specimen determined using a separate analytical balance.

2.3.1. Results.

The same test temperatures were used as in the vibration work, (600°, 700°, 750°, 800° and 900°C), usually for exposure times of at least 25 hours. The specimens used were cut from the 0·2" diameter

centreless ground rods, degreased in trichloroethylene, washed in iso-propyl alcohol, and then usually vacuum annealed at 950°C for one hour, although some specimens were tested in the as received condition. The specimens were measured and weighed before testing, weighed after oxidation, and then preserved for metallographic examination.

The results obtained are shown in Figs. 2.14. to 2.18., which show the range of values obtained at the various temperatures, expressed as mass gain per unit of original surface area, mgm./sq.cm., plotted against time at temperature. Also shown in these figures are results calculated from mass gains in the vibration experiments on the 6" long specimens. Since these results largely fall within the scatter, it shows that the imposed vibration is not radically affecting the rate of oxidation. Most specimens used in the thermobalance were approximately 0·5" long, which was the most suitable size for the mass gain capacity of the thermobalances used. Since any effects of the specimen ends on the oxidation will be more important with shorter specimens, several specimens 1" in length were tested at each of the test temperatures for comparison. All of the results obtained with the longer specimens were within the scatter of the results for the ½" long specimens when expressed as mass gain/unit total original area. Similarly, specimens which were not annealed before testing showed mass gains slightly higher than the average value obtained for annealed specimens for the first one or two hours of oxidation, but the results again fell within the general scatter band. This shows that the non-annealed surface only affected the oxidation rate during the early stages, and became unimportant at longer times.

The irregularity observed in the initial stages of oxidation at 750° and 800°C, Figs. 2.16. and 2.17., may be explained in terms of the changing oxide composition in the region of 800°C (1). These irregularities confirm the results obtained in the vibration work. The effect of the Fe_2O_3 becoming a stable phase in the scale means that transformations are occuring in these early stages, and since the three oxides have different densities and rates of growth, the overall growth rate must be irregular. After a few hours, when the Fe_2O_3 is established as a stable phase, the oxidation may continue at a rate more nearly approximating to the parabolic.

The difference in kinetics at these two temperatures is more clearly shown in Fig. 2.19., where the mass gain data are plotted on a logarithmic basis. If growth was truly parabolic this figure should show a series of straight lines all having a slope of 0·5. the actual slopes of these lines were measured at various

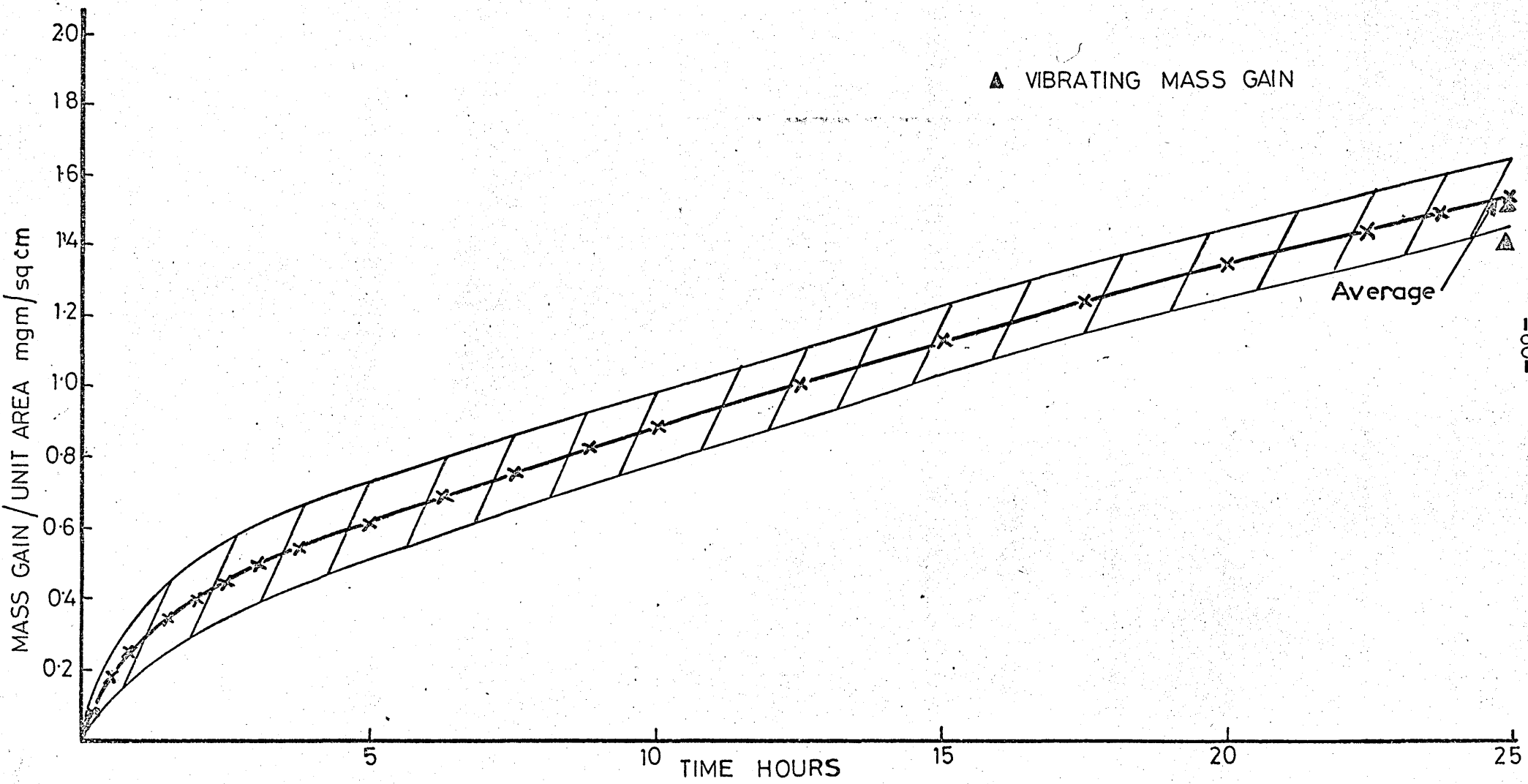

FIG. 2·14 MASS GAIN / UNIT AREA AT 600°C

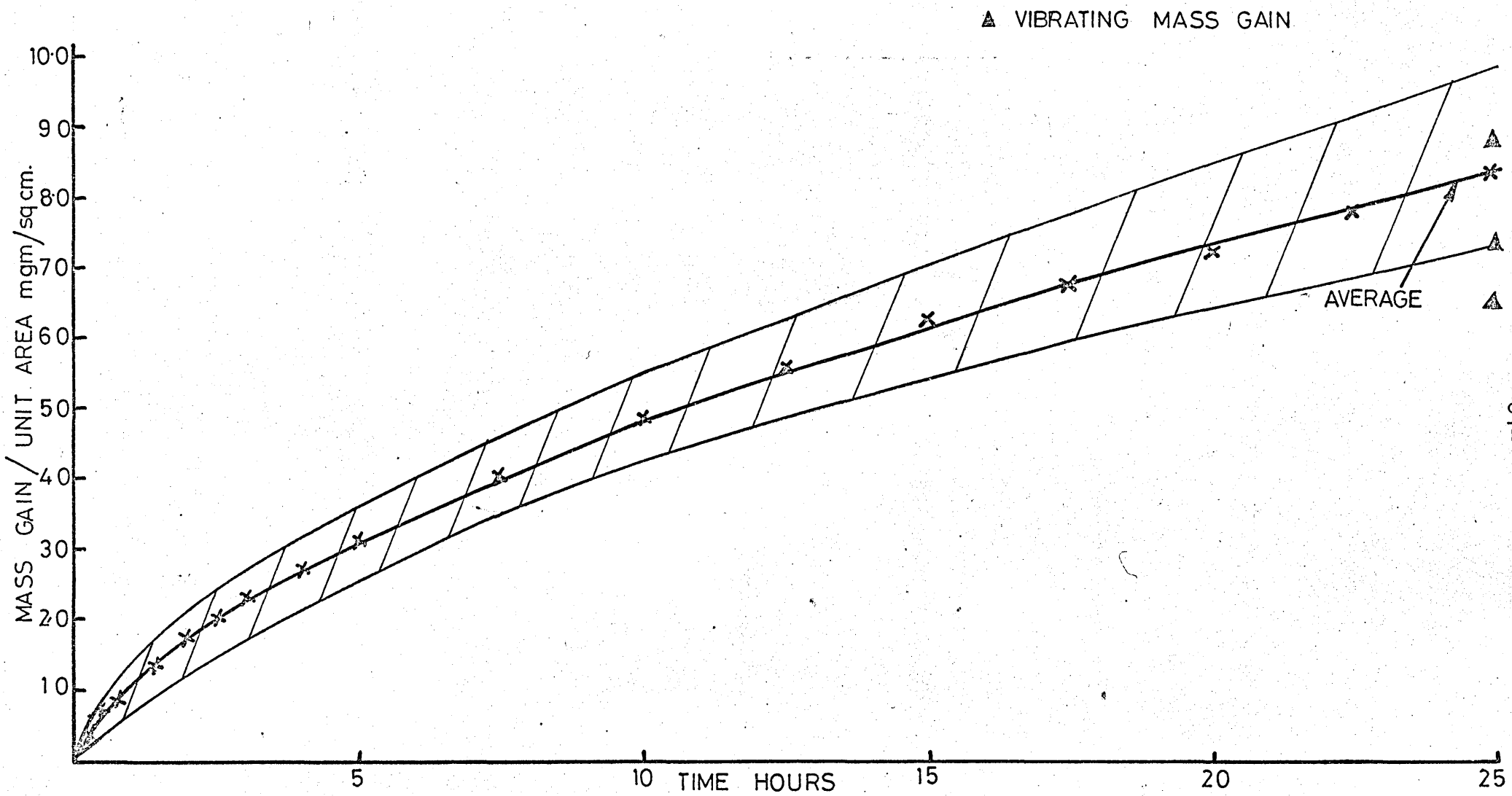

FIG.2-15. MASS GAIN / UNIT AREA AT 700°C

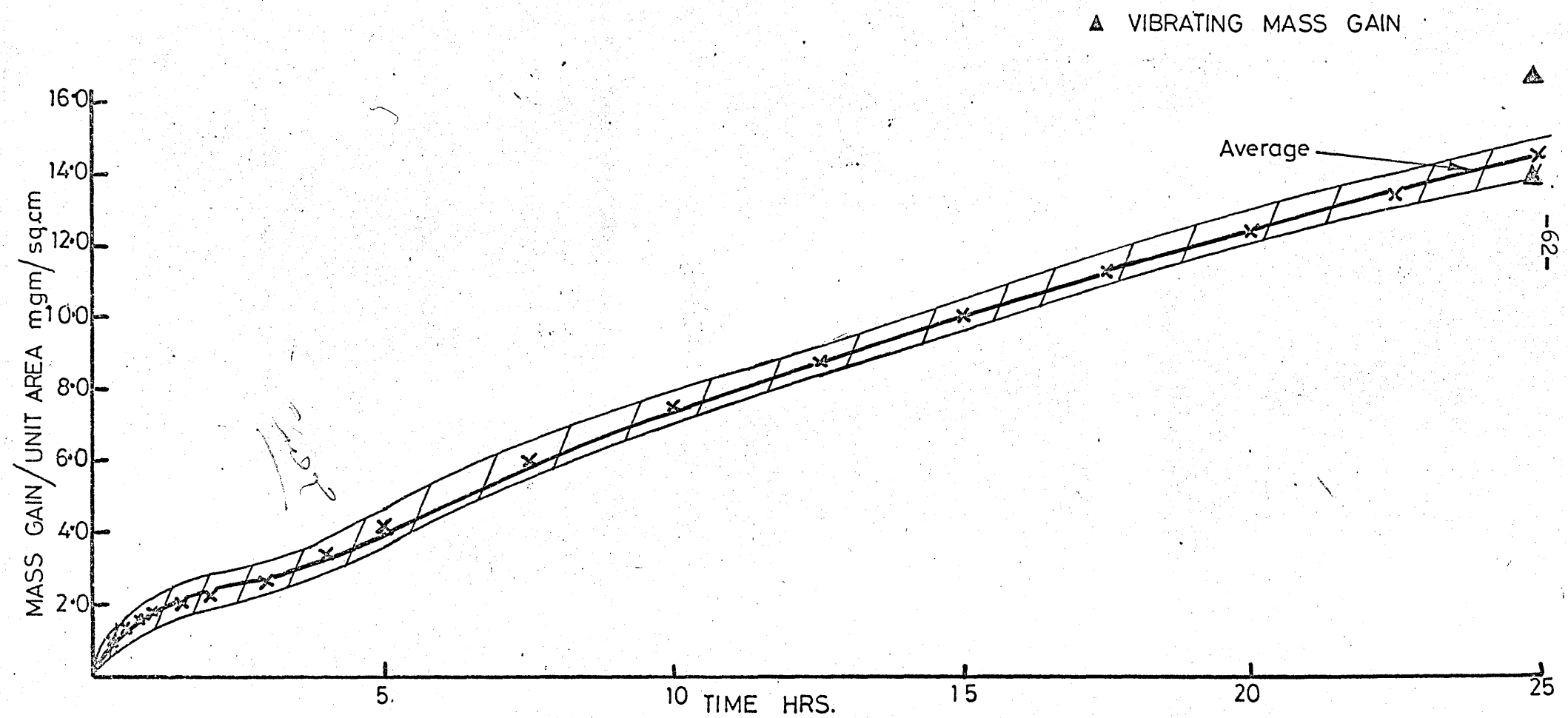

FIG. 2·16 MASS GAIN UNIT AREA AT 750°C

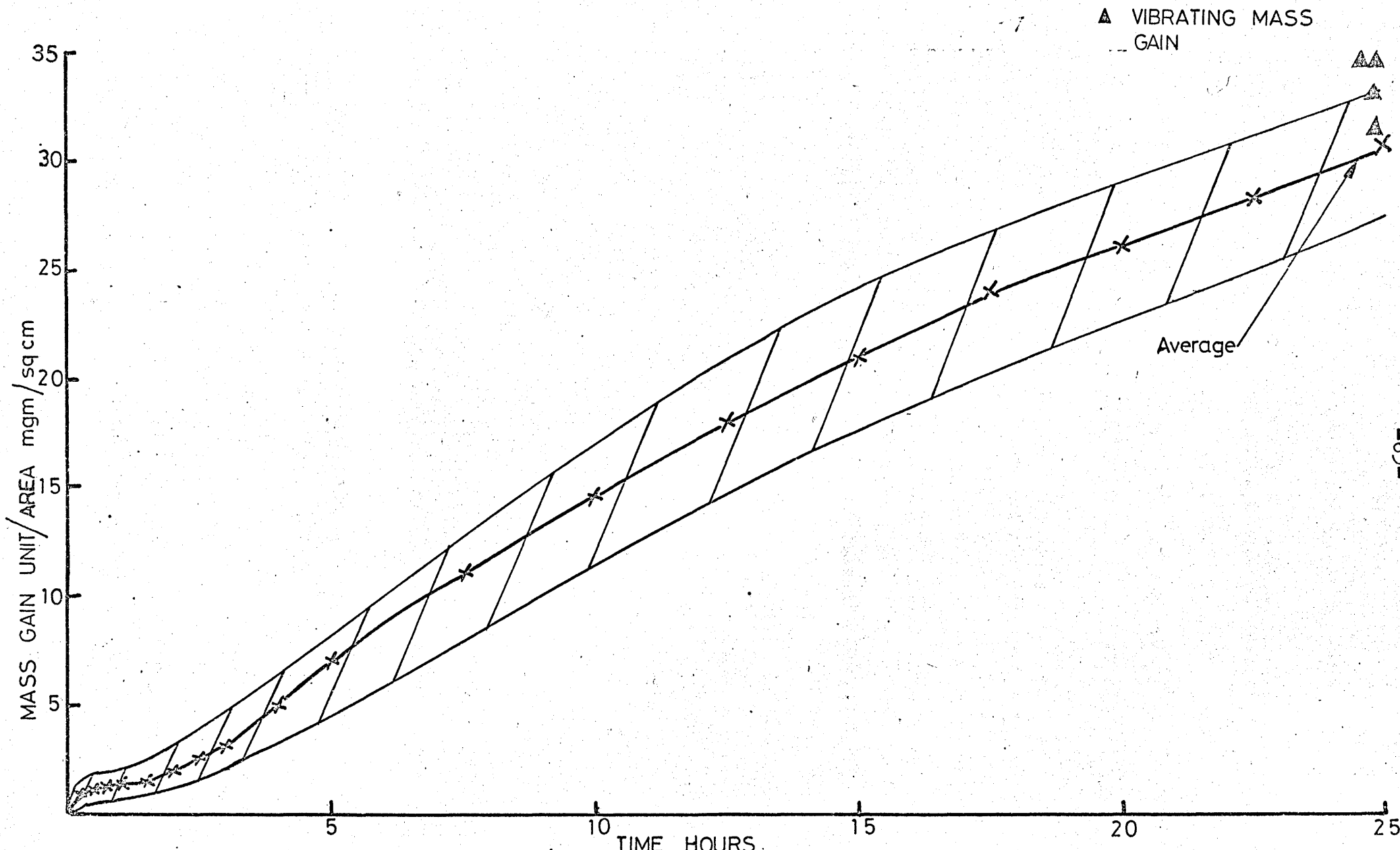

FIG.2-17 MASS GAIN / UNIT AREA AT 800°C

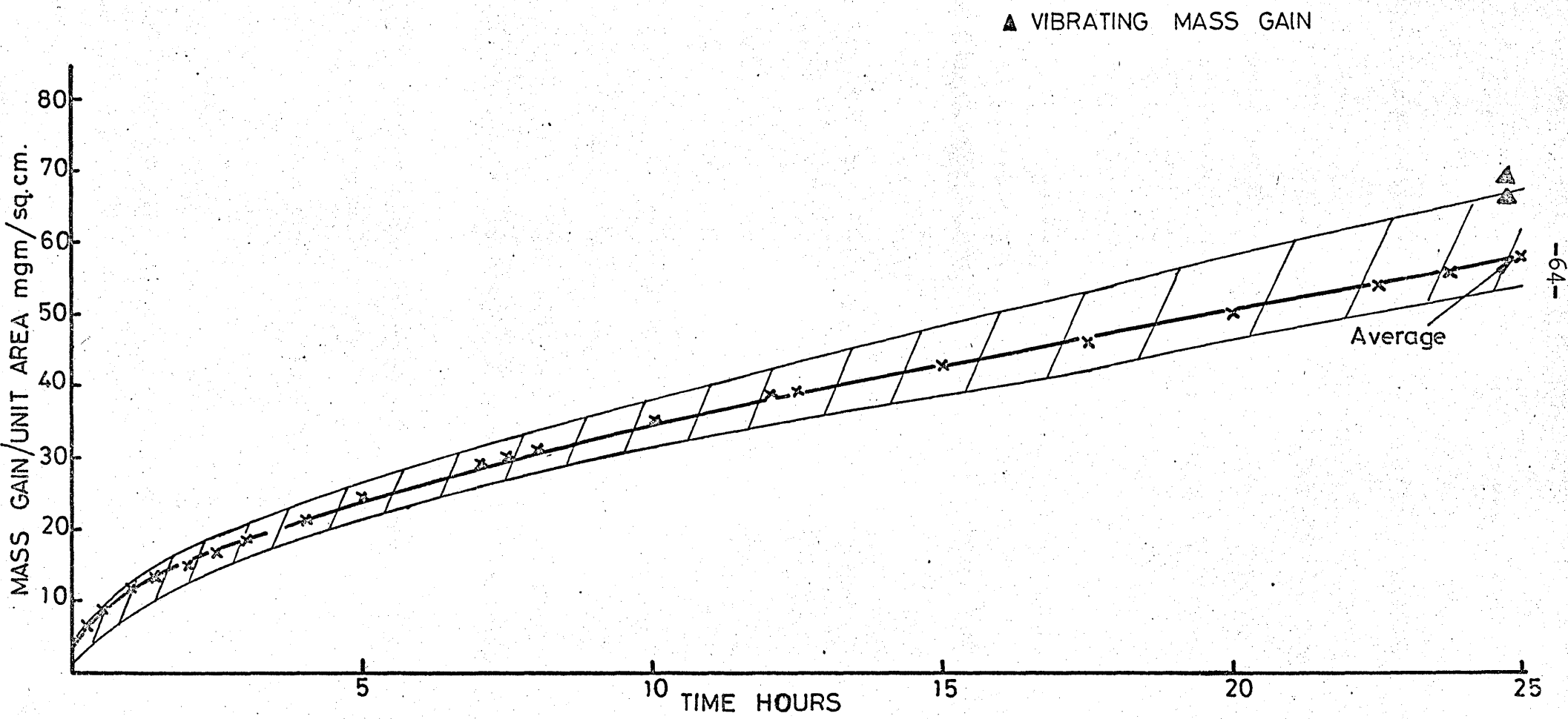

FIG 2·18 MASS GAIN / UNIT AREA AT 900°C

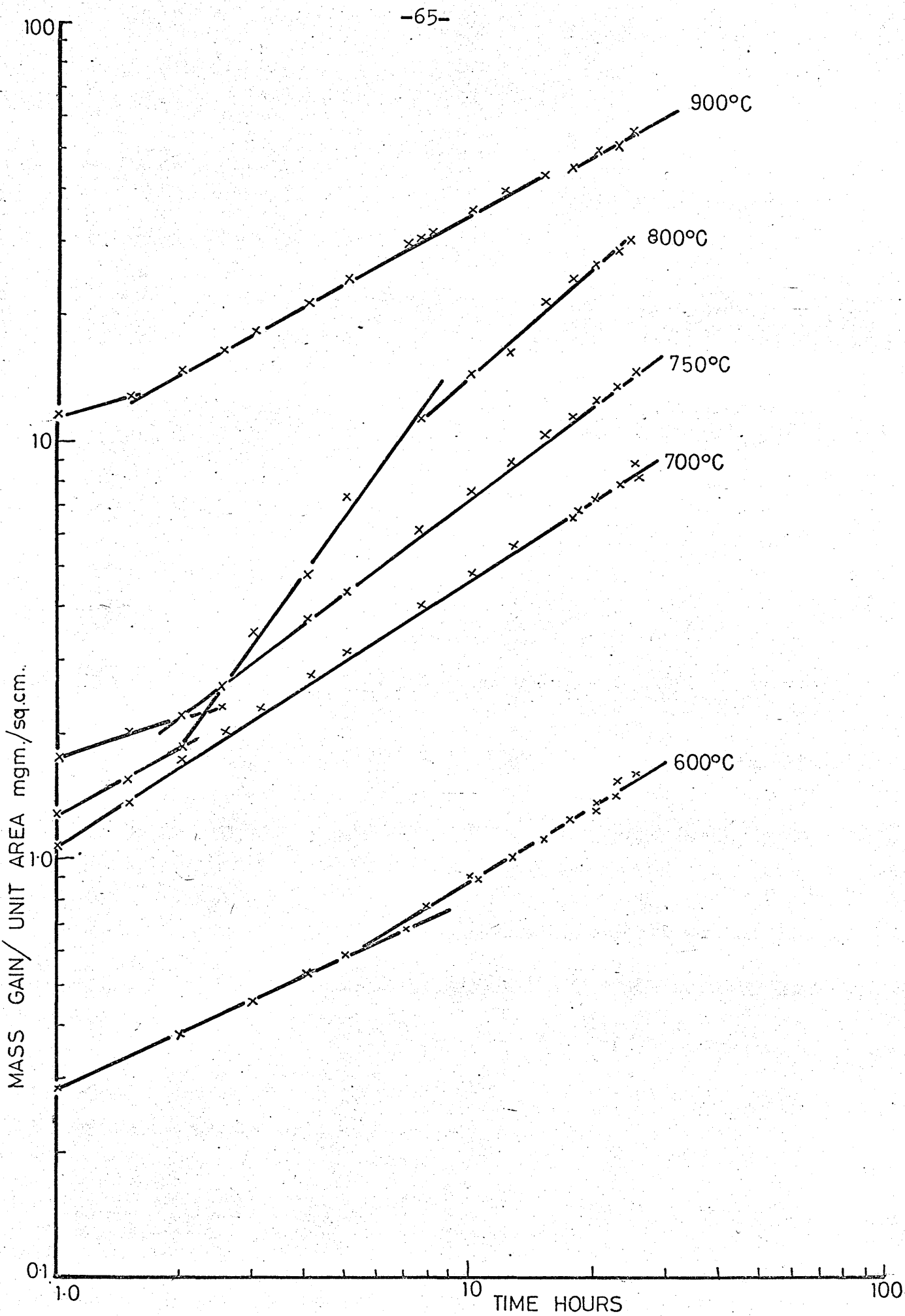

FIG.2-19 AVERAGE MASS GAINS AT VARIOUS TEMPERATURES

oxidation times, and the results are given in Table 3:-

Table 3

Temperature °C	Time interval hours.	Slope mgm./sq.cm. Time
600	1 - 5	0·4375
600	5 - 25	0·625
700	1 - 25	0·625
750	1 - 2·5	0·300
750	2·5 - 25	0·750
800	1 - 2	0·250
800	2 - 7·5	1·375
800	7·5 - 25	0·875
900	1 - 1·5	0·250
900	1·5 - 25	0·500

It may be seen that even neglecting the first hour of oxidation, where growth rate might be expected to be other than parabolic, the agreement with the parabolic law is not particularly good. This is especially so for the 800°C tests where a very steep slope of 1·375 is determined for part of the oxidation. This type of deviation from the ideal parabolic rate law might be expected for a number of reasons, viz:-

(a) The test procedure adopted involves the oxidation of specimens with a rough, ground surface, in air rather than in pure oxygen, and certainly with oxidation occuring before the isothermal temperature is reached i.e. whilst the specimen is heating after the furnace has been placed over it.

(b) The cracking and decohesion that has been shown to occur will have a marked influence on the growth rate, and will generally serve to increase it above the ideal parabolic rate, which is in agreement with the results quoted above.

(c) Since these scales are multilayer, at any given time and temperature the oxide composition and properties are likely to be altering. This will affect the dependance of the rate constant on temperature.

From the data shown in Fig. 2.19., it is possible to calculate the rate constant k for the various test temperatures, and these are shown in Table 4:-

Table 4

Temperature °C	k $gm.^2cm.^{-4}sec.^{-1}$	1/T $10^{-4}\ K^{-1}$
600	$2{\cdot}84 \times 10^{-11}$	11·45
700	$7{\cdot}22 \times 10^{-10}$	10·30
750	$2{\cdot}44 \times 10^{-9}$	9·79
800	$8{\cdot}67 \times 10^{-9}$	9·30
900	$4{\cdot}83 \times 10^{-8}$	8·52

Most kinetic studies are carried out under more stringent conditions of atmosphere, surface finish, etc., so that the values obtained here are not strictly relatable to other results. They do however show quite reasonable agreement with most of the available data, e.g. (1)(4).

The temperature dependance of k may also be used to calculate the activation energy for the process, on the basis of an Arrhenius relationship:-

$$k = A_e^{-Q/RT}$$

A graph of k against 1/T Fig. 2.20. should then have a slope of Q/R where Q is the activation energy. As can be seen in this figure there are not really enough points to definitively identify any inflections in the graph, but it is fairly clear that a major inflection does occur in the region of 800° - 900°C, agreeing with several other researchers (1)(5)(7).

From this graph a value of activation energy of 27·1K. Cals. per mole may be obtained, although it is somewhat speculative as to what this actually means under these test conditions and with a multilayer oxide suffering periodical mechanical damage.

As mentioned in the introduction 1.1., several interpretations have been suggested for an inflection in such cases, e.g. $\alpha - \gamma$ phase change (7), magnetic transformation (7), the presence of Fe_2O_3 as a stable component in the scale (1). With a scale that is suffering periodic damage, particularly at the lower

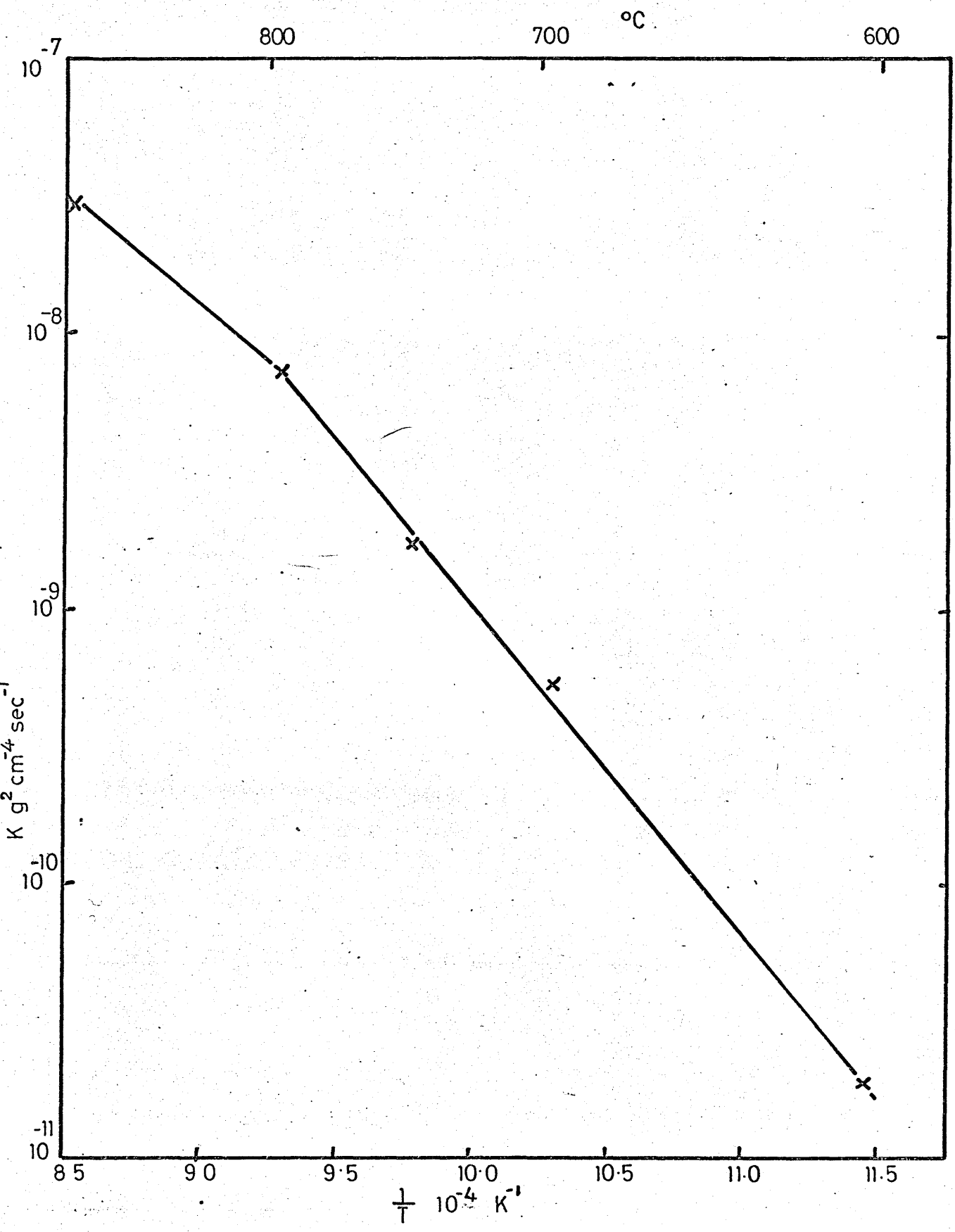

FIG 2·20 CHANGE OF RATE CONSTANT WITH TEMPERATURE

temperatures, a likely explanation might well be that at high temperatures oxide plasticity is sufficient to produce a more stable adherent scale with more regular growth characteristics. The inflection could therefore represent a change from irregular growth, due to oxide damage, to a more uniform oxidation typified by a parabolic relationship. Further speculation along these lines will not be made on the basis of the experimental evidence described, since this work was not undertaken to specifically examine the kinetics of oxidation. It does seem, however, that this examination of kinetics does indicate the important role played by the mechanical condition of the oxide.

2.4. Oxide dynamic modulus

2.4.1. Introduction.

In order to determine the oxide dynamic modulus it was necessary to use some form of the basic frequency equation:-

$$\frac{f^2 - f_o^2}{f_o^2} = \Delta \left[\frac{2\beta M_1}{M_2 - M_1} - \frac{M_2 + M_1}{M_2 - M_1} \right] \qquad (5)$$

Of these terms, $\frac{f^2 - f_o^2}{f_o^2}$ was determined during oxidation, Δ was determined either from weighing the vibration specimen before and after oxidation, or from thermobalance data, and this leaves only the molecular weight terms and the β term to be evaluated.

where $\beta = \frac{E_2 \rho_1 M_2}{E_1 \rho_2 M_1}$ (4)

ρ_1, and M_1, the density and molecular weight of steel are known and the metal modulus has been calculated at the various temperatures from the vibration experiments in vacuo. Therefore, in order to determine the oxide modulus E_2 the oxide density and molecular weight have first to be determined accurately by examination of the oxide since these two quantities obviously have a large effect on the value of oxide modulus calculated.

2.4.2. Metallographic examination of the oxides formed in vibration and thermobalance experiments.

All oxidised specimens from the vibration and

thermobalance experiments were retained and weighed. On some specimens damage to the oxide had occured during unloading and these specimens were not further examined. All other specimens were set in a mixture containing 50% marble flour, and 50% of a 10:1 Araldite mix of resin MY750 and hardener HY951. The specimens in the Araldite mix were then placed in an evacuated chamber for a few minutes, to remove entrapped air bubbles, and then allowed to set. The mounted specimens were then sectioned, usually transversely, and polished in the usual manner for metallographic examination. This procedure proved to be quite adequate for the examination of the surface oxides.

A total of 36 specimens were examined after oxidation and the remaining metal diameter and oxide thickness was measured for each of them, using a calibrated vernier scale on a Reichert microscope. Generally the oxide thickness was not uniform around the circumferance and similarly the final metal diameter was also variable. This was due to the process of oxidation producing detachment of the oxide at various points and this also led to varying amounts of oxide porosity. An example of this non-uniform growth is shown in Fig. 2.21.. A further indication of the random nature of the cracking and decohesion may be seen from Fig. 2.22., which is a section through a specimen, originally 0·2" diameter, which was oxidised to completion in 550 hours at 950°C. This variation of oxide thickness meant that for any given section a great many measurements were necessary (10 - 20 typically, depending on the oxide uniformity) and average values obtained. Several 6" long vibration specimens were mounted and prepared longitudinally and the variation in oxide thickness along the length was measured and found to be typically ± 5%. This longitudinal examination also indicated that the strains induced by the applied vibration were not affecting the oxidation rate, since the maximum amplitude of vibration is at the centre of the specimen, and the oxide in that area was not thicker than the average thickness. This is also confirmed by Figs. 2.14 to 2.18. in which thermobalance mass gains are compared to vibrating mass gains.

At the same time as total oxide thickness was measured, measurement of the thickness of the layers of the three oxides Fe_2O_3, Fe_3O_4 and decomposed FeO were also noted. The relative proportions of these oxides also varied greatly within any specimen due to the cracking and decohesion occuring at temperature or during cooling, so again average values had to be taken. This variability may also be seen in Fig. 2.21..Whether cracking or decohesion occured at temperature or during cooling could be ascertained, since cracking at

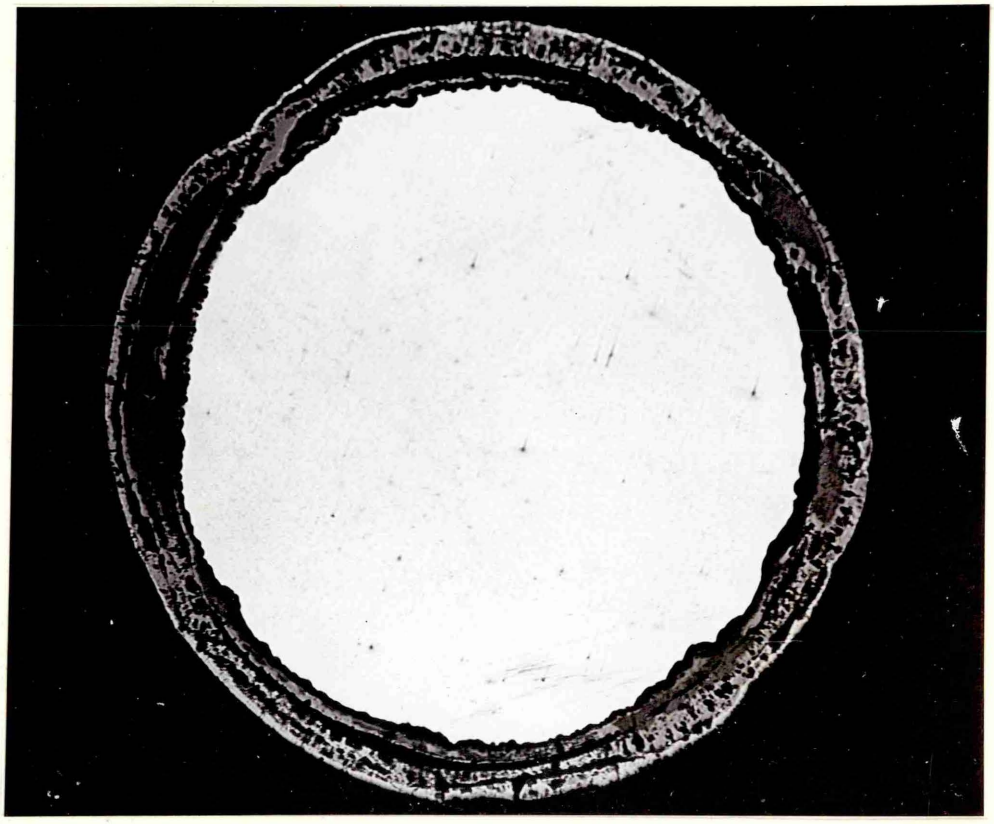

Fig. 2.21. Transverse micrograph of thermobalance specimen oxidised at 900°C for 25 hours (Mag. x 18)

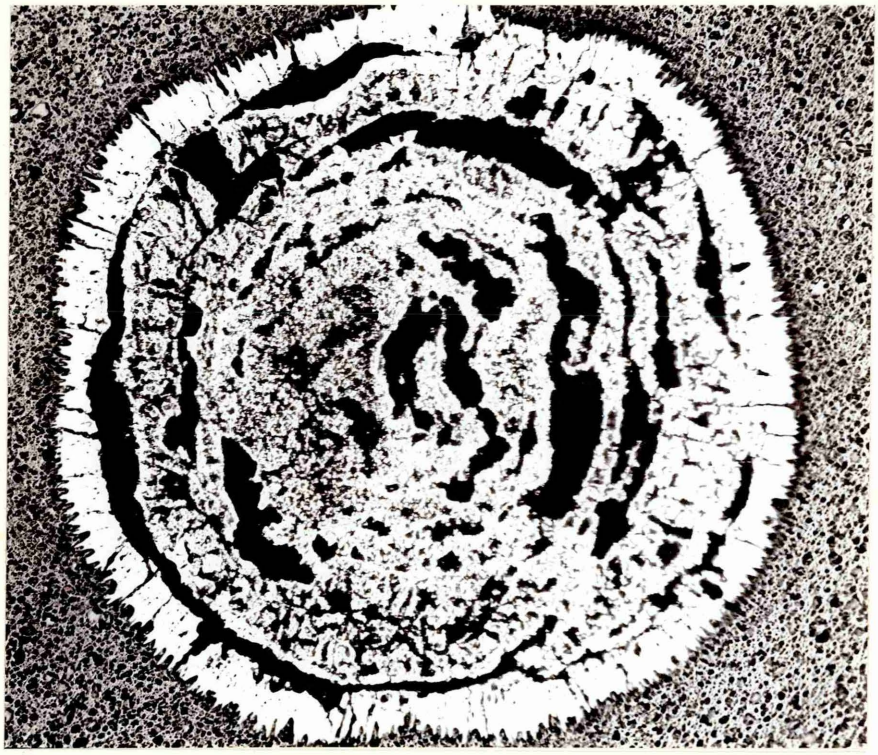

Fig. 2.22. Specimen completely oxidised at 950°C (Mag. x 18)

temperature is accompanied by transformation to the higher oxide in that region, whilst cracking on cooling shows no such transformation. Examination of the areas of oxide that had transformed at temperature did not clearly identify the cause of the irregularities in the frequency response, since although there was much evidence of decohesion occuring at temperature some radial cracking was also identified.

A further attempt at these measurements was made by photographing complete transverse sections of the specimen, enlarging a print of these photographs so that total magnification was of the order of x40, and using a planimeter to determine the areas of oxide and metal present. This technique had the advantage that measurements were effectively made around the whole circumference of the section, and averaging of discrete measurements was not involved. However, it was found that the inaccuracies introduced by the photographic enlarging technique, for example in determining the exact magnification produced, far outweighed any potential gains in accuracy, so this system was not employed.

2.4.3. Oxide density.

From measurements of total oxide thickness and final metal diameter for a specimen of known total weight, the effective oxide density was calculated using the following system.

Original metal diam. = D cm.

Final metal diam. = d cm.

Original metal length = l cm.

Steel density = 7·8 gm./cc.

Total composite wt. = W gms.

If we assume that the specimen length is reduced by the same amount as the diameter is reduced, and that oxide thickness at the specimen ends is the same as the oxide thickness at the diameter then the following calculations may be made:-

$$\text{Wt. of steel remaining } (w_1) = \left(\frac{d}{2}\right)^2 \pi \left[L - (D - d)\right] \times 7{\cdot}8 \text{ gm.}$$

Therefore weight of oxide $W_o = W - W_1$

$$\text{Volume of oxide } V = \left[L - (D - d)\right] \pi \left[\left(\frac{d + 2t}{2}\right)^2 - \left(\frac{d}{2}\right)^2\right] + 2t\pi \left(\frac{d + 2t}{2}\right)^2$$

$$\text{Oxide density} = \frac{W_o}{V} \text{ gm./cc.}$$

This is the effective oxide density, including porosity, cracks, etc., and is the value that should be used for the oxide modulus calculation. The values obtained by this method of calculation are shown in Table 5.

Measurement of oxide density was also attempted using a specific gravity bottle. Weighed large pieces of oxide were first placed in the weighed bottle containing water, and the 'bulk' density was obtained. The oxide was then removed, finely ground, and the procedure repeated to give the 'true' oxide density. This method was unsuccessful in giving suitable effective oxide densities for two reasons. Firstly, the effective density values obtained depended strongly on the size of oxide pieces used, and, secondly with water as the medium the pores and cracks in the oxide pieces were penetrated by the water and high values of density were obtained. Different immersion media were tried, notably mercury, paraffin and glycerol, none of which proved suitable. However, density measurements of the powdered oxide were used as a cross check on the calculated values of oxide molecular weight.

2.4.4. Oxide molecular weight.

The values of oxide molecular weight used in the modulus calculations were calculated from the measurements of the proportions of the three oxides present. The molecular weights of the three oxides are:-

$FeO = 55{\cdot}85 + 16 = 71{\cdot}85$

$Fe_3O_4 = 55{\cdot}85 + (1{\cdot}33 \times 16) = 77{\cdot}13$

$Fe_2O_3 = 55{\cdot}85 + (1{\cdot}5 \times 16) = 79{\cdot}85$

The composite oxide molecular weight was then calculated using:-

$$M_2 = \frac{(71{\cdot}85 \times \%FeO) + (77{\cdot}13 \times \%Fe_3O_4) + (79{\cdot}85 \times \%Fe_2O_3)}{100}$$

Table 5.

Temp °C	Time hours	Actual oxide density gm/cc	% FeO	% Fe_3O_4	% Fe_2O_3	Mol.wt.	Calcd. oxide density gm/cc	% Porosity
600	30·5	2·0	65·0	35·0	nil	73·7	5·518	63·76
"	30·25	-	42·8	39·2	18·0	77·6	5·413	-
"	74·0	2·03	81·6	18·4	nil	72·8	5·604	63·78
"	25·0	2·51	82·6	17·4	nil	72·8	5·610	55·42
700	9·3	-	82·6	17·4	nil	72·8	5·610	-
"	24·75	3·495	74·3	21·8	3·9	74·42	5·569	36·17
"	25·0	4·171	94·0	6·0	nil	72·13	5·669	26·42
"	25·0	2·155	-	-	-	-	-	-
"	25·0	2·455	79·0	16·6	4·4	73·04	5·594	56·11
"	40·25	4·049	93·0	7·0	nil	72·1	5·664	28·51
"	42·9	3·933	68·0	28·4	3·6	73·77	5·536	28·96
"	70·0	4·39	79·2	17·8	3·0	73·18	5·594	21·52
"	71·0	3·59	86·7	13·3	nil	72·5	5·631	36·25
750	65·0	3·351	92·5	7·5	nil	72·2	5·661	40·81
"	51·0	3·743	74·1	21·9	4·0	73·5	5·568	32·78
"	25·0	3·564	78·1	19·4	2·5	73·06	5·588	36·22
"	31·5	3·369	90·4	8·8	0·8	72·36	5·651	40·38
800	29·0	4·141	88·3	8·7	3·0	72·58	5·641	26·59
"	9·9	4·362	93·2	5·7	1·1	72·31	5·665	23·00
"	24·9	5·199	86·8	10·0	3·2	72·64	5·634	7·88
"	25·0	4·68	73·4	21·2	5·4	73·45	5·565	15·90
"	25·0	3·439	72·0	21·2	6·8	73·7	5·559	38·14
"	25·0	3·857	84·0	11·4	4·6	72·9	5·620	31·37
"	25·0	3.98	95·0	5·0	nil	71·96	5·674	29·86
"	42·9	3·59	80·0	13·6	6·4	73·28	5·600	35·89
"	43·5	3·536	93·4	6·6	nil	72·1	5·576	36·59
"	50·0	4·176	70·1	27·3	2·6	73·84	5·546	24·70
900	78·0	4·491	67·0	27·4	5·6	74·12	5·532	18·82
"	7·25	3·604	83·2	14·7	2·1	72·73	5·614	35·80
"	21·5	3·875	82·5	11·2	6·3	73·05	5·613	30·96
"	25·0	3·168	73·0	19·1	7·9	73·7	5·564	43·06
"	25·0	4·396	80·5	17·1	2·4	72·98	5·600	21·50
"	26·25	3·380	74·0	22·2	3·8	73·34	5·567	39·29
"	36·5	4·339	79·0	16·9	4·1	73·08	5·593	22·42
"	75·25	4·353	93·0	5·4	1·6	71·83	5·665	23·16
"	25·0	4·793	80·5	13·0	6·5	73·15	5·603	14·46

The values of the oxide percentages, and the calculated molecular weights are also shown in Table 5. Although the proportions of oxides varies greatly the calculated molecular weights are in quite good agreement with each other, and show no obvious temperature dependence. The average oxide molecular weight from all of these calculated values was 73·11, and this average value was used for the modulus calculations. This figure compares with a value obtained of 70 for molecular weight, using the specific gravity measurements described previously. Samples of powdered oxide were sent for chemical analysis of the iron content, and from these analyses an average value of oxide molecular weight of 75·5 was calculated.

If the oxide composition was the usually quoted one of 95% FeO, 4% Fe_3O_4, 1% Fe_2O_3, (11), with densities of 5·7, 5·18 and 5·24 gm./cc. respectively, then the oxide density would be 5·6 gm./cc.. The calculated values of non-porous oxide are also shown in Table 5. This shows that widely varying oxide composition has little effect upon composite oxide density, whereas the presence of porosity and cracking has a major effect.

Also shown in Table 5 is the calculated percentage porosity in the oxide scales, calculated from the bulk oxide density. These values are apparently very high, (e.g. Bruce (94) quotes 3% porosity in Armco iron), but they are completely consistent with the metallographic examination.

2.4.5. Effective dynamic modulus of the oxide.

The oxide modulus E_2 was calculated in two ways. Firstly, from isothermal thermobalance and vibration data, usually from 25 hour experiments.

$$\frac{f^2 - f_o^2}{f_o^2} = \Delta \left[\frac{2\beta M_1}{M_2 - M_1} - \frac{M_2 + M_1}{M_2 - M_1} \right] \qquad (5)$$

where $\Delta = \dfrac{m - m_o}{m_o}$

Graphs of $\dfrac{f^2 - f_o^2}{f_o^2}$ against average values of Δ

were plotted for temperatures 600 - 900°C and are shown in Figs. 2.23. to 2.27.. The values were calculated for a 6" length from the thermobalance data obtained on shorter specimens by first calculating mass gain/sq.cm.,,

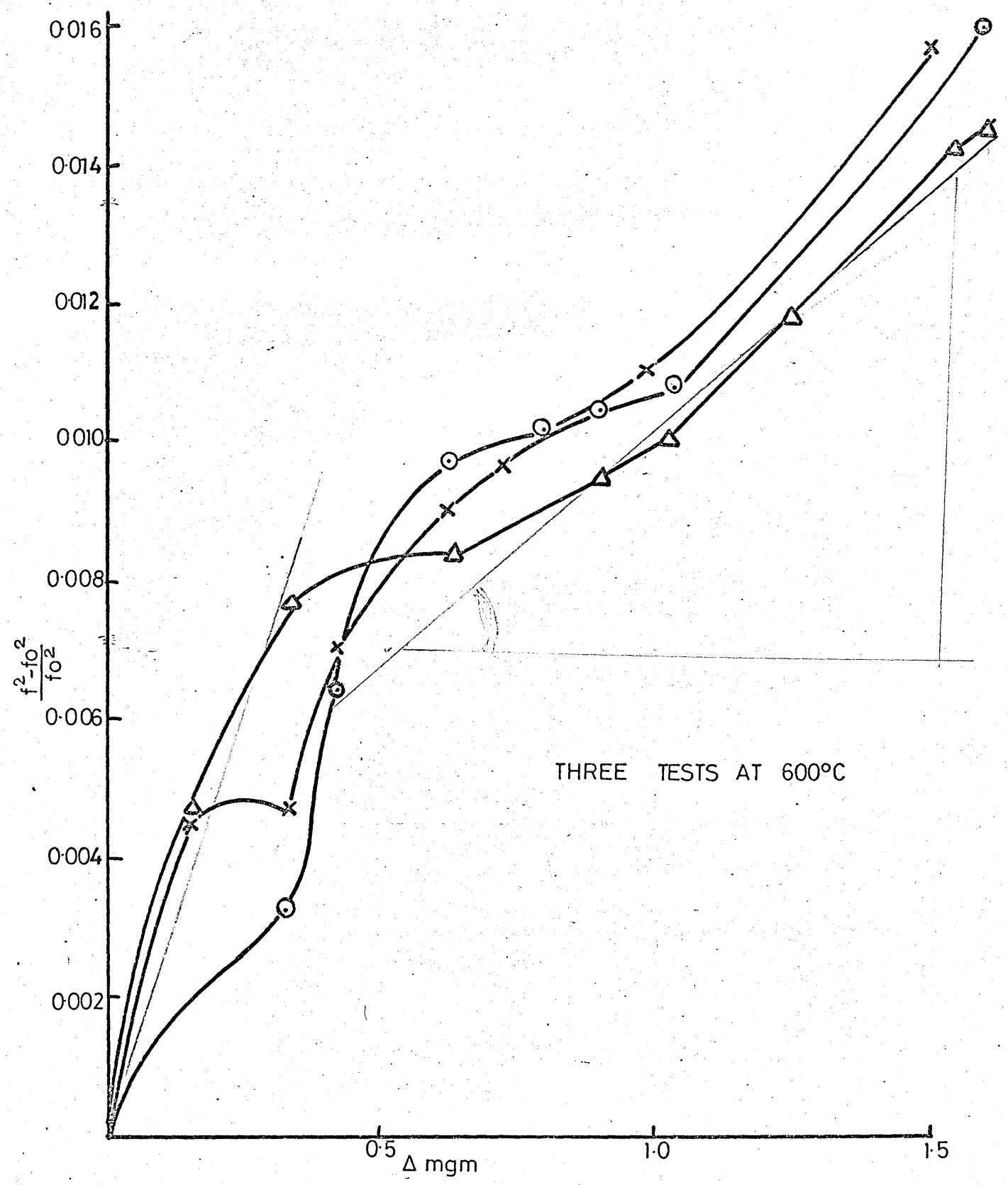

FIG 2·23. RELATIONSHIP OF MASS GAIN TO FREQUENCY CHANGE DURING ISOTHERMAL OXIDATION

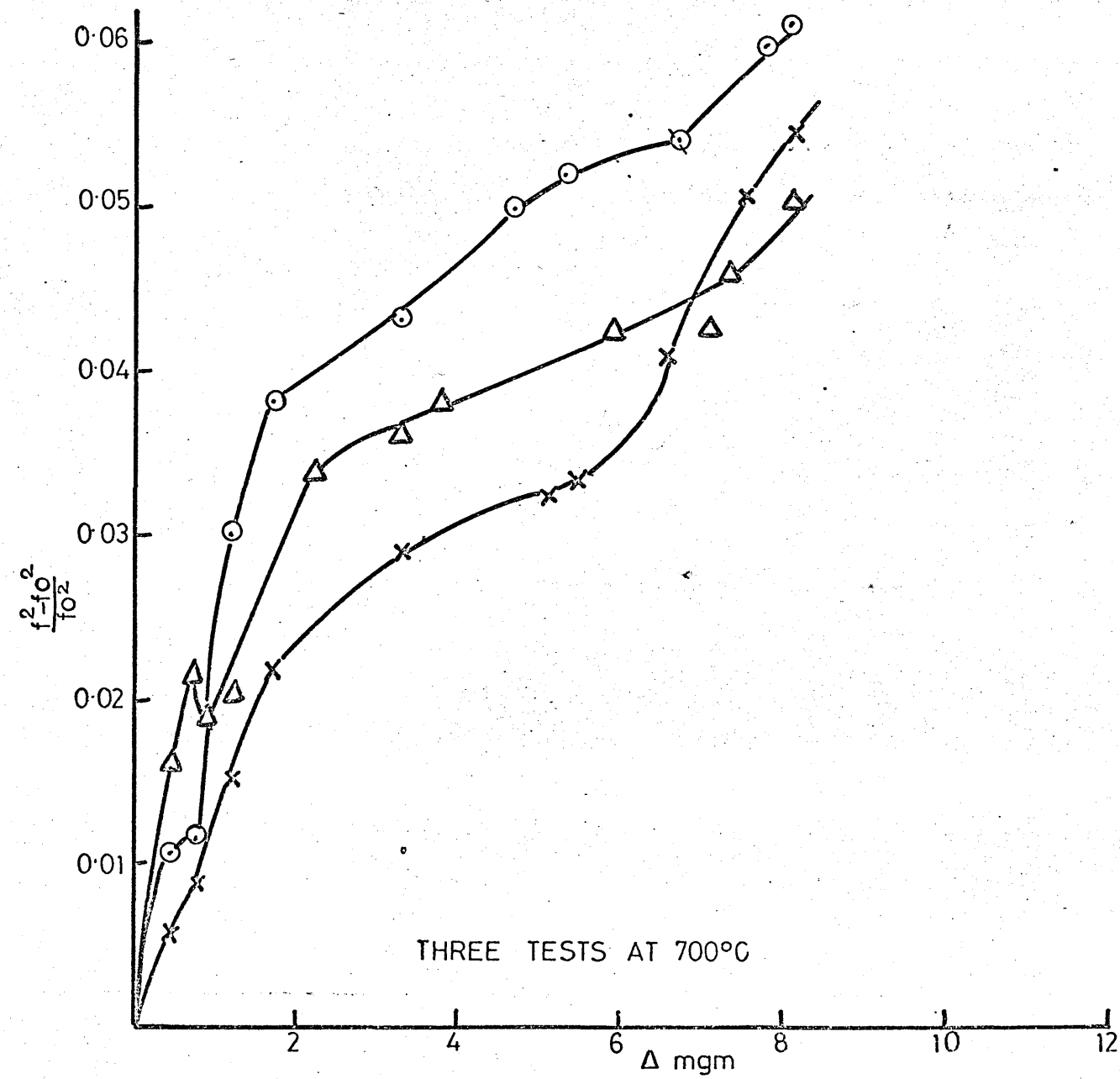

FIG. 2-24 RELATIONSHIP OF MASS GAIN TO FREQUENCY CHANGE DURING ISOTHERMAL OXIDATION

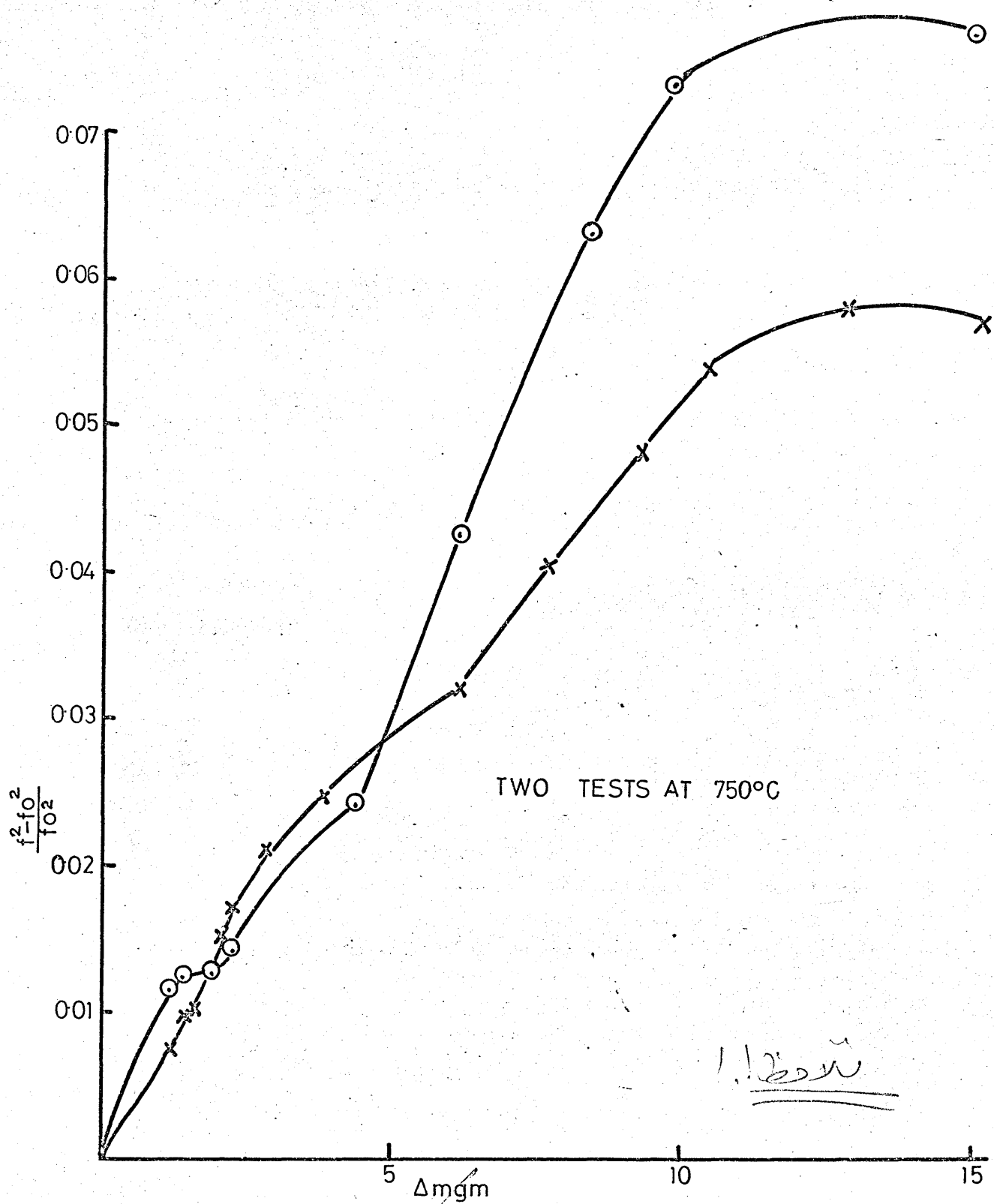

FIG. 2·25 RELATIONSHIP OF MASS GAIN TO FREQUENCY CHANGE DURING ISOTHERMAL OXIDATION

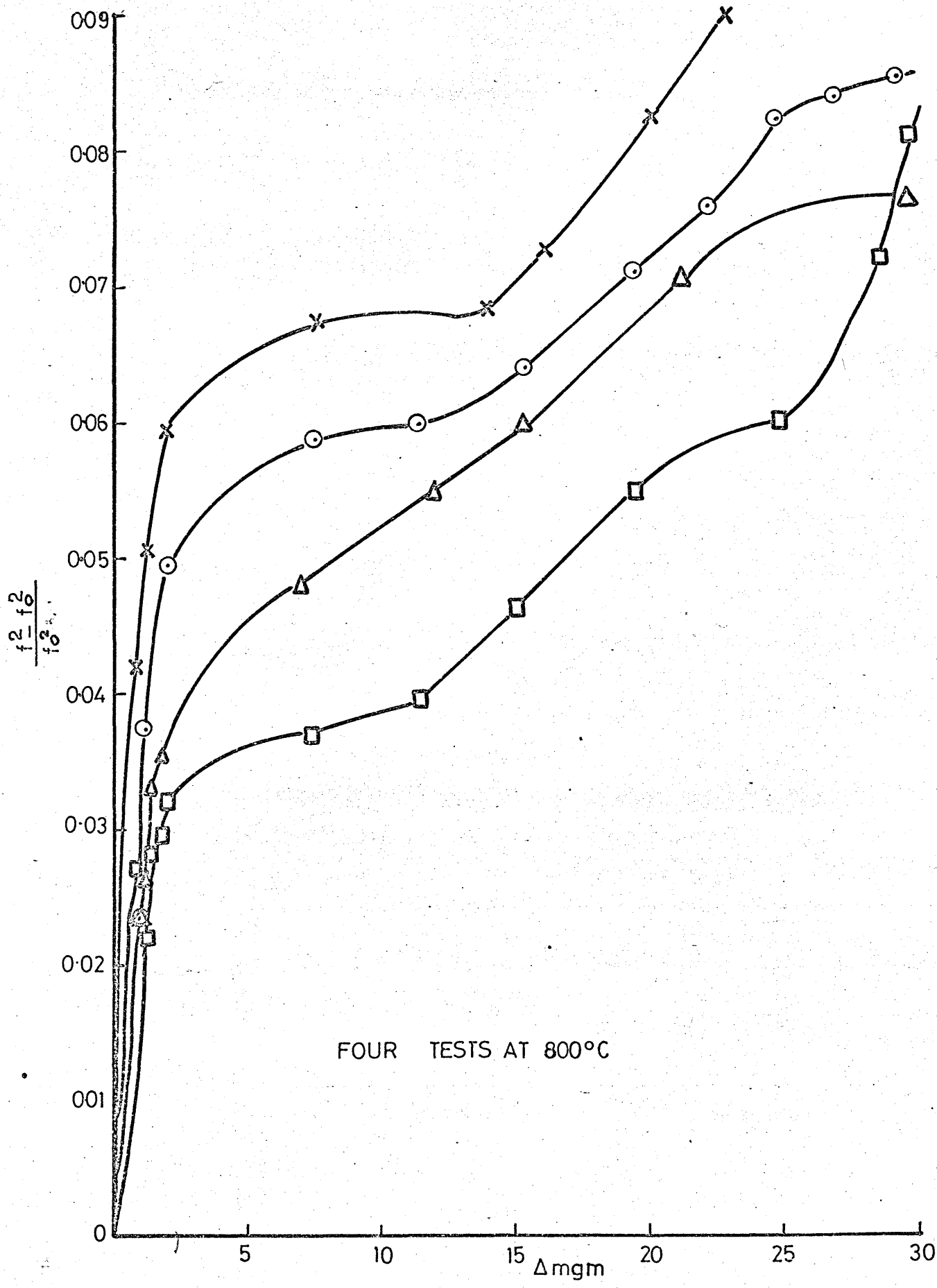

FIG. 2·26. RELATIONSHIP OF MASS GAIN TO FREQUENCY CHANGE DURING ISOTHERMAL OXIDATION

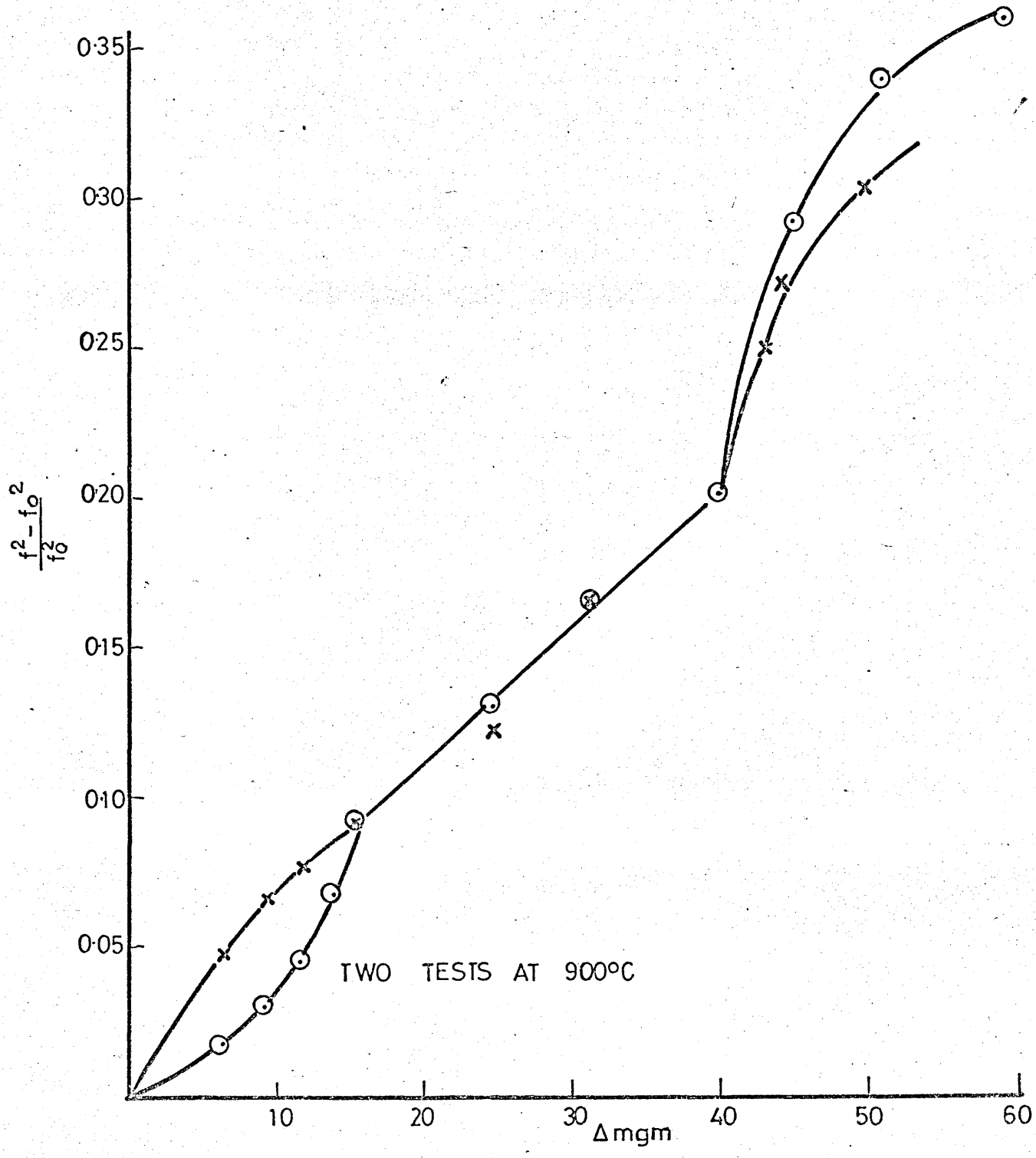

FIG. 2·27 RELATIONSHIP OF MASS GAIN TO FREQUENCY CHANGE DURING ISOTHERMAL OXIDATION

and multiplying by surface area of a 6" long specimen (these predicted Δ values for 6" specimens agreed fairly well with values from vibration experiments). The gradient of these graphs, in the region where reasonably uniform oxide growth was occuring, was measured and is equal to :-

$$\left[\frac{2\beta M_1}{M_2 - M_1} - \frac{M_2 + M_1}{M_2 - M_1}\right]$$

Taking values of $M_1 = 55{\cdot}85$ gm.

$M_2 = 73{\cdot}11$ gm.

This may be reduced to:-

$$\beta = (g + 7{\cdot}474) \times 0{\cdot}1545$$

Where g = gradient of the graph

$$\text{Therefore } \frac{E_2 \, \rho_1 \, M_2}{E_1 \, \rho_2 \, M_1} = (g + 7{\cdot}474) \times 0{\cdot}1545$$

Taking $\rho_1 = 7{\cdot}8$ gm./cc.

$$\text{Then } E_2 = (g + 7{\cdot}474) \times 0{\cdot}1545 \times E_1 \, \rho_2 \times 0{\cdot}0978 \times 10^6 \text{psi}$$

Where E_1 and ρ_2 are the metal modulus at the test temperature, and the oxide density respectively for the relevant test. In tests for which the actual oxide density value was not available, the average oxide density for the relevant time and temperature was used. The metal modulus at temperature was calculated from frequency measurements during heating and cooling of steel specimens in vacuum The modulus was then calculated using the formula:-

$$f_o^2 = \frac{(4{\cdot}73)^4 \, E \, a^4}{16 \pi \, l^3 \, m_o} \qquad (1)$$

Specimen length l was calculated at the relevant temperatures using the coefficient of thermal expansion. Typical values of modulus at temperatures up to 950°C are shown in Fig. 2.28..

The second method of calculating oxide modulus was by using frequency data taken from the heating and cooling cycles and the weights before and after the vibration experiment.

At any given temperature $\left(\frac{f^2 - f_o^2}{f_o^2}\right) / \Delta$ could be

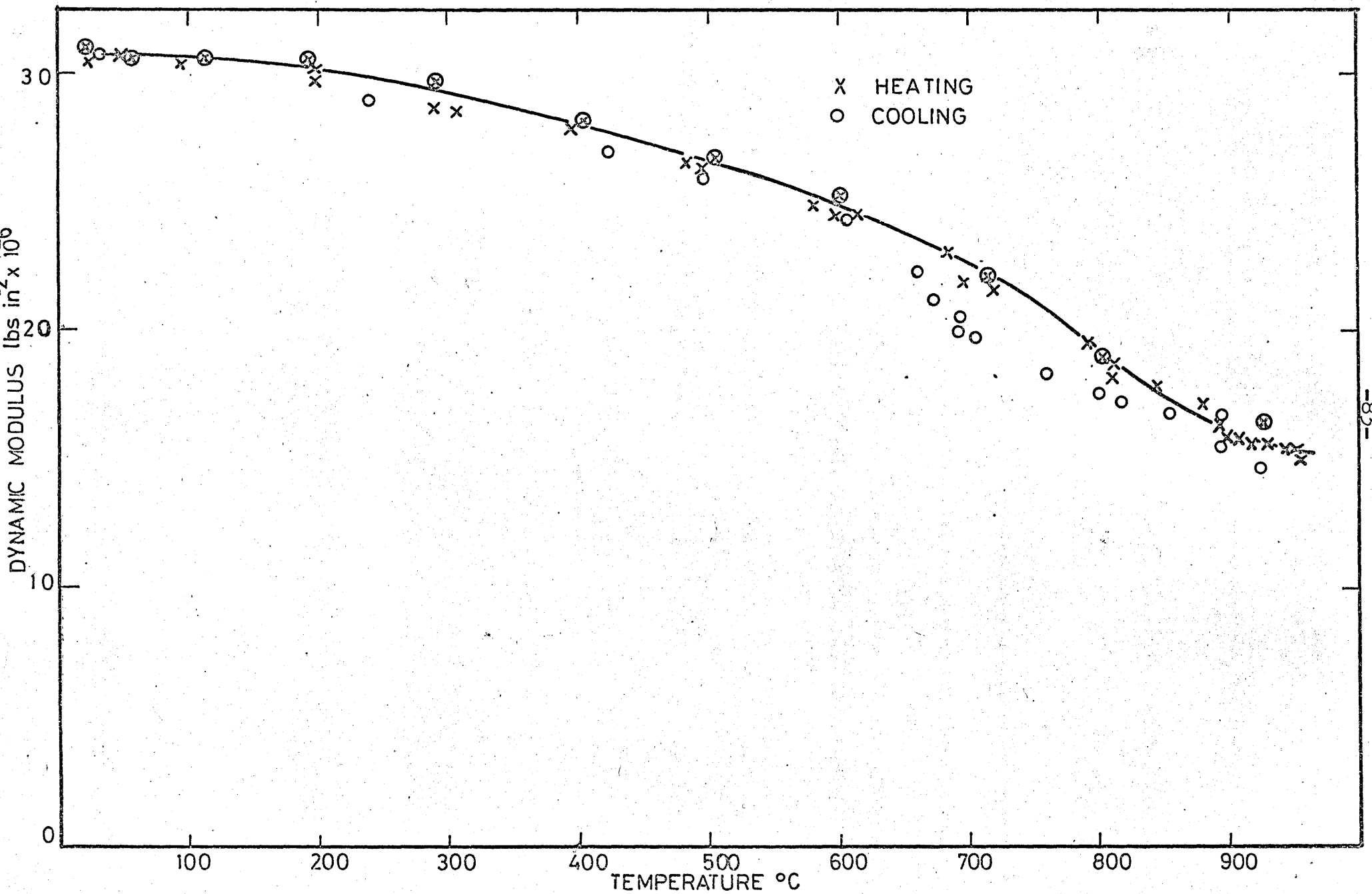

FIG. 2·28 CHANGE IN METAL DYNAMIC MODULUS WITH TEMPERATURE

calculated where f_o was the frequency at that temperature during heating, and f was the frequency at the same temperature during cooling in vacuum. The modulus value could then be calculated using the method outlined for isothermal tests. This method of determining modulus during cooling was only valid at temperatures down to the point where discontinuities occured in the frequency due to cracking, etc.. This was usually only down to about 500°C but occasionally with very thin oxides a smooth curve was obtained right down to near room temperature and a modulus value was calculable over most of the temperature range.

All the oxide modulus values calculated are presented in Fig. 2.29.. Since the composition and mechanical condition of the scale are altering during oxidation we are really measuring effective dynamic modulus which will be less than the intrinsic value for the oxide. This graph shows that the effective dynamic modulus of the oxide scale is very variable at any given temperature. This is to be expected in view of the obviously highly defective scale layers observed metallograpically, and evidenced by the irregular change in resonant frequency during isothermal oxidation. The curve shown in this figure was obtained by computer analysis of all the data, using curve fitting programme Z01A. This computer programme carries out progressive polynominal regression analysis, and the curve actually produced was a third order fit.

This curve shows a definite minimum in the region of 760°C, which is further strong evidence of the change in oxide composition, and therefore properties, occuring in this temperature region.

2.5. Summary and conclusions

The main points, deriving from the work described in this chapter, may now be summarised and some conclusions reached.

The vibration technique is certainly able to follow the progress of oxidation of steels, and is now able to sensitively detect damage in the oxide or at the oxide/metal interface. It has been shown that at all test temperatures up to 900°C oxide damage occurs during isothermal oxidation of EN2 steel. This damage could be either decohesion or cracking, or a combination of both. The most likely explanation is that the principle damage detected is due to failure at or near the oxide/metal interface. The metallographic evidence for this is that in virtually every specimen examined a gap was found between the bulk scale and a thin oxide layer left on the metal surface. This thin adherent oxide layer will be discussed in detail later. The bulk scale

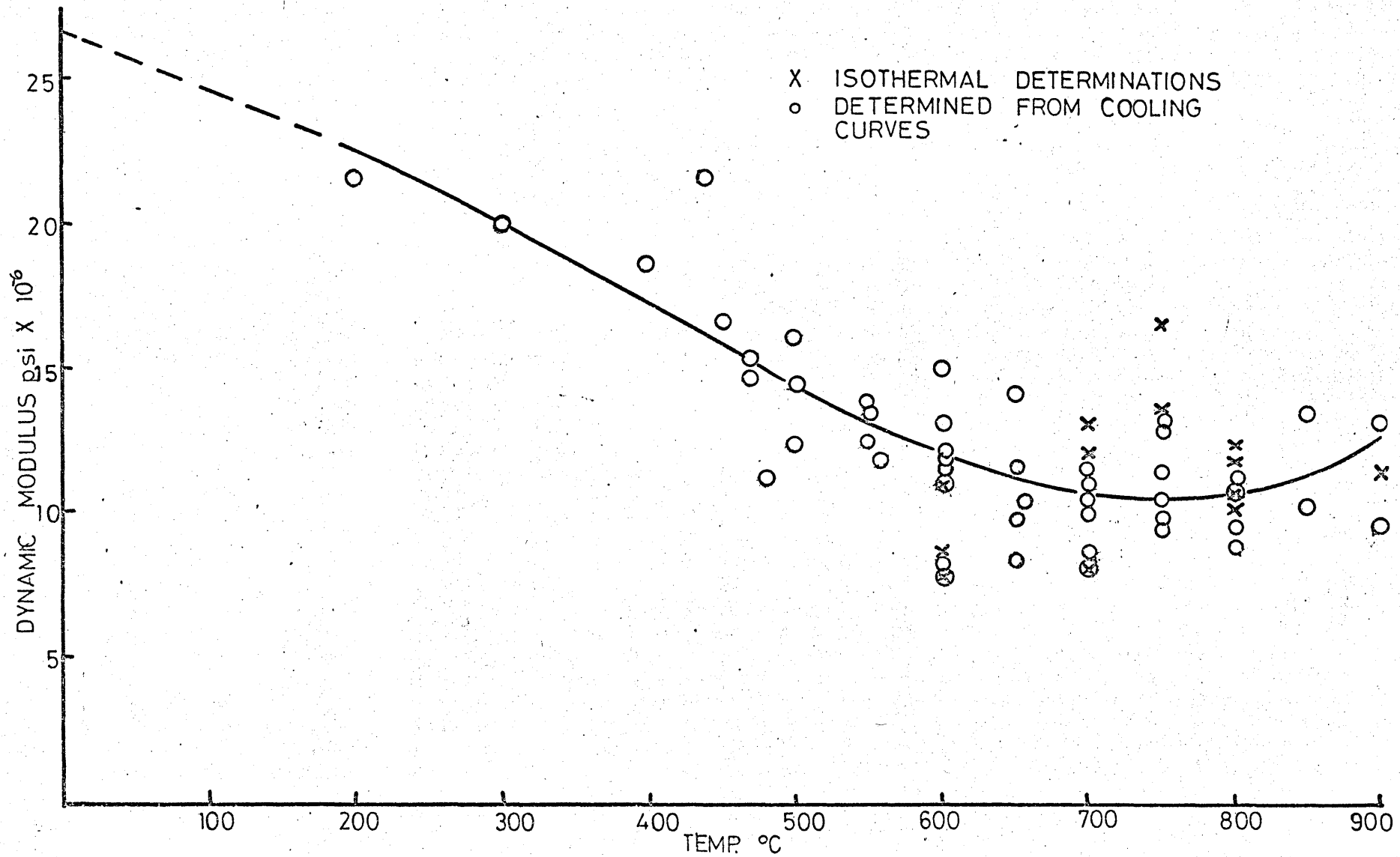

FIG 2·29 VARIATION OF OXIDE MODULUS WITH TEMPERATURE

was often very largely transformed to the higher oxide indicating that the decohesion occured at high temperature. In addition, if the damage was simply cracks in the oxide scale which subsequently healed, it would be extremely unlikely that the effective modulus of the composite would be recoverable rapidly and completely. This rapid recovery is indicated by the shapes of the natural resonant frequency curves after the frequency falls observed in the initial stages.

It therefore seems likely that failure due to geometry and growth stresses occurs by decohesion, probably leading to some cracking of the scale. Air will then penetrate these cracks and will either oxidise any exposed metal surface, if the decohesion is at the interface, or oxidise the bulk scale further if a protective oxide layer remains on the metal surface. Either of these processes would lead to a rapid recovery of the resonant frequency, and the subsequent increase in frequency often observed.

The thermobalance experiments have been found to give suitable data for correlation with the vibration work, and to give some indication of the effects of oxide damage on the kinetics of oxidation. The rate equation describing the oxidation process was found to vary over the whole range of temperatures, and in some cases to be far removed from a parabolic relationship. An activation energy for the process was calculated at 27·1k Cals. per mole, but this does not really have any useful significance in view of the contribution of a combination of diffusion and random oxide damage, to the kinetics of the oxidation process.

The oxide porosity was found to be high and variable, which is again highly consistent with the evidence of scale damage. This also had a large effect on the effective oxide modulus calculated. The modulus calculated for the oxide was very variable at any temperature, and decreased with temperature up to about 760°C, and then increased at higher temperatures up to 900°C. This change in oxide properties at around 760°C is in agreement with the change in kinetics observed in this temperature region. This effect is attributed to the presence of stable Fe_2O_3 at temperatures above about 760° - 800°C. This modulus data may be compared with similar data obtained for the EN2 steel in vacuum, and it may be seen that for all temperatures up to 900°C the average oxide modulus is less than that of the metal.

The room temperature oxide modulus, predicted by extrapolation of the best fitted curve is in the region of $26{\cdot}5 \times 10^6$ psi, which is considerably less than that quoted by Doraiswanie (100) of 38×10^6 psi, but this was determined on naturally occuring magnetite crystals, again indicating the effect of oxide defects on its dynamic modulus.

CHAPTER 3

3. THE INFLUENCE OF STRESS ON THE OXIDATION OF STEEL

3.1. Stresses induced by cooling

Since the coefficients of thermal expansion of iron and its oxides are different, any cooling of an oxidised steel bar must result in the production of stresses at the metal/oxide interface. Under the action of these stresses three possibilities arise: firstly the oxide may be able to withstand the stress without cracking; secondly the oxide may crack, if adhesion is good; or thirdly failure may occur at the interface if adhesion of the oxide to the metal is poor relative to the cohesive strength of the oxide. Obviously, some combination of these phenomena may occur in practice. If an oxidised sample has been cooled sufficiently to damage the oxide or oxide/metal interface in this manner, subsequent reheating will produce an increase in the oxidation rate since oxygen may now have easy access to the metal surface. This presence or absence of any increase in the oxidation rate after cooling and reheating has been used to indicate strains at which oxide failure occurs in both the thermobalance and vibration experiments.

3.1.1. Thermobalance.

A total of 22 experiments were carried out in the thermobalance in which the oxidising specimen was subjected to thermal shocks, either at a fast rate of cooling by raising the furnace, or a slow cooling rate in which the furnace was switched off. The rate of weight gains was then monitored once the specimen had again reached the oxidation temperature. With any given specimen this process of cooling and reheating was continued at intervals using progressively greater temperature drops in each case. It was found that generally even cooling to room temperature from all test temperatures did not have the effect of increasing the oxidation rate on subsequent reheating. An increased rate was produced on reheating on only two occasions. These two isolated results are shown in Fig. 3.1., but it should be emphasised that many other tests of equal severity did not produce comparable results. It can be seen from the graph of the 600°C test some scale had actually been lost due to the thermal shock.

The metallographic examination detailed previously indicated that oxide failure during cooling was by further detachment of the oxide from the inner adherent oxide layer, already partly detached during isothermal oxidation. In these thermal shock experiments for an increased oxidation rate to be observed must mean that

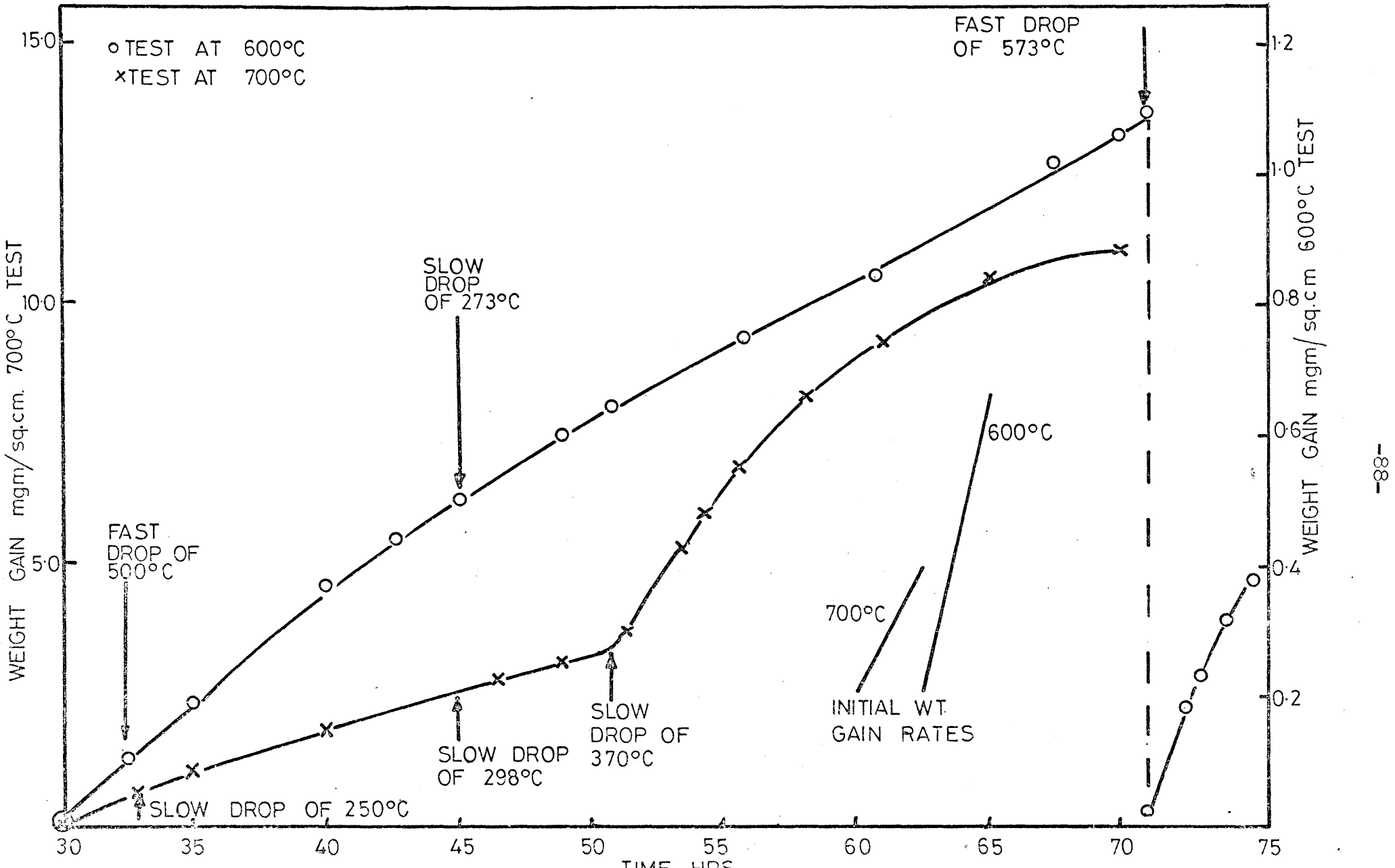

FIG. 3·1 EFFECT OF THERMAL SHOCKS ON THERMOBALANCE WEIGHT GAIN EXPERIMENTS

the inner adherent layer must also be damaged, in fact it is highly likely that the bulk scale is detached and damaged by much smaller shocks, but if the adherent scale remains intact oxidation rate does not increase.

For an oxide layer failing by detachment due to circumferential stresses, the value of the adherence may be calculated from:-

$$A = \frac{E_2 (\alpha_m - \alpha_o) Ta \delta}{C}$$

where

α_m and α_o are the coefficients of thermal expansion of the metal and oxide respectively.

δ is the oxide thickness.

Ta is the maximum temperature drop that just produces cracking.

C is the metal diameter.

E_2 is the oxide modulus at the mean temperature during the temperature drop.

Using Tylecotes' (59) values of $\alpha_m = 12{\cdot}2 \times 10^{-6}$, and $\alpha_o = 15{\cdot}3 \times 10^{-6}$ deg C^{-1}, and values of oxide thickness and metal diameter from the metallography, then values of adhesion (expressed as the force/unit area of surface acting perpendicular to the interface) were calculated for these two experiments. The thermal shock from 600°C gave an adhesion value of 177 psi, and the 700°C experiment gave a value of 755 psi. Whilst these fit in with the general order of the results obtained by Bruce and Hancock (54), they are of limited value in view of the fact that only two isolated experiments showed this type of behaviour. Also, this calculation assumes only elastic behaviour which is not likely at these temperatures.

During cooling of an oxidised specimen through T°C, the total strain in the oxide may be obtained from:-

$$\varepsilon = (\alpha_m - \alpha_o)\ T$$

Again, for these two thermal shocks, the value of oxide strain to fracture has been calculated to give a strain of $1{\cdot}8 \times 10^{-3}$ for the 600°C test, and $1{\cdot}15 \times 10^{-3}$ for the 700°C test. These values are very much higher than those obtained by Bruce and Hancock (54) using an identical method and similar materials. The only

apparent difference between the materials is the presence of the inner adherent oxide layer on this EN2 steel, which was not present on the mild steel examined by Bruce and Hancock.

In addition to the stress produced due to the difference in thermal expansion coefficients a further source of stress during cooling would be expected to be produced at around 570°C. Below this temperature, FeO decomposes to form a mixture of Fe_3O_4 and iron, and the reaction is accompanied by an expansion. Also, if cooling is carried out in air, there exists the further complication of the possibility of further oxidation occuring, either of the FeO directly:-

$$3FeO + \tfrac{1}{2} O_2 = Fe_3O_4$$

or, of the iron particles produced from the decomposition of the FeO:-

$$3Fe + 2\ O_2 = Fe_3O_4$$

Both of these reactions would increase the compressive stresses present in the oxide film. Thus it seems that although the stresses produced during cooling are able to produce further damage to the bulk oxide layer, they are generally unable to seriously impair the protectiveness of an inner adherent oxide layer observed on this EN2 steel.

3.1.2. Vibration experiments.

Similar thermal shock experiments were attempted using the vibration apparatus. The procedure was similar to that employed in the thermobalance work in that after various oxidation times over the range of test temperatures, the furnace was switched off and then re-heated after the required temperature drop. On no occasion did an increase of frequency result from such a procedure confirming the thermobalance findings that it was extremely difficult to produce serious penetration of the oxide film by thermal shock. However, on several occasions the resonant frequency of the specimen on regaining the oxidation temperature was slightly below the resonant frequency before cooling which is indicative of damage to the bulk outer scale, with the inner adherent scale remaining protective.

The frequency change during cooling was monitored for most specimens at the end of each oxidation test. Cooling in air generally produced a smooth curve down to around 570°C followed by an irregular serrated curve at lower temperatures which was presumably due to oxide cracking induced by the transformation and oxidation of the FeO around its decomposition temperature. This type

of irregular curve was rarely seen during vacuum cooling presumably indicating that the oxidation occuring during cooling has a prime role to play in disruption of the oxide film.

Some typical frequency curves produced during vacuum cooling are shown in Fig. 3.2., and several distinct types of curve are apparent. These curves are classified into three types labelled A - C in Fig. 3.2., and are each typical examples from several tests. Also included in this figure is a typical heating curve.

These curves may be interpreted as follows:-

Type (A). This oxide produced at 600°C was very thin, approximately 0·02mm, and had been subsequently vacuum annealed at 950°C. Very slow cooling, produced by gradually turning down the furnace control in 50°C steps, gave the straight line relationship with two inflexion points as shown in Fig. 3.2.. The two straight lines intersecting at about 600°C are representative of the change in modulus of the steel/FeO composite above 600°C, and the change in modulus of the steel/Fe_3O_4 composite below 600°C. The high temperature annealing, coupled with the very slow cooling and the presence of only a thin oxide has enabled equilibrium to be reached at each temperature. The inflexion at about 790°C, is presumably due to decomposition of some of the Fe_2O_3 layer.

Type (B). This again is a very thin oxide produced at 500°C and is largely Fe_3O_4. A smooth curve is produced indicating no cracking or decohesion. The cooling rate in this case is somewhat higher than that for the Type (A) curve, the furnace was merely swtched off and allowed to cool naturally, and the presence of a slight temperature lag between the specimen and furnace is presumably the reason for the slight curve in the frequency change graph.

Type (C) This oxide is very thick, approximately 0·5mm and the cooling rate is again faster than in Type (A). In this case it is suggested that the decomposition of FeO, commencing at around 570°C, produces sufficient stress to initiate damage of the scale layer. Metallography shows this to be by detachment of the bulk scale at its interface with the inner adherent scale. This results in a fall in effective modulus of the composite giving rise to the observed fall in frequency. At a lower temperature, when the scale is largely detached, frequency again begins to rise due to the increasing modulus of the metal core.

The form of damage to the scale produced by growth stresses, cooling stresses or compositional stresses, or a combination of all three, will depend on oxide plasticity, adhesion properties and oxide thickness. All of these factors are obviously greatly influenced by temperature of oxidation.

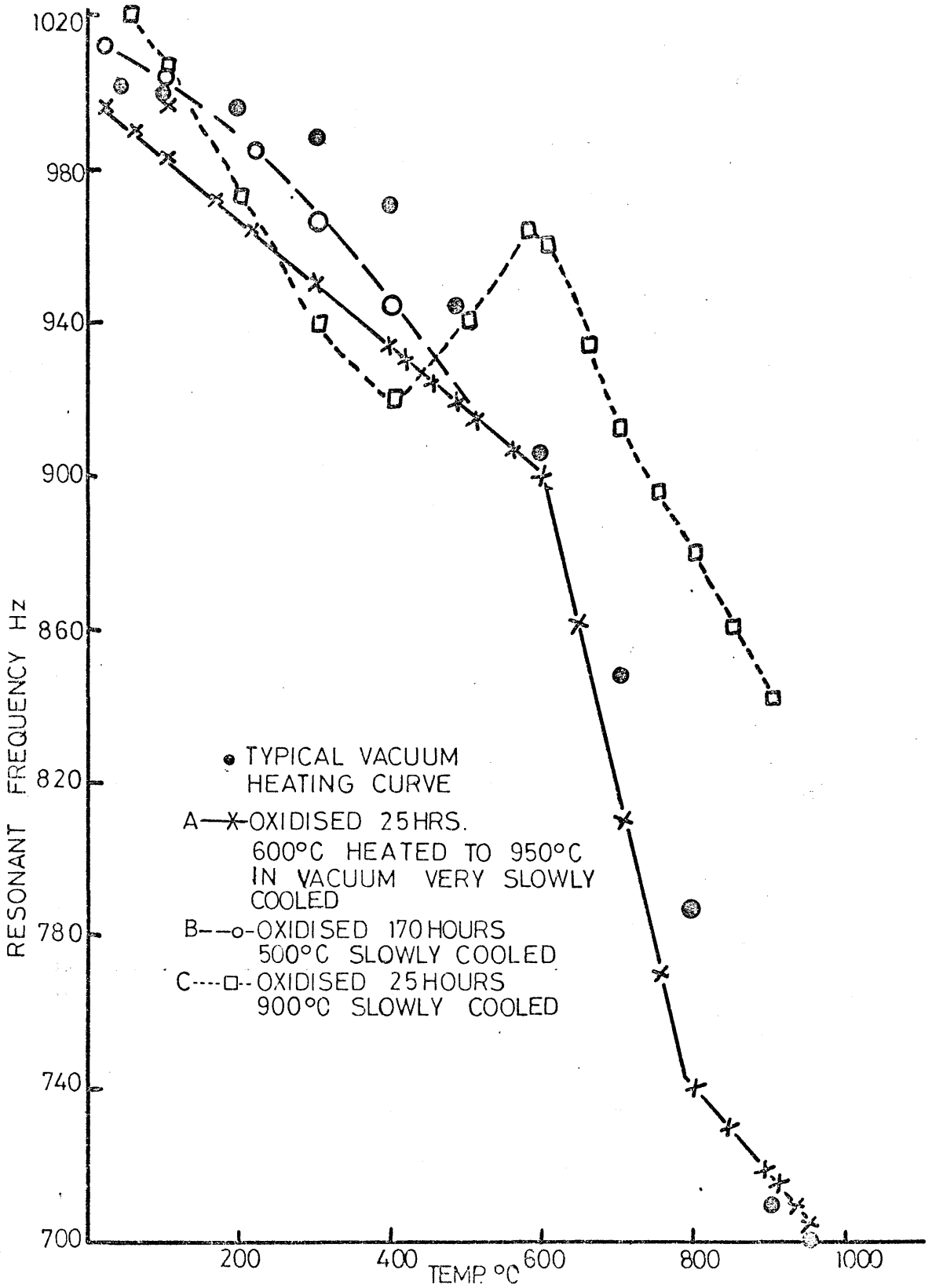

FIG. 3·2 RESONANT FREQUENCY DURING COOLING IN VACUUM AFTER OXIDATION

Fig. 3.3. show the surface oxide produced on a vibration specimen oxidised for 25 hours at 600°C. The tensile stress at the free oxide surface has been sufficient to crack the oxide and cause it to curl up in the manner shown. This behaviour indicates two things. Firstly the oxide has considerable plasticity even at these comparatively low temperatures, and secondly the oxide adhesive strength is low.

Fig. 3.4. shows a vibration specimen after oxidation at 700°C for 21 hours. After cooling the oxide on this specimen appeared adherent, smooth and uncracked. Upon removal from the furnace this specimen was soaked in paraffin, and then sprayed with acetone. As the acetone was drying the very fine cracks shown in Fig. 3.4. were outlined by the paraffin being drawn out of them. This type of fine cracking with no evidence of blistering or decohesion is indicative of an oxide which has good adhesion and low fracture strength.

Fig. 3.5. illustrates the effect of a superimposed tensile stress on the form of oxide damage produced. This is a tensometer specimen which had been oxidised at 750°C for one hour and then elongated by 10%. The longitudinal tensile stress had cracked the oxide along its length, and the oxide had then become detached at points around the circumference. The cooling stresses had then caused the circumferential blistering shown in the Fig. 3.5.

3.2. Stress due to specimen geometry effects

Another way in which stress may be generated in a growing oxide is by varying the specimen geometry such that the normal growth stresses may be either diminished or increased. A series of approximately 30 specimens were tested to attempt to evaluate this geometry effect. Holes of various diameter were drilled and reamed in steel blocks, and also cylinders of varying internal and external diameters were prepared. The hole sizes varied from 0·15 cm. to 2·7 cm. and the outside diameter from 0·6 cm. to 1·25 cm.. All specimens were carefully cleaned and measured prior to oxidation at various times and temperatures between four hours at 800°C and 18 hours at 900°C. Specimens after oxidation were usually photographed, mounted in Araldite, sectioned and prepared for metallography and measurement.

Typical cylindrical specimens before and after oxidation at 800°C for eight hours, are shown in Fig. 3.6.. An individual specimen after oxidation is shown in Fig. 3.7..This clearly shows the difference between oxidation on a concave and a convex surface, and also the plasticity of the oxide on the inner surface at this temperature. The concave surface had imposed a compressive stress on the oxide which had led to decohesion and

Fig. 3.3. Vibration specimen after oxidation at 600°C for 25 hours.

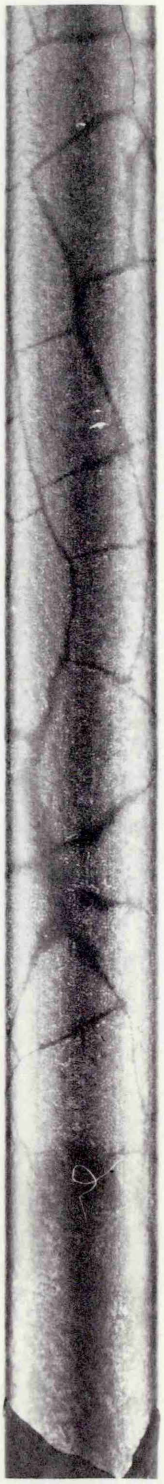

Fig. 3.4. Vibration specimen after oxidation at 700°C for 21 hours.

Fig. 3.5. Tensometer specimen oxidised 1 hour at 750°C then elongated by 10% (Mag. x 10approx.)

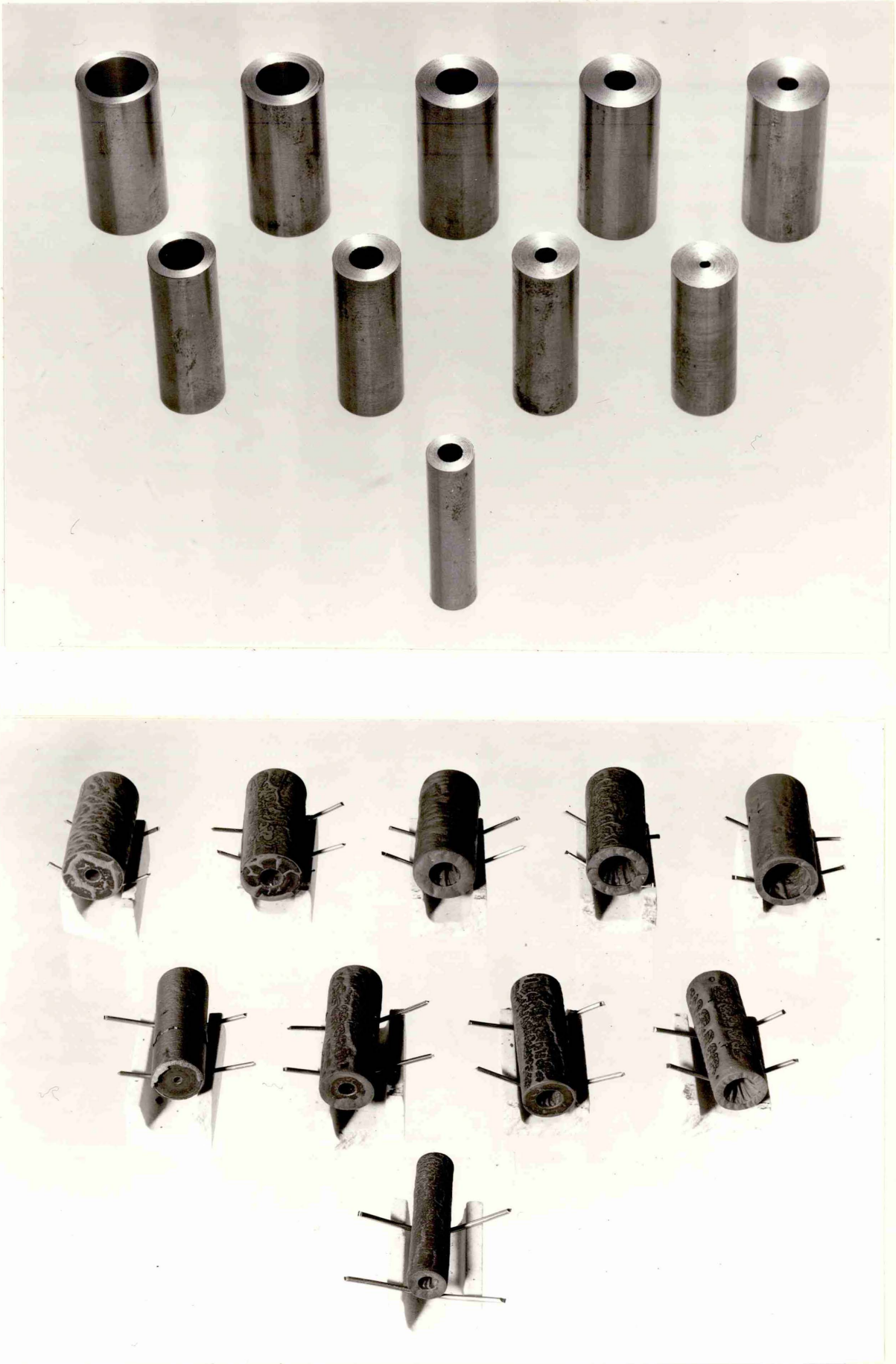

Fig. 3.6. Geometry specimens before and after oxidation at 800°C for 8 hours

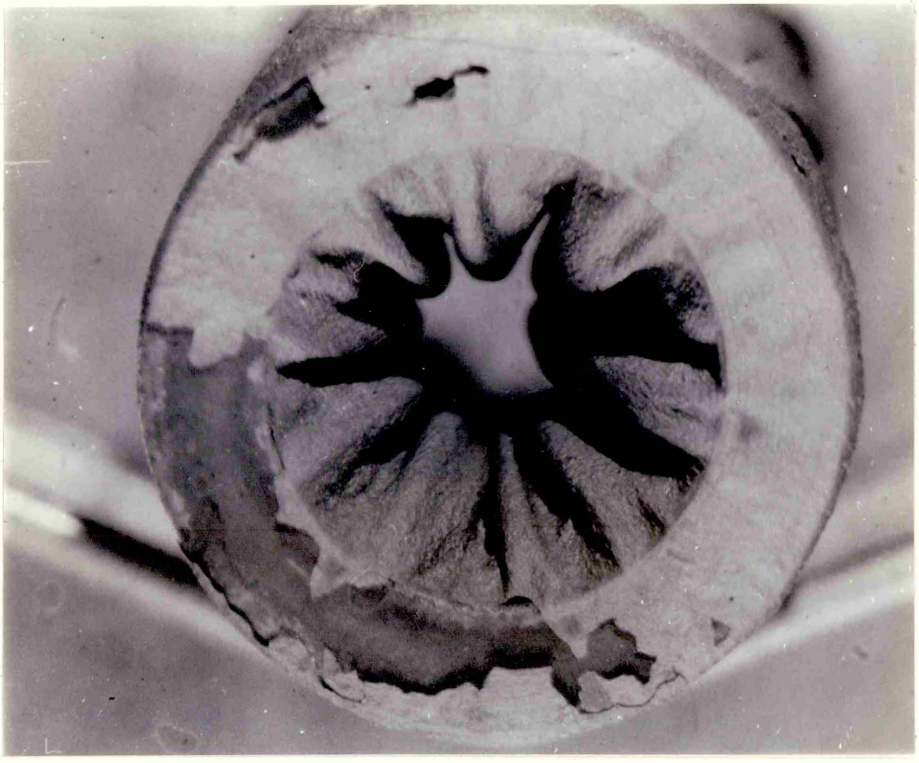

Fig. 3.7. Typical geometry specimen (Mag. x 5)

buckling. Measurement of the increase in length of this oxide on the surface of the hole indicates an extension up to 30%, for the cylinder with the smallest wall thickness. Since presumably the hole is also acting as a vacancy sink for the oxidation of the outer surface decreasing adhesion of the oxide on the inner surface. Metallography shows that this buckling and high plasticity is largely confined to the outer oxide layers, i.e. largely Fe_3O_4 and Fe_2O_3 which are said to have only limited plasticity (66).

Thicker oxides grown for longer times and at higher temperatures on surface and holes often exhibit radial cracking. This is illustrated in Fig. 3.8. which is a micrograph of a hole oxidised at 900°C for 18 hours. These radial cracks are produced by tensile stresses induced in the oxide near the interface as the metal surface receeds, and indicates good adhesion in the early stages of oxidation. Also shown is the Pfeil type porous layer near the interface, presumably accentuated by this inner hole acting as a vacancy sink for the oxidation of the outside of the specimen.

The effects of geometry were also indicated by oxidising specimens which had either holes drilled or grooves turned, having different profiles ranging from a smooth semicircle to a sharp angled V section. The oxide formed on all of these profiles was found to be cracked, the severity of cracking increasing with increasing sharpness of section. In no case however was the inner adherent scale of the EN2 steel broken even when the bulk oxide was severely damaged.

Measurements of the specimen and oxide dimensions did not show any clear relationship between outside or hole dimension and thickness of oxide produced. The only consistent result obtained was for any given hole diameter and wall thickness the oxide thickness on the surface of the hole was 20% $\mp$ 5% less than the oxide thickness on the outer convex surface. This is to be expected because of the constraints placed on the oxide growing on a concave surface whereas the oxide on the convex surface will be in tension at the free surface during growth, and therefore more likely to become cracked and less coherent giving a thicker oxide scale.

3.3. Applied stress

3.3.1. Preliminary.

Most methods that have been applied to measure mechanical and adhesive properties of oxides suffer from severe limitations. For example, the testing of bulk oxides rather than surface oxides, the interference of the oxidation process, or often the ability to test only at room temperature.

The vibration technique has been shown capable of

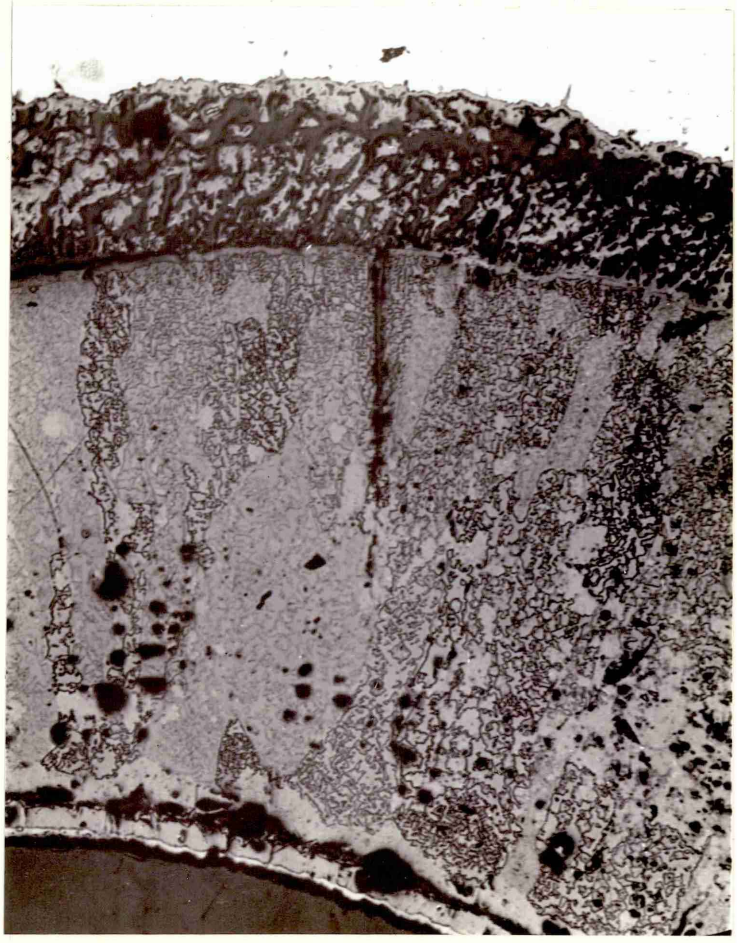

Fig. 3.8. Microsection of geometry specimen oxidised at 900°C for 18 hours (Mag. x 100)

sensitive detection of oxide cracking or decohesion. It was decided to try and incorporate this capability into equipment for applying stress to the oxidising specimen, in such a way that oxide failure could be detected after load application.

In order to apply a load to a vibration specimen several requirements had to be met:-

(a) Some means of applying the load to the specimen, without damaging the oxide, was required, such that the resonant frequency could still be determined quickly and accurately.

(b) The specimen could not be bent during loading, (e.g. a three point bend method) because of the effects of bending on the specimens resonant frequency.

(c) Since changes in the specimen dimensions alter the resonant frequency it was necessary to monitor any dimensional changes if any plastic deformation of the specimen occured.

The capability of applying a tensile load to the specimen was required in such a way that it was unnecessary for grips to be permanently attached to the specimen. The method of attaching the grips should not damage the oxide in any way. In order to accomplish this, tests were carried out to determine the effect on resonant frequency of fixing small Nimonic bars to the specimen ends. Welding was considered, but was discounted because of the likely metallurgical effects, and the irregularity of section introduced.

The Nimonic bars were 1" long, 3/16" diameter, with a small seating flat, and they were attached to the specimen by 6BA Nimonic screws 3/8" long. The effect of the two drilled and tapped holes in the specimen ends was to increase the natural frequency by approximately 4·8%, due to loss in mass and section. When the bars were in position the frequency decreased further, so that the overall effect was a reduction of 33% in the resonant frequency of the specimen.

The amplitude of output signal increased greatly, since the bars acted as inertia bobs, and a clear, single resonant peak could be dtermined. This prototype specimen was then heated to ensure that the changes in resonant frequency could be followed in the usual manner. This was found to be the case, and curves of frequency change against temperature during heating and cooling followed the normal form, with a total frequency change similar to that for the usual type of vibration specimen.

3.3.2. Apparatus.

The final design of the apparatus used is shown schematically in Fig. 3.9., and photograpically in Fig.3.10. It consists of a furnace chamber formed from fire bricks, housed in a Sindanyo box, and heated by three Crusilite

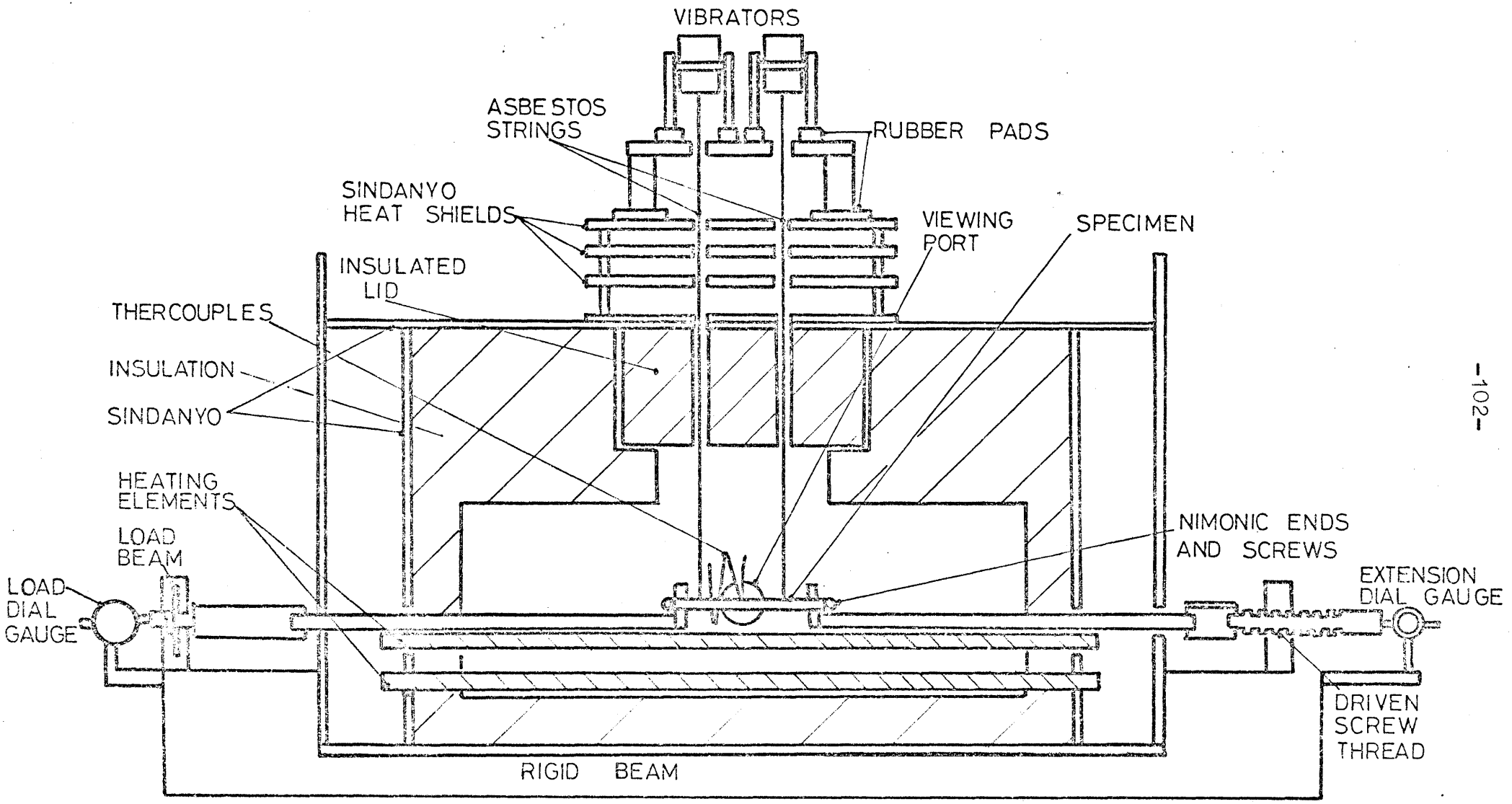

FIG.3-9 SCHEMATIC DIAGRAM OF HOT TENSILE DEFORMATION RIG

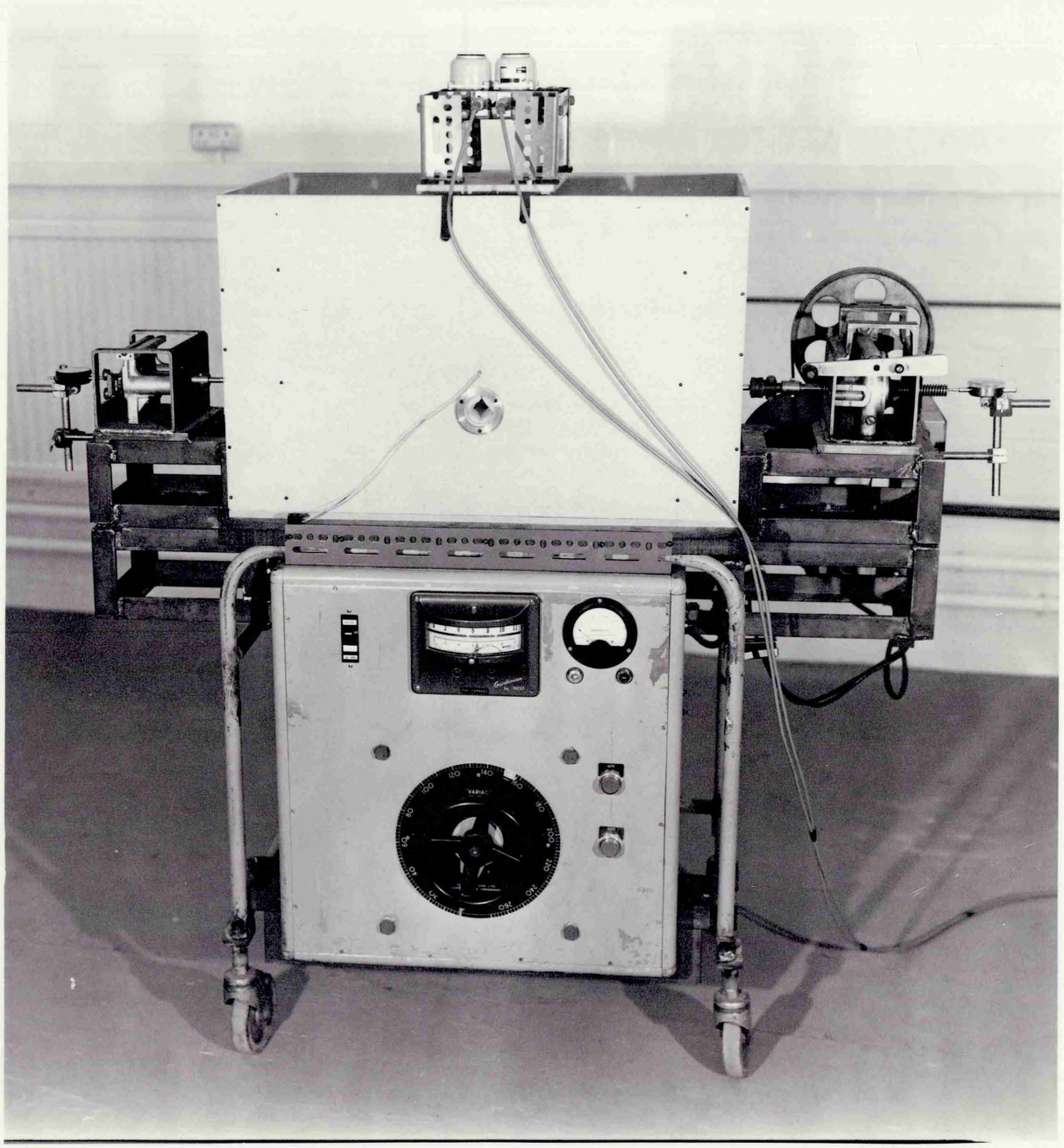

Fig. 3.10. General view of hot tensile deformation rig.

rod elements 14 mm. diameter, 650 mm. long. The temperature was controlled by means of a variac and a West Guardsman Pt/Pt.Rh. controller unit. Beneath this furnace a fabricated box section, made from 1¼" angle iron, was situated in order to act as a mounting beam for the loading system. A standard Hounsfield tensometer machine was removed from its base and the two separated ends were then remounted at either end of the box section beam. The arrangement of these ends are shown in Figs. 3.11. and 3.12., and the method of loading the specimen in the Nimonic pulling grips is shown in Fig. 3.13.. Before this apparatus could be used to measure oxide fracture stresses and strains, it was necessary to calibrate the system, and to determine the strain in the apparatus at varying temperatures.

The deflection of the load beam was measured with a dial test indicator, to an accuracy of 4×10^{-5} of an inch, was calibrated against load using a two ton force elastic proof ring. This ring was prviously calibrated at the National Physical Laboratory for movement of a Sogenique transducer against applied load. The proof ring was placed in position in the Nimonic grips (after removal of the heating elements), and the slack in the system taken up using the Hounsfield manual drive. The dial test indicator was adjusted to zero, and the zero deflection of the proof ring was balanced on the Sogenique hand set. The load was then increased incrementally using the motor drive, and both beam deflection and proof ring deflection were noted. This procedure was repeated several times for each of the two load beams to be used, rated at 500 lb.f. and 1120 lb.f. respectively. The deflections of the proof ring were converted to loads from the N.P.L. calibration graph, and load beam deflection was plotted against applied load, as shown in Fig. 3.14. for the 500 lb.f. beam.

The standard Hounsfield machine is inherently "soft", which means that it exhibits high strains under load thus making accurate measurement of specimen strains extremely difficult. This modified Hounsfield apparatus was expected to be even softer, and because no suitable method of extensometry was formulated, a method was devised to attempt to determine the strain in the system at the operating temperature.

The actual specimens initially used were the normal vibration ones of 0·2" diameter 6" long EN2 steel, but for calibration, a 3/8" diameter 6" long bar of Nimonic 90 was prepared with the 6BA tapped holes. This was used since it should not extend significantly at the loads and temperatures to be used. The Nimonic end bars, screws and grips were the same ones to be used for the steel testing. Working loads were applied to the calibration Nimonic bar and both beam deflection and travel of the drive screw were recorded. This was repeated

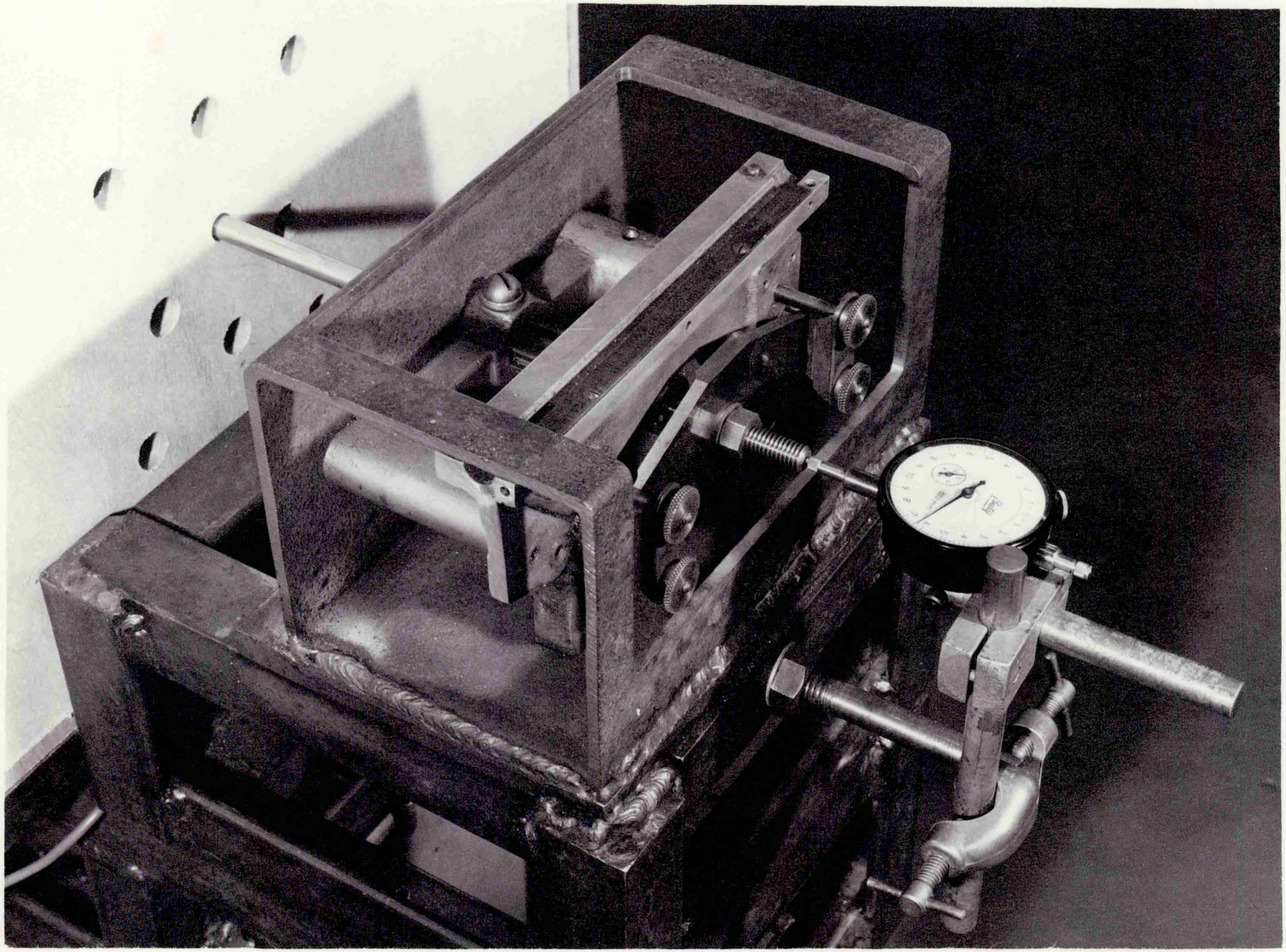

Fig. 3.11. Load beam end of hot tensile deformation rig

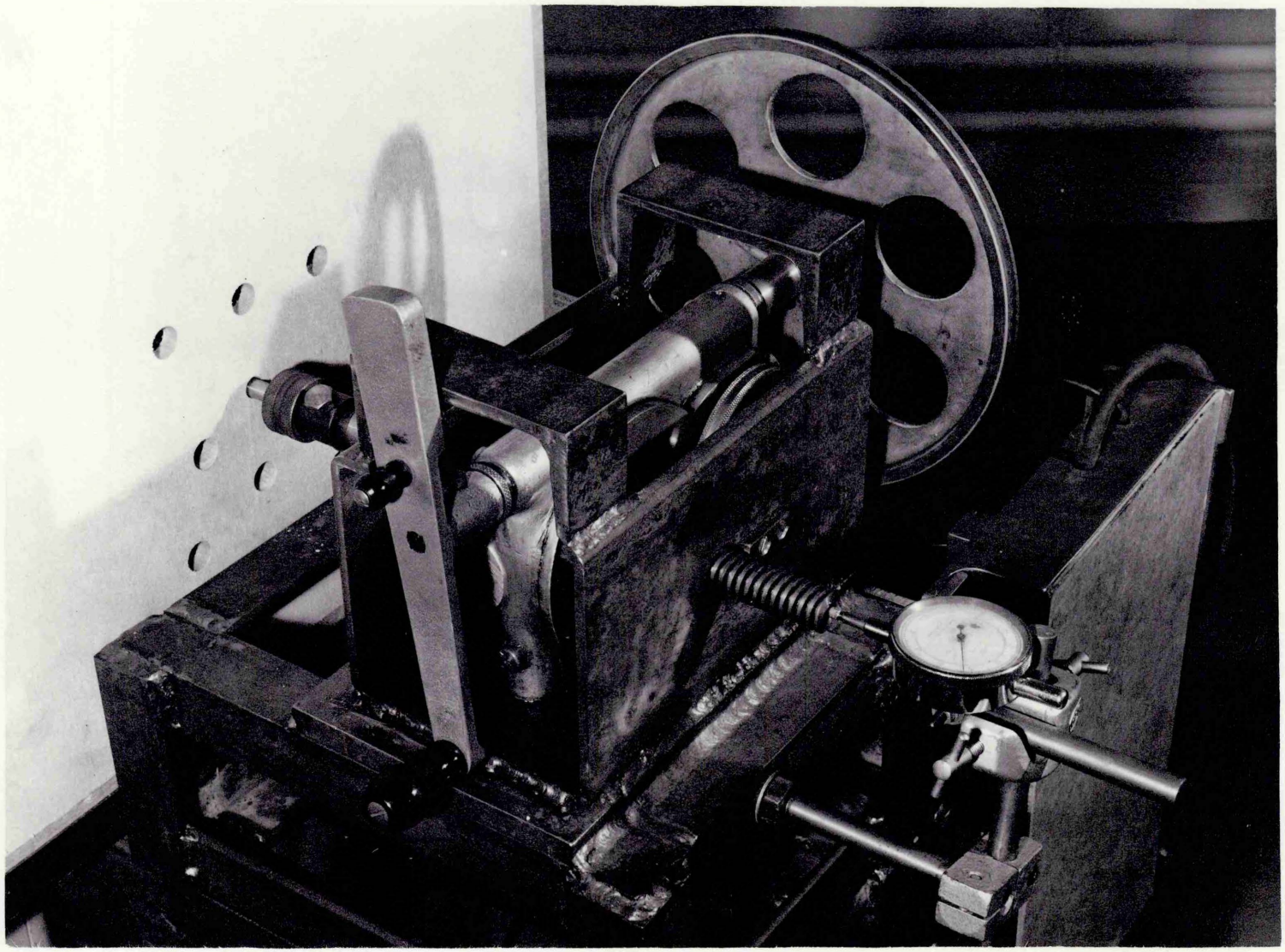

Fig. 3.12. Drive end of hot tensile deformation rig

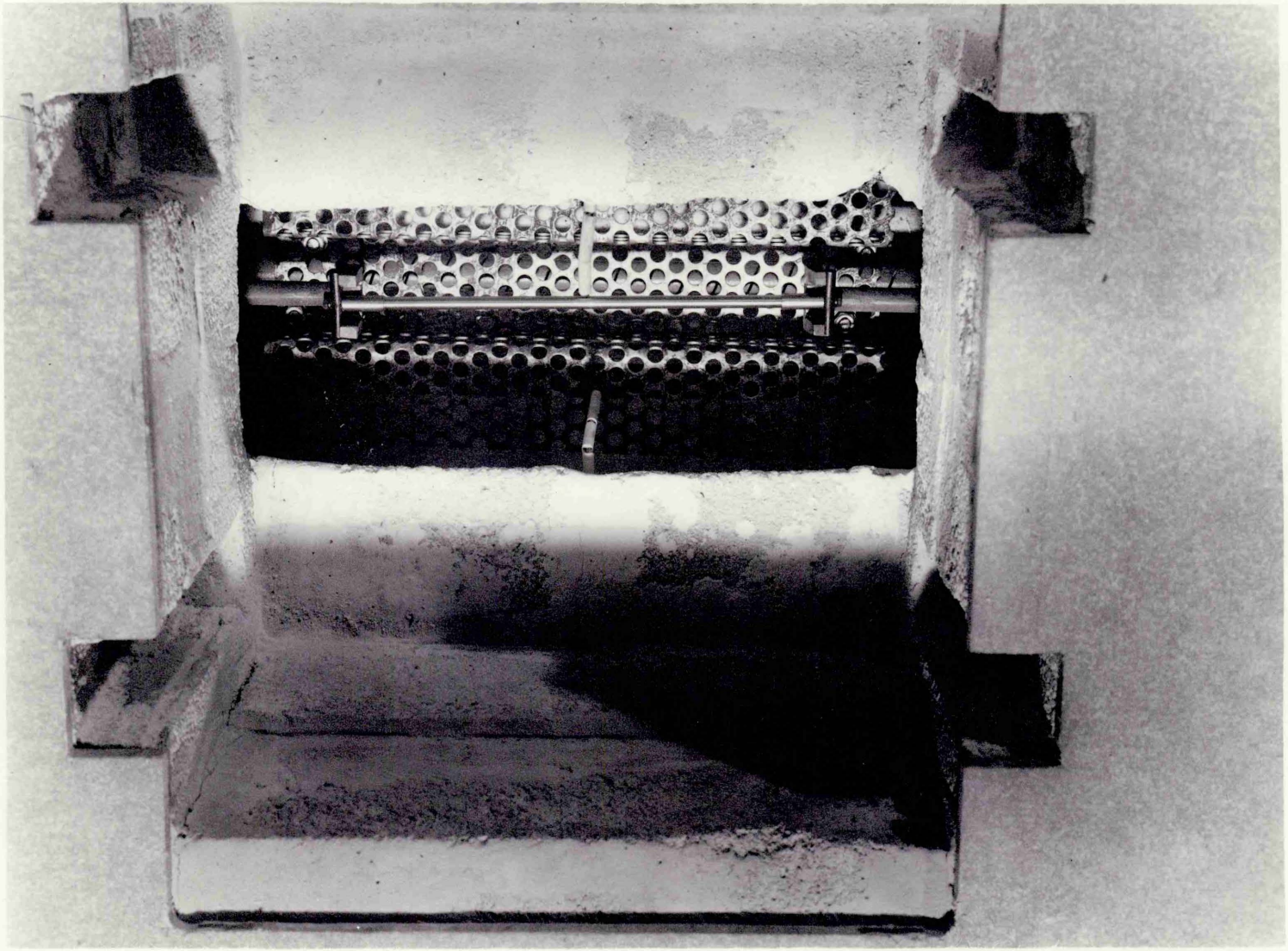

Fig. 3.13. Specimen in position within hot tensile deformation rig furnace

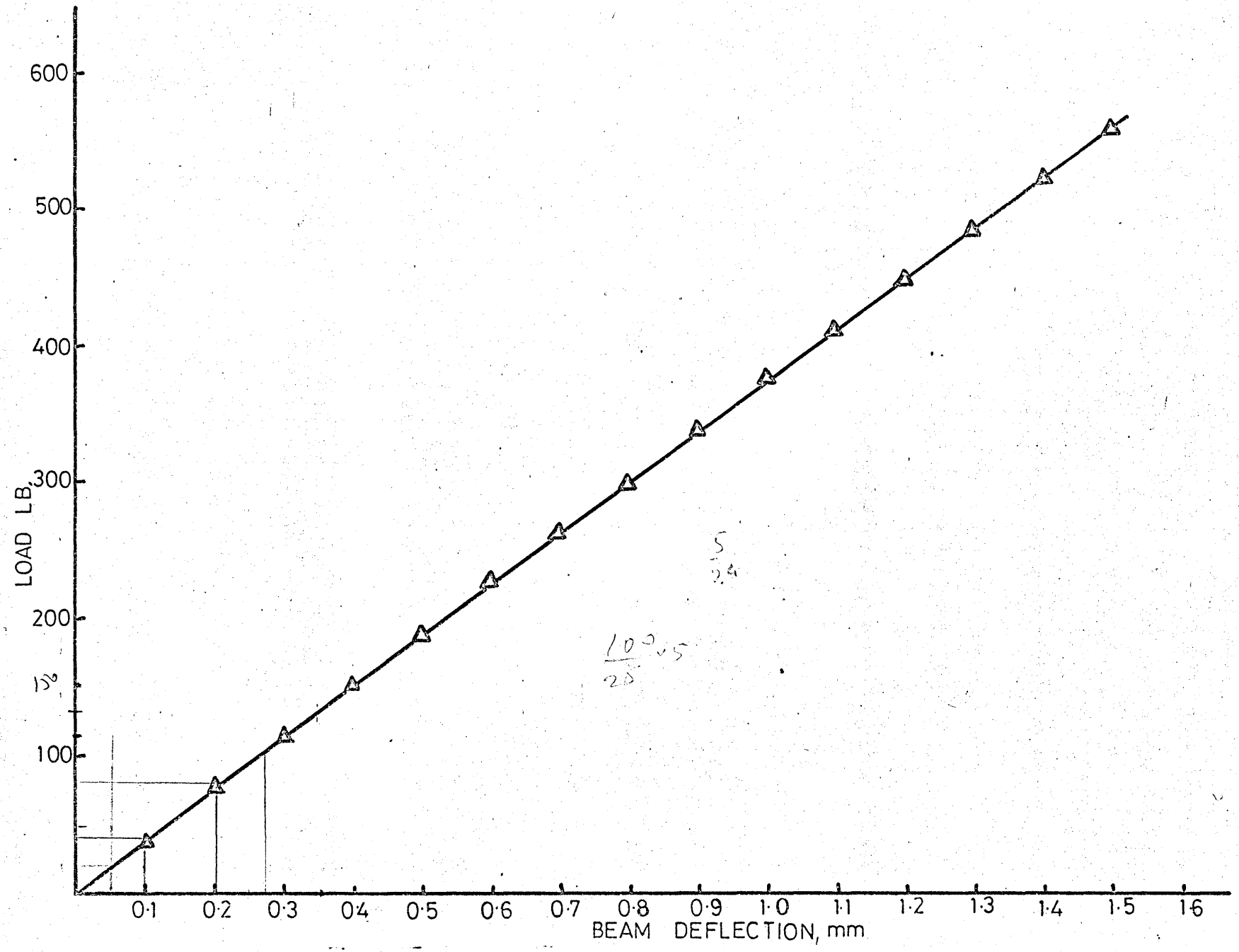

FIG 3·14 CALIBRATION CURVE 500 lb LOAD BEAM

for each of the proposed working temperatures. The extension of the Nimonic bar was calculated for each load and temperature from published hot tensile data, which was subtracted from the recordings of drive screw movement. This meant that for any given temperature and load beam deflection, a value of system extension was available. The difference between these two movements was due to the elastic deformation of all the separate parts of the load application system. The strain in the specimen could then be calculated, by subtracting the recorded extension when calibrating from the recorded extension during testing, for the load beam deflections measured.

A standard steel specimen, with three fibre glass coated thermocouples welded at points along its length, was placed in position in the furnace in order to determine the temperature gradient over the specimen length. The furnace was then heated up to 900°C and the temperature was allowed to equalise at several points in the heating range. The temperature along the specimen length, and the corresponding temperature of the controlling thermocouple, were noted throughout the working temperature range. It was found that the temperature of the controlling thermocouple agreed with the temperature of the central portion of the specimen to within 1°C over the entire temperature range, and the temperature of the specimen centre was constant to within $\mp \frac{1}{4}$°C. It was also found that the temperature was the same at both ends of the specimen, but was between 2° and 5°C less than the temperature of the specimen centre. This was a function of the rod heating system used, and unfortunately, no method of improving this temperature distribution was found.

Once these preliminary calibrations had been completed, a test specimen 0·2" x 6", fitted with the Nimonic ends, was heated to 750°C and oxidised for several hours. Loads were then applied incrementally and the resonant frequency monitored. It was found that only a small drop in resonant frequency was produced after 0·2% strain. The specimen was cooled and examined. It was seen that all of the extension had occured in the region of the tapped holes, where obviously the section is thinnest. To overcome this problem, several different designs of contoured specimens were tested, and the one finally adopted is as shown in Fig. 3.15.

3.3.3. Experimental and results.

Several specimens were produced from both mild steel and the EN2 steel (analyses shown in Table 2. P.36), to the dimensions given in Fig. 3.15.. These were then vacuum annealed at 950°C for one hour and then accurately measured. The Nimonic end pieces were then fitted using the 6BA Nimonic bolts, and the specimen

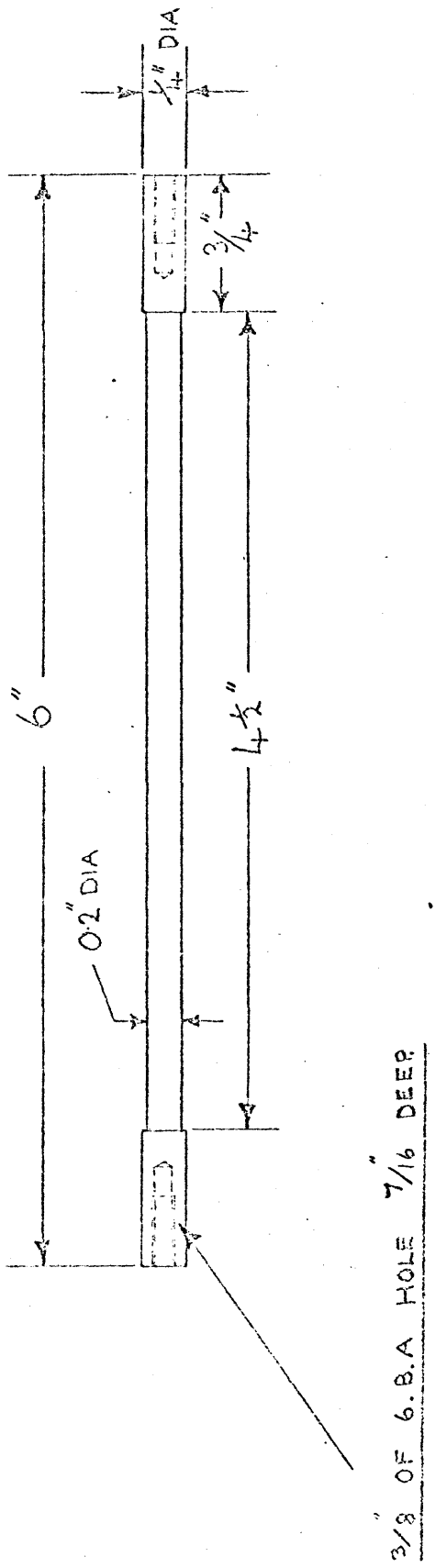

3.81
11.43
15.24

Fig. 3.15. Specimen used in hot tensile deformation rig

suspended symmetrically from the vibrators using asbestos string. The furnace top, heat shield, vibrators and suspended specimen were then placed in position in the furnace enclosure. The specimen position in relation to the Nimonic grips was adjusted when necessary whilst viewing through the quartz glass ports. The funace was then heated to the required oxidation temperature and the specimen oxidised for the desired time, with the specimen resonant frequency being monitored in the usual manner. The grip at the load beam end of the specimen was then moved outwards until it contacted the Nimonic bar attached to the specimen, again using the quartz glass ports for viewing. The other grip was next withdrawn until a movement of the load beam was indicated on the relevant dial guage, whereupon the drive gear was locked. At this stage all of the slack in the system had been removed, and no load was being applied to the specimen. Both dial guages were then set to zero. Loads were applied incrementally to the specimen using the motorised drive movement were recorded. After each load increment both grips were moved inwards so that they no longer contacted the specimen end bars, and the resonant frequency was determined. This procedure was repeated until a major change in resonant frequency (i.e. at least 5 - 10 cycles) was detected. The subsequent recovery of resonant frequency was then monitored during further oxidation.

The form of cracking produced at 700°C by a stress of 5000 psi in the steel is shown in Fig. 3.16.. A result which is typical of the type of response observed in all specimens is shown in Fig. 3.17.. In order to ensure that such a fall in frequency was due to the presence of the oxide film, and not to some change in the metal, a test was carried out in which a specimen was charged into the furnace held at 700°C. Once temperature had been allowed to equilibrate and the specimen was only slightly oxidised, loads were applied to the specimen and its resonant frequency monitored. It was found that after applying a stress of approximately 6000 psi the resonant frequency was unchanged. Therefore the fall in resonant frequency due to load application during oxidation could not be due to any changes produced in the metal by the stress.

Initially, arbitrarily selected oxidation temperatures and times were used, in order to formulate suitable conditions for a rational test programme. During these first tests it was noted that the specimen strains determined using Nimonic calibration data were much greater than strains calculated from the steel elastic modulus values determined previously. For example, a test at 700°C indicated a strain to oxide damage of 0·31% using the Nimonic calibration, and 0·01% by calculating strain from the stress applied and the

Fig. 3.16. Oxide cracking produced at 700°C.

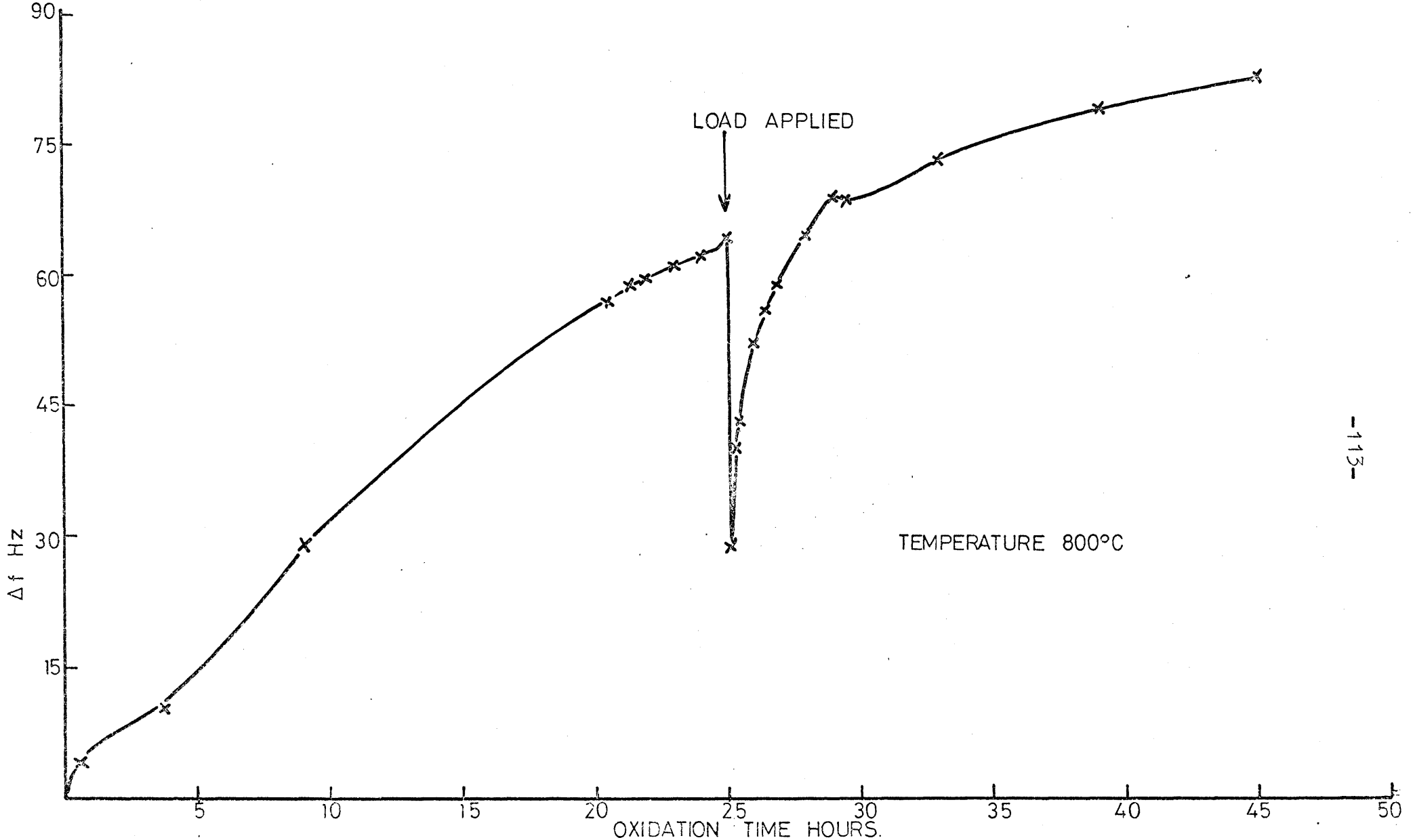

FIG. 3·17 TYPICAL RESPONSE OF EN 2 SPECIMEN TO LOAD APPLICATION

dynamic modulus value, even though no plastic deformation had been detected. The absence of plastic elongation was indicated by the return of both dial guages to zero when the load was removed, and by measurement of the length of the specimen after test. This problem of high strain value was further highlighted by attempting to measure the specimen dynamic modulus both at room temperature and at elevated temperatures. At room temperature using the Nimonic calibration, E was found to equal approximately 3×10^6 psi, compared with the actually determined value of 31×10^6 psi. Similarly a specimen which was loaded directly into the furnace already heated to 700°C, and then loaded once the temperature had equilibrated, indicated $E = 3{\cdot}5 \times 10^6$ psi compared with the value, previously calculated from the natural resonant frequency of $21{\cdot}5 \times 10^6$ psi. These results are presented in Fig. 3.18., from which it may be seen that the elongation required to be measured is a very small proportion of the total elongation of the equipment plus specimen. It was therefore decided that test results obtained under elastic conditions would be analysed separately from those in which plastic flow had occured. The elastic results were calculated from the load applied and using the dynamic modulus data, and the plastic plus elastic strains could only realistically be quoted as maximum values.

Tests were carried out in which specimens were oxidised for varying times and loads were applied at approximately 24 hour intervals. A typical result of these tests is shown in Fig. 3.19.. This shows that the damage produced by elastic deformation of the specimen increases dramatically above a certain threshold stress of around 5000-6000 psi, and this result was reproducible for any given temperature and time. The effect of oxidation time on the frequency drop produced by constant loads is shown in Fig. 3.20.. The stresses quoted in this figure are somewhat in error since they have been calculated on the basis of initial specimen diameters, but even assuming that the load is only effective over the remaining steel section, i.e. that the oxide layer is not attached to the metal, the error involved would be less than 5%. It may be seen that this relationship is approximately linear and not apparently related to any form of parabolic relationship. This is probably because the specimens were all air heated, and consequently the initial fast oxidation rate is not included, so that oxidation is proceeding at a comparatively uniform rate. The interpretation of the effects of oxidation time on the fall in resonant frequency for a given load is that the strain in the steel is transmitted via the parts of the interface that

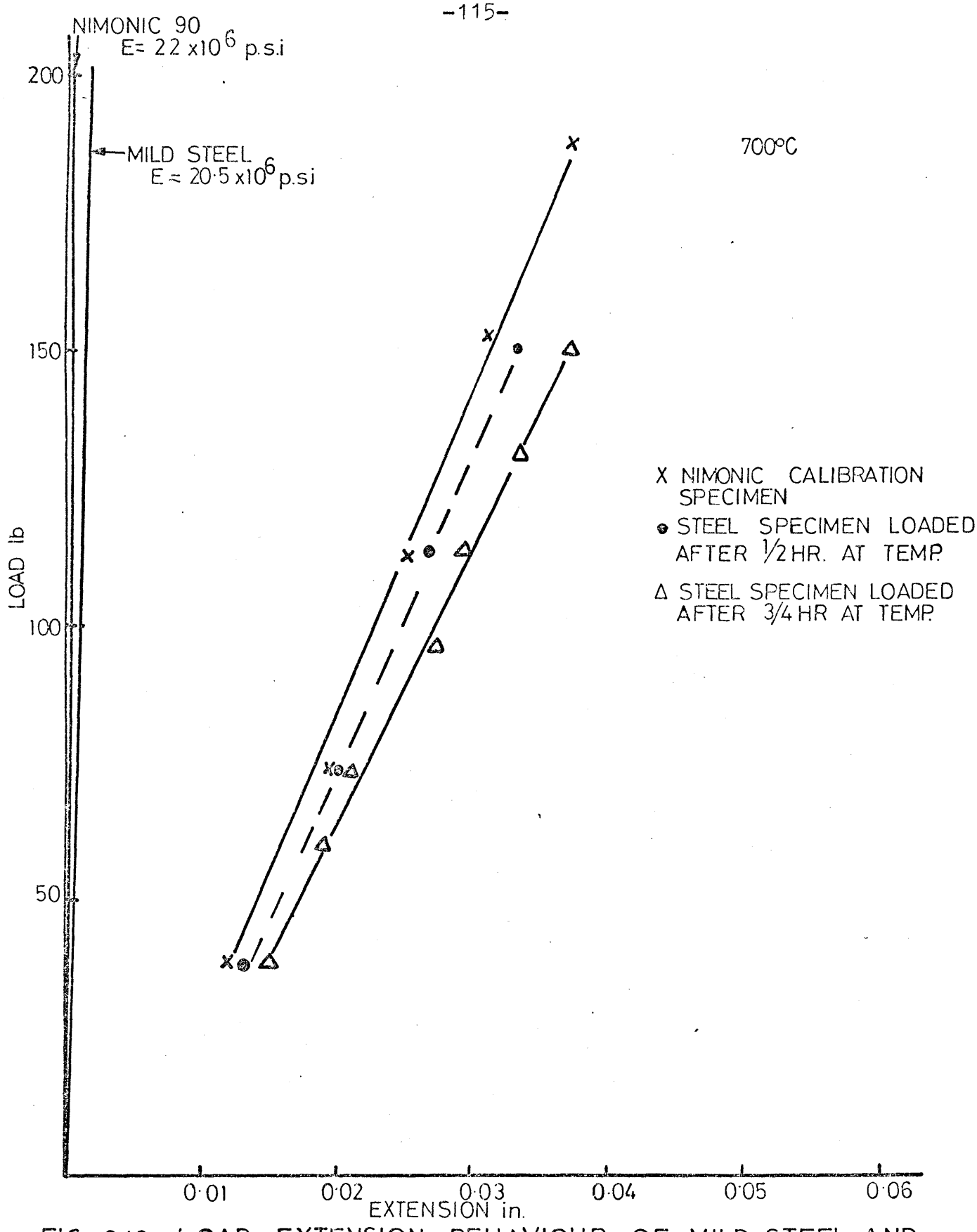

FIG. 3·18 LOAD EXTENSION BEHAVIOUR OF MILD STEEL AND NIMONIC CALIBRATION SPECIMEN

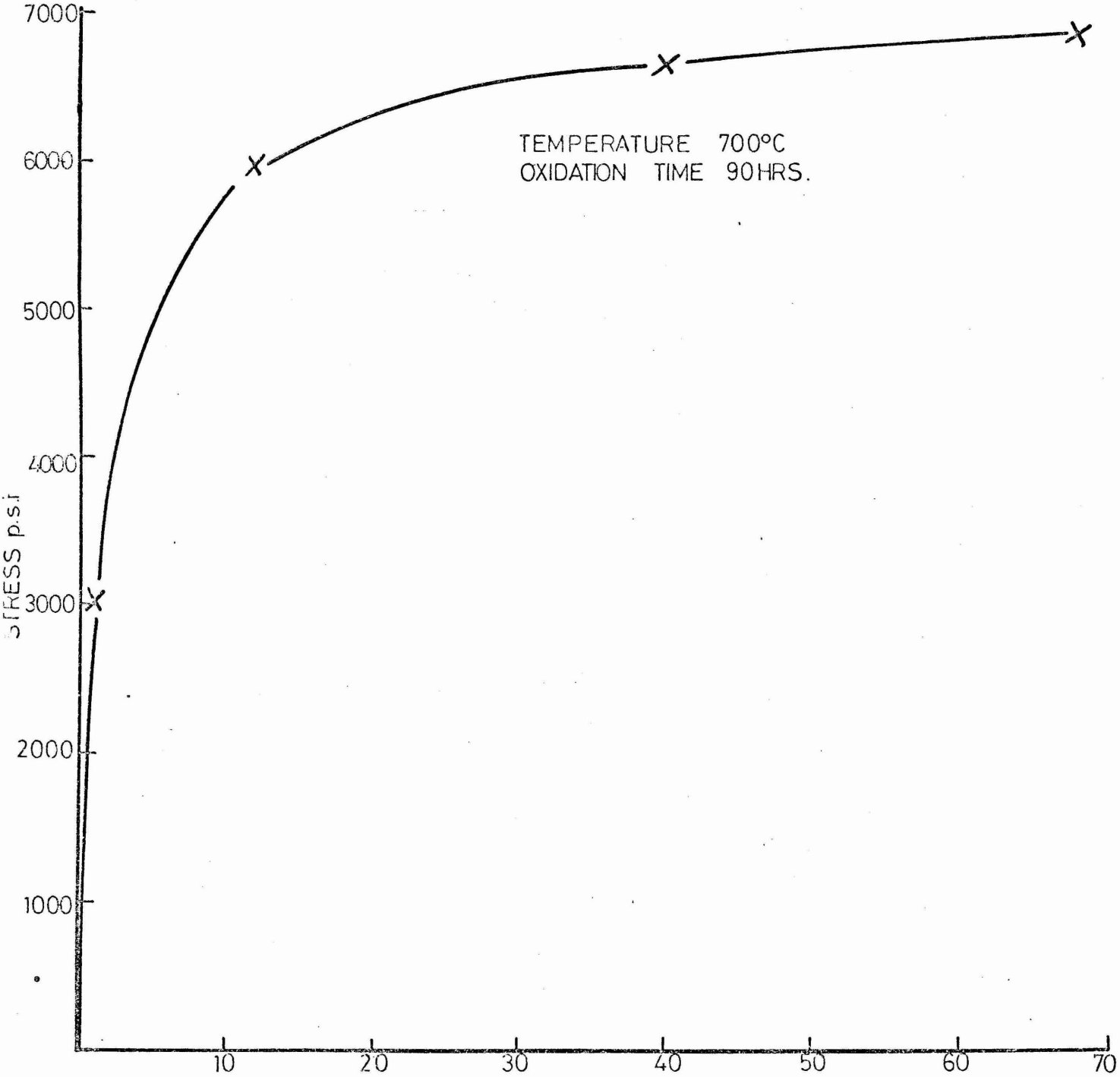

FIG. 3-19 TYPICAL RESPONSE OF EN2 SPECIMEN TO INCREASING STRESS

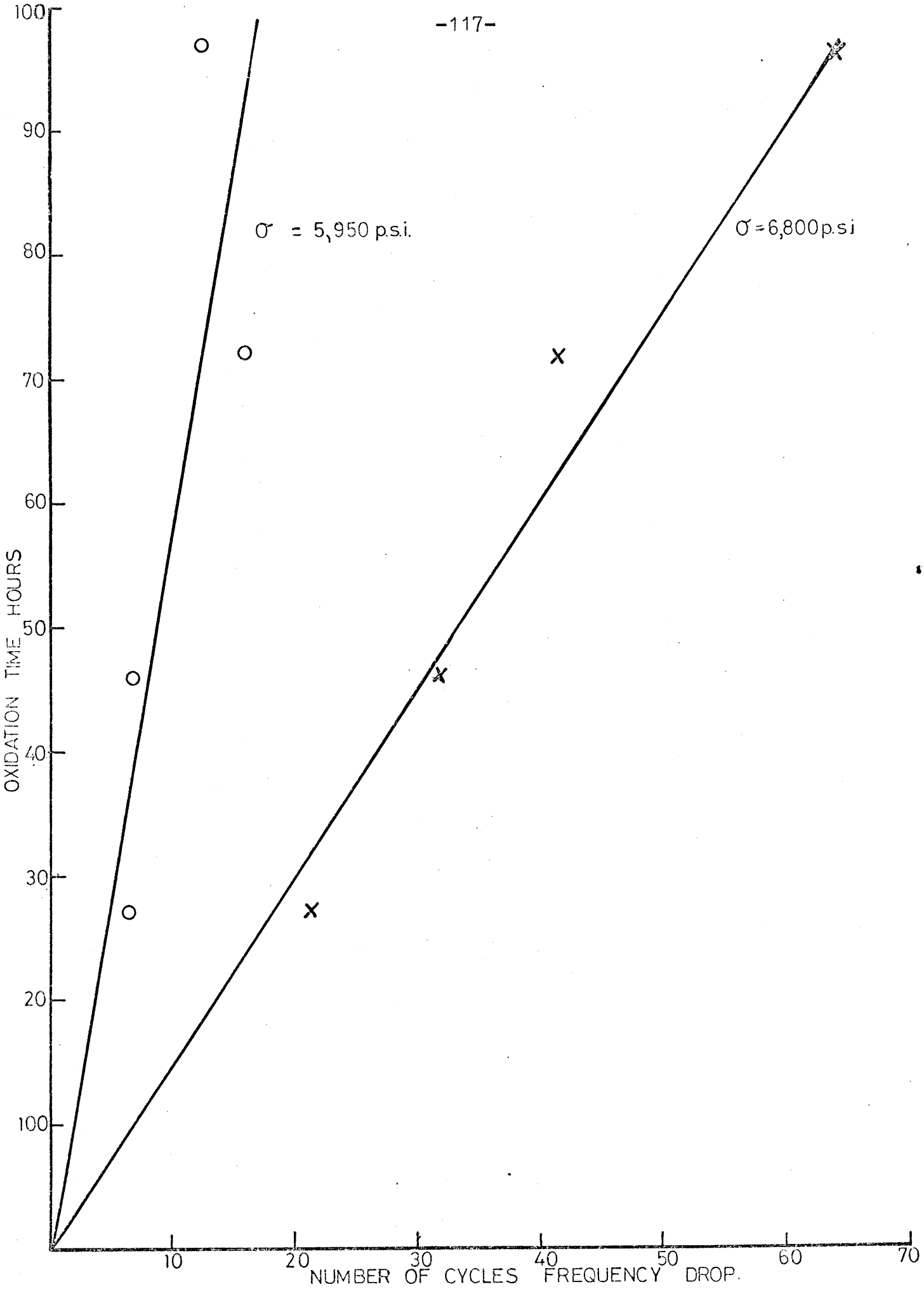

FIG. 3·20 EFFECT OF OXIDATION TIME ON FREQUENCY DROP AT 700°C

remain intact, and produces radial cracks spaced along the specimen length. It has been found that the crack spacing remains virtually constant for any stress level, and that the majority of cracks extend through the complete oxide thickness. In this way oxidation time would affect the frequency drop only in as much as the oxide thickness cracked would be greater the longer the oxidation time. The form of cracking is shown metallographically for the EN2 steel in Fig. 3.21. which shows cracks in the bulk scale that have healed, and also shows another crack which has probably become enlarged during cooling. Metallography of all the specimens tested showed very similar types of cracking in all cases, some of the cracks had healed and some had not. The only obvious difference between the mild steel and the EN2 steel was that the mild steel specimens tested at 900°C showed extensive internal oxidation, particularly beneath the cracks in the bulk scale, and this was never observed in the EN2 steel. There was no evidence for any general damage occuring to the inner adherent scale on the EN2 steel.

The test conditions adopted for the bulk of the specimens,were to oxidise all specimens (suspended in position in the furnace), at 900°C for four hours and then either to test immediately at 900°C, or to drop the furnace temperature to 600°, 700°, 750°, or 800°C and to test immediately the temperature became equilibrated. In this way the potentially important variable of oxide thickness could be eliminated. Using the values of dynamic modulus of the steel shown in Fig. 2.28. and the loads required to cause major oxide damage, the strains to oxide cracking were calculated. These calculated strains, with the steel deforming elastically, are shown in Fig. 3.22., which indicates that at higher temperatures the oxide coating is able to withstand greater strains before fracture than at the lower temperatures.

As has been discussed previously it proved to be very difficult to determine or calculate strains to oxide failure once the steel had been plastically deformed. The figures that were obtained using the Nimonic calibration varied from 0·577% to 1·05% strain, having no obvious relationship with temperature. All of these strains naturally produced major falls in resonant frequency, far in excess of what might be expected due to the change in length of the specimen. If we assume that the radius is not appreciably altered during loading it follows that:-

$$f^2 \propto k \frac{1}{l^3} \quad \text{where k is a constant}$$

On this basis with all of the extension occuring on a $4\frac{1}{2}$" guage length, a strain of 0·65% would produce a 5 cycle

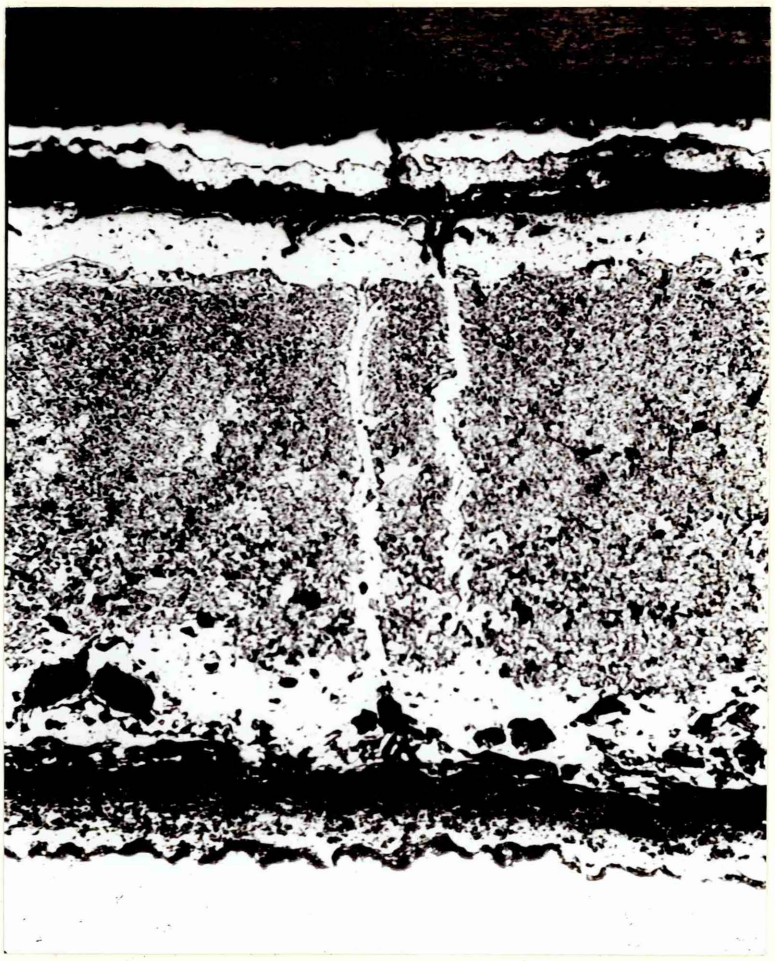

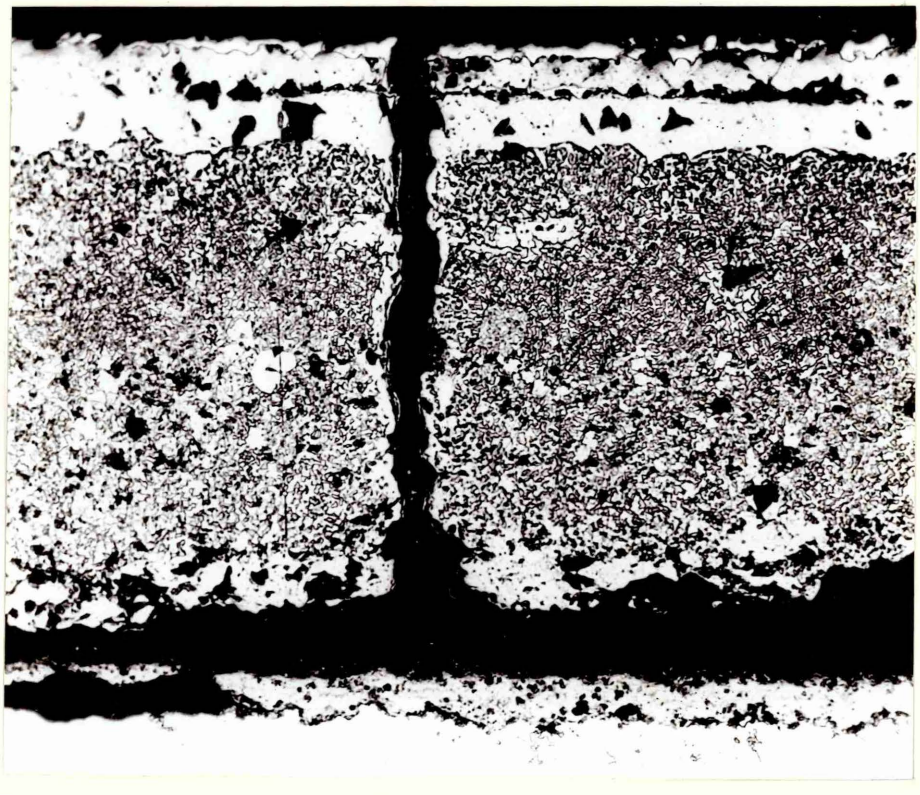

Fig. 3.21. Micrographs of cracks produced in oxide on EN2 steel by tensile loading (Mag. x 200)

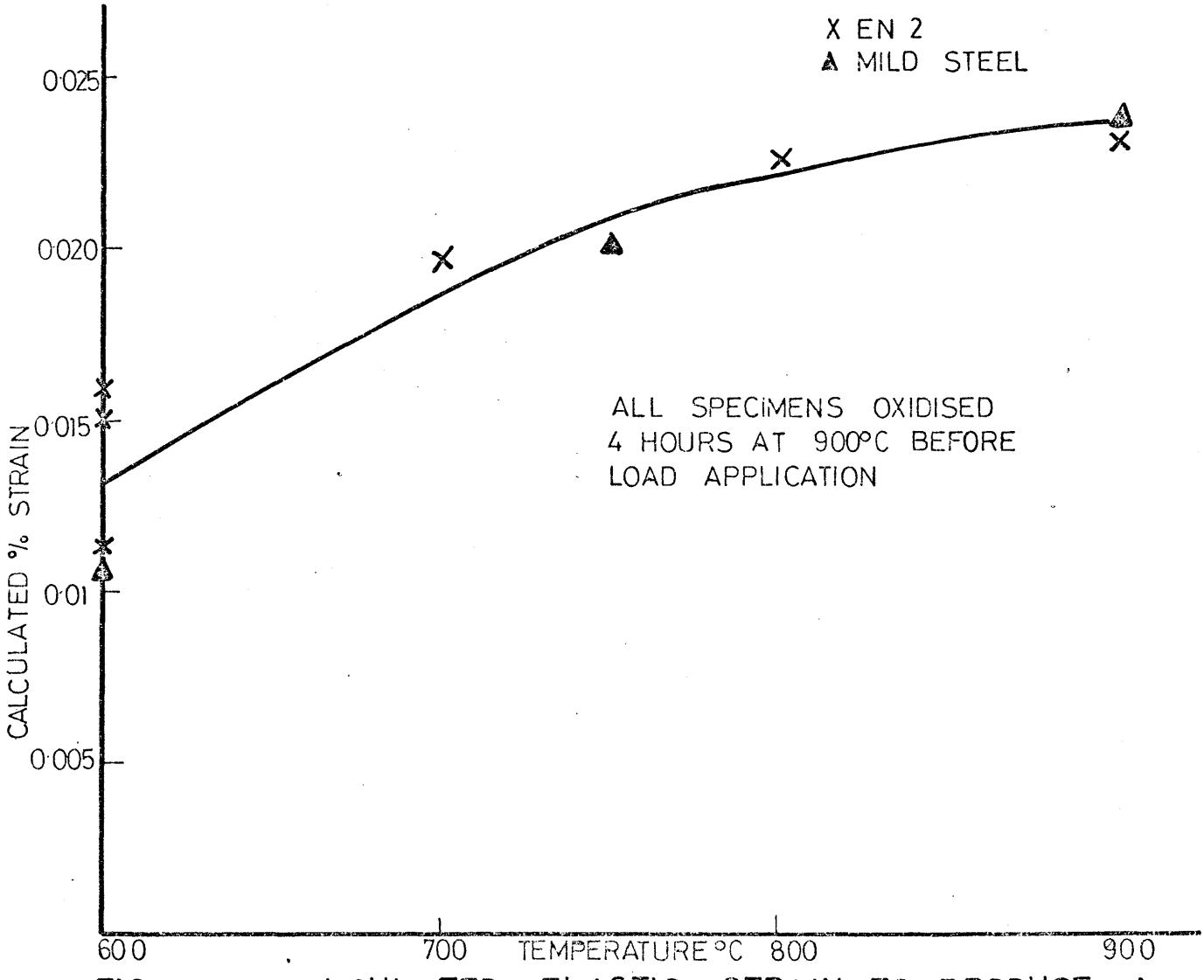

FIG. 3·22 CALCULATED ELASTIC STRAIN TO PRODUCE A FALL IN RESONANT FREQUENCY

drop in resonant frequency at 700°C. In fact the minimum fall in frequency produced by plastic extension of the specimen was 23 cycles, and falls of 40 - 50 cycles were not uncommon, so that the change in frequency observed could not be due only to changes in specimen length.

3.4. Summary and conclusions

The main points arising from the work described in this chapter may now be summarised. The effects of thermal stresses have been investigated using both thermobalance and vibration experiments. The thermobalance method relies on an increased rate of oxidation upon reheating to indicate oxide damage. It was therefore unable to generally detect any such damage on this EN2 steel which has an inner adherent protective scale, not normally disrupted by thermal shock. The vibration technique however could detect damage occuring during cooling by monitoring the form of the frequency change during cooling. This showed that the superimposition of the stresses due to the decomposition of FeO at around 570°C has a major disruptive effect on the scale. The suggested form of oxide damage during cooling is an extension of the detachment of the bulk scale from the inner scale, started isothermally, coupled with some cracking of the bulk scale.

Experiments concerned with the effects of specimen geometry have shown that oxide grown on a concave surface is generally thinner than that on a convex surface, due to the superimposition of the compressive geometry stresses. Oxides grown on the inside of cylinders has also been found to have considerable plasticity, substantiating the results of Vagnard (65) concerning the effects of stress system on the oxide ductility.

The method of monitoring oxide damage, due to imposed tensile loading, using the vibration technique has been found to be satisfactory. Oxide cracks normal to the interface are produced, being detected by the change in natural resonant frequency of the oxidised specimen. It has been shown that such a change in frequency is not due to any changes occuring in the steel. The method of measuring specimen strains using a Nimonic calibration has not been found to be suitable due to the excessive extension of the load application system employed. However, since load could be accurately determined it has been possible to calculate the strains by using the dynamic modulus values determined previously for the steel. This was of course only possible for elastic extension of the specimen, and the Nimonic calibration method was used to estimate maximum oxide strains to fracture in cases where the steel specimen had extended plastically. It was found that oxide cracking increases markedly at stresses greater than a certain

threshold limit of around 5000 - 6000 psi. The crack distribution has been found to depend on the stress level used, with most of the cracks extending right through the bulk scale layer. Since little increase in the rate of oxidation after loading was observed for either the EN2 or mild steels, it must be assumed that the cracks heal rapidly allowing only limited access of air to the steel surface. It has also been shown that with increased temperature a given thickness of oxide is able to withstand a greater strain prior to fracture, indicating the effect of temperature on oxide plasticity. Maximum strains to fracture measured, with the steel plastically deforming, have been 0·577 - 1·05%.

CHAPTER 4

4. THE EFFECTS OF CONTAMINANTS ON HIGH TEMPERATURE OXIDATION

4.1. Introduction

The influence of contaminants on the high temperature oxidation of metals and alloys is generally to accelerate the rate of oxidation. In particular, chloride and sulphate contamination of high temperature atmospheres has been shown to increase the oxidation of components operating in gas turbines, in coal or oil - fired boilers and in marine environments (15)(23). The influence of sodium chloride contamination on the mechanical failure of the scale on high temperature superalloys (96), and on Armco iron (101) has been investigated previously. The effects of sodium chloride and/or sodium sulphate on the high temperature oxidation of the irons and steels whose compositions are presented in Table 2 (P.36), was the purpose of this investigation. This investigation was carried out using a combination of several techniques which will be discussed separately.

4.2. Hot stage experiments

The equipment used was a standard Leitz hot stage as shown in Fig, 4.1.. This hot stage was mounted on a low power binocular microscope fitted with a 35mm. camera attachment as shown in Fig. 4.2.. This enabled the surface reaction occuring on the end of a specimen, during oxidation and corrosion, to be recorded. The specimens used were standard cylinders with dimensions of 7·64mm. diameter and length 18mm., with the end polished to $\frac{1}{4}\mu$diamond finish, ultrasonically degreased in trichloroethylene and rinsed in acetone prior to testing.

One grain of sodium chloride, when placed directly on the polished metal surface, produced a general attack beneath the oxide film formed during heating on all the materials tested. The oxide scale then grew and blistered as shown by Figs. 4.3. and 4.4.(EN2) and 4.5.(mild steel). In this work, as in the previous study (97), the effect of increasing temperature was always to increase the rate and extent of oxide blistering. Indeed, complete oxide failure by cracking or spalling always occured on cooling to room temperature from test temperatures above 801°C (the melting point of salt) whereas cooling from lower test temperatures did not necessarily result in oxide failure over the whole surface.

The actual mechanism of blistering which results from steel/chloride interaction, whether by pressure from volatile species formed such as oxychlorides, or more

Fig. 4.1. Leitz hot stage showing specimen in position

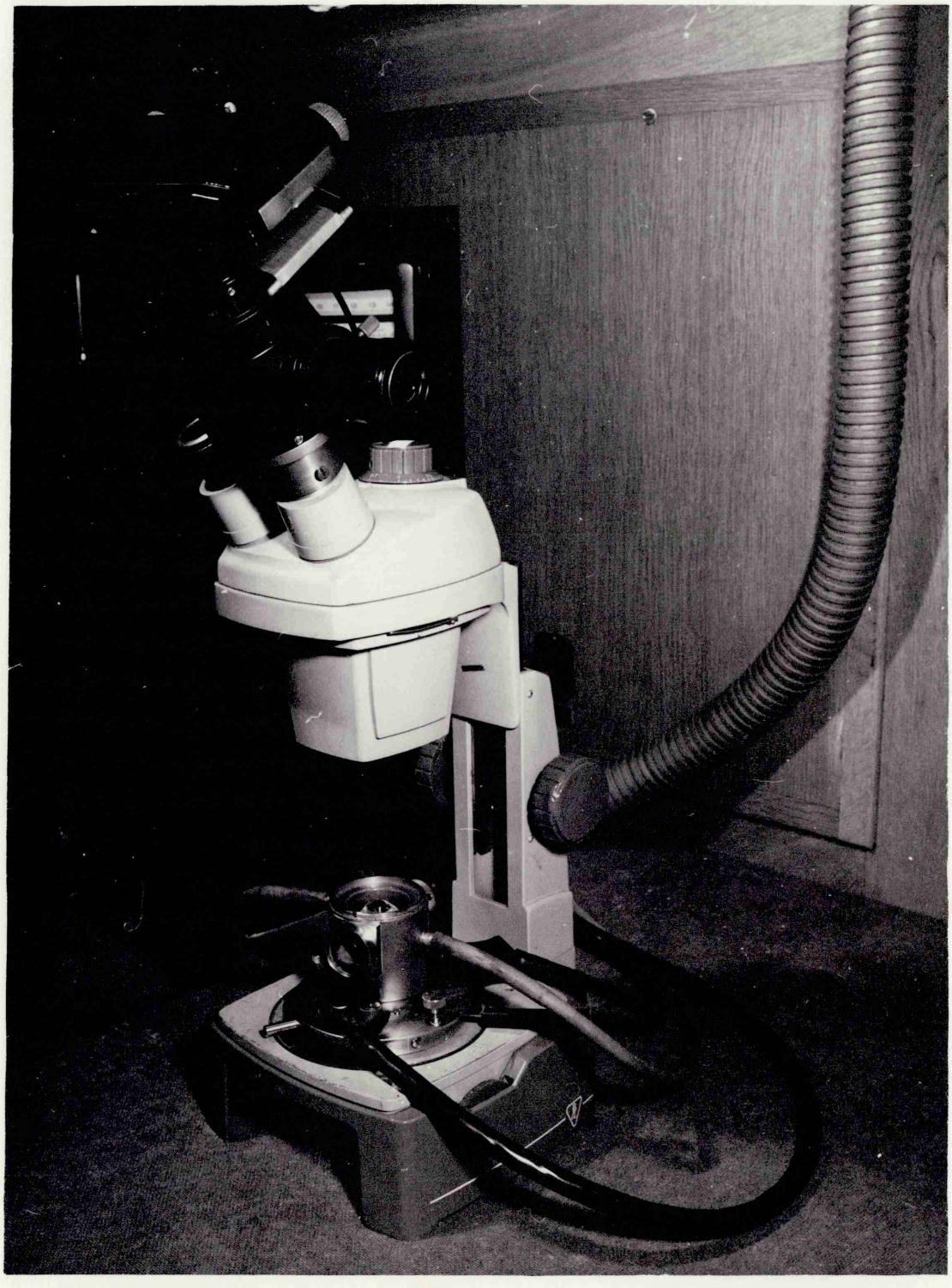

Fig. 4.2. Leitz hot stage fitted with camera attachment.

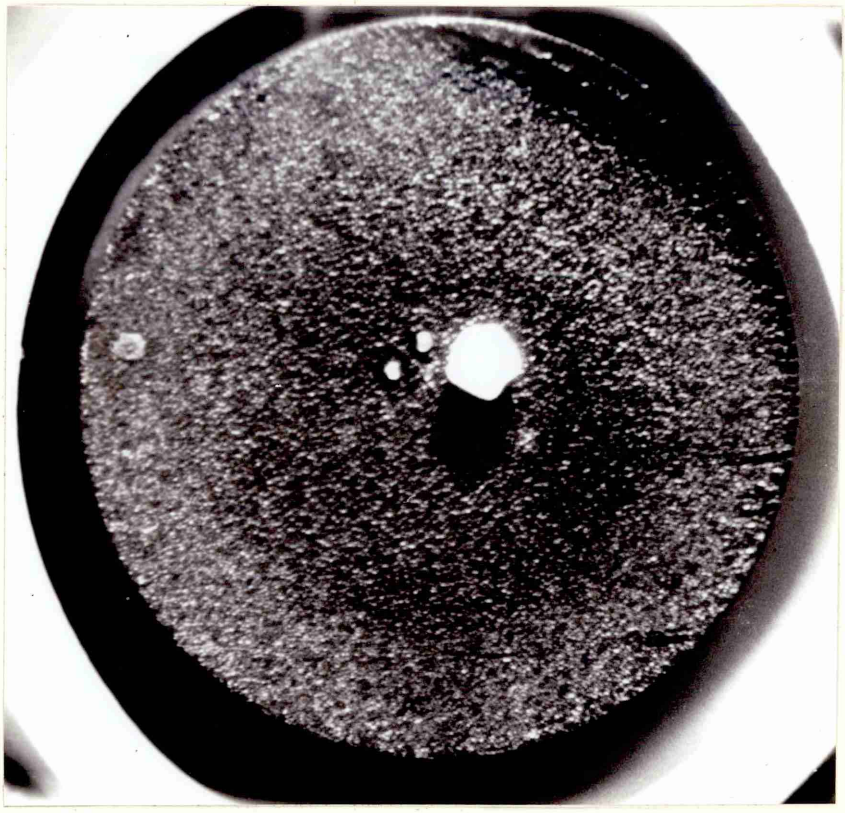

Fig. 4.3. NaCl on polished EN2, at 600°C during heating to 900°C (Mag. x 12)

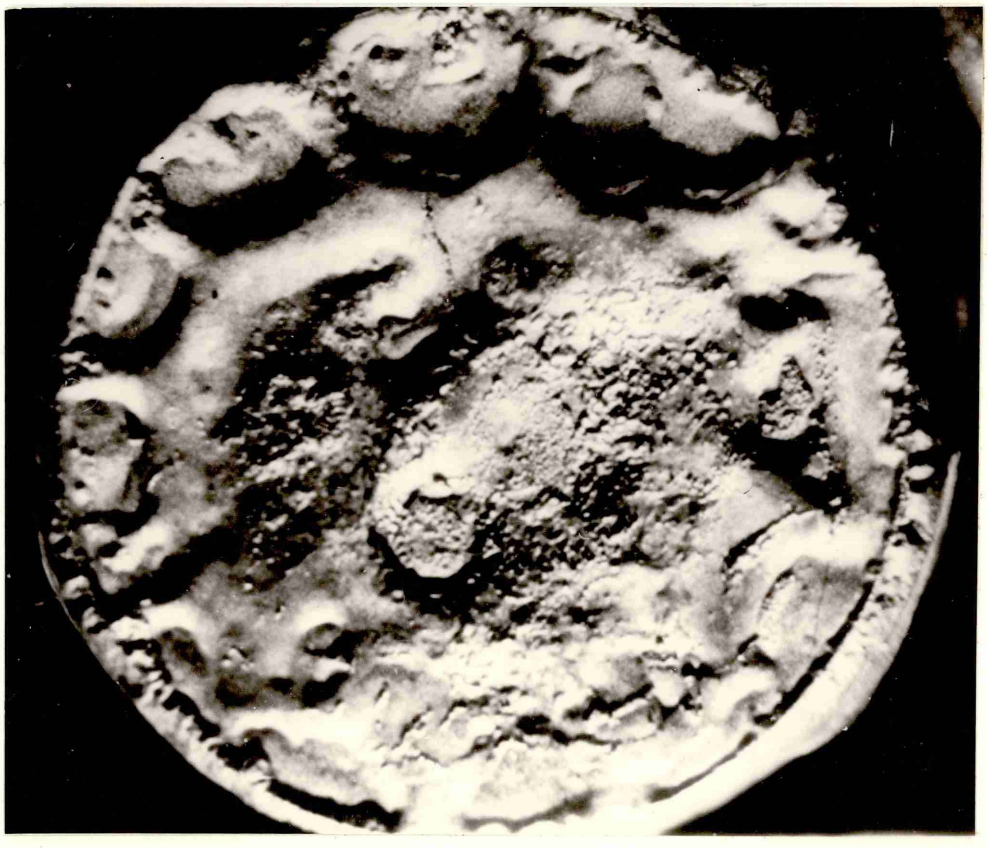

Fig. 4.4. Hot stage photograph of EN2 at room temperature after salt corrosion at 900°C (Mag. x 16)

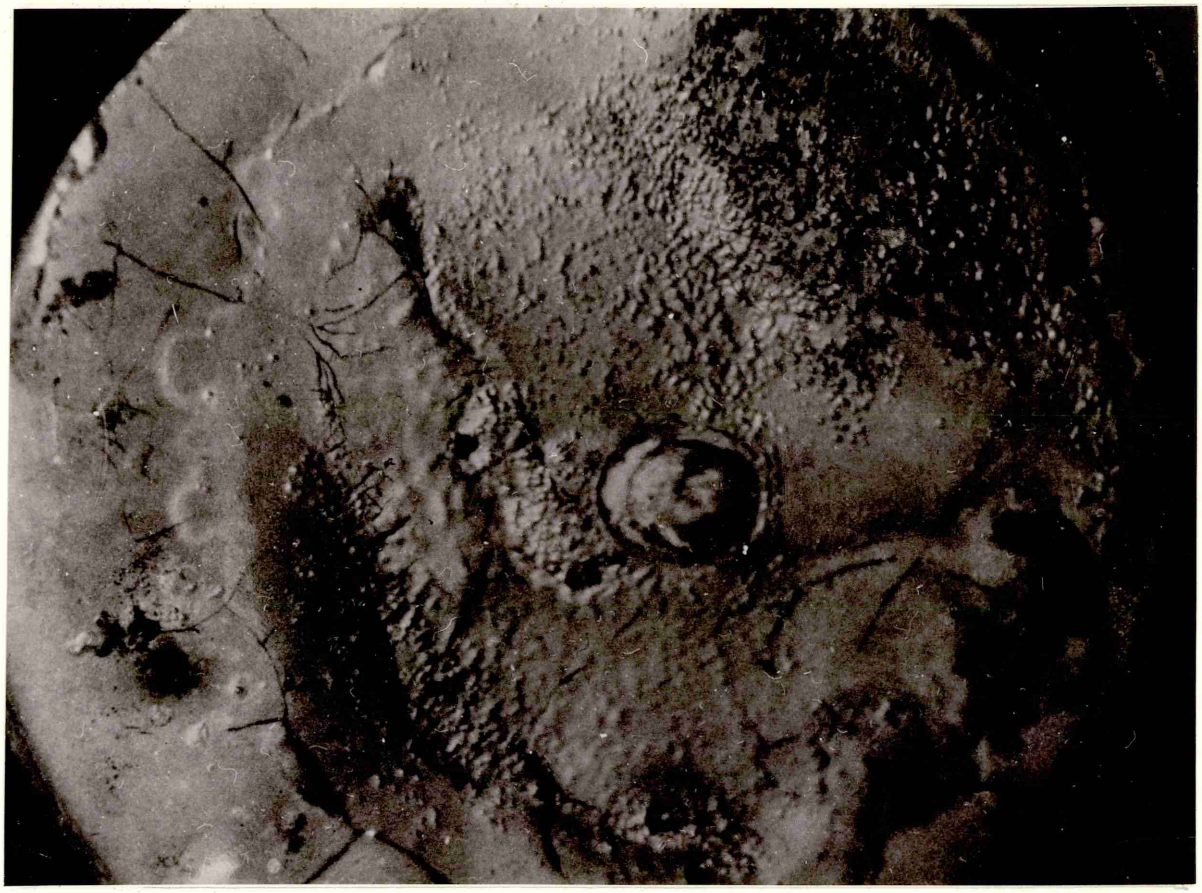

Fig. 4.5. Hot stage photograph of mild steel at room temperature after salt corrosion at 950°C (Mag. x 20)

simply due to evaporation of sodium chloride at the scale/metal interface, is subject to much conjecture (15)(23). It has been suggested that the anionic may be important in determining the extent of corrosion (48), and, in order to assess this possibility, the corrosive action of both potassium chloride and sodium nitrate was evaluated. It was found that potassium chloride had exactly the same effect as sodium chloride whereas sodium nitrate tended to be protective and apparently decreased the rate of oxidation. This strongly indicated that chloride was the active radical in the corrosion reaction.

In order to evaluate the protection rendered by surface scales in preventing access of sodium chloride to the metal surface the mild steel was preoxidised for two hours at 850°C prior to salt attack in the hot stage. A blistered scale was observed, even on this preoxidised specimen, and a longitudinal section beneath the blister was examined metallographically, Fig. 4.6., and it will be noted that no part of the scale adheres to the metal. The distribution of chlorine across this section, as determined using electron probe microanalysis, is shown in Fig. 4.7. where it can be seen that a high concentration of chlorine was found at the metal surface after corrosion at 700°C, for example, indicating that the scale on this steel was not impervious to the salt. However this is not surprising for it has been shown in this work, and previously (54), that the oxide on Armco iron and mild steel cracks continually during growth.

The influence of preoxidation was then evaluated for the EN2 steel. The extent of preoxidation, using the hot stage microscope, ranged from 15 minutes at 680°C, to three hours at 950°C, in air. The addition of small amounts of NaCl resulted in no visible effects on the scale at test temperatures up to 950°C even for the least preoxidised specimen. This is in direct contrast to the behaviour of mild steel described above.

The effect of sodium sulphate during the oxidation of the EN2 steel has also been evaluated. Crystals of sodium sulphate, placed on a polished metal surface, produced attack of the steel and svere blistering, Fig. 4.8., but the attack of the steel was to a lesser extent than that produced by sodium chloride. The combination of chloride and sulphate, Fig. 4.9., on the polished surface resulted in greater attack than either contaminant acting alone, because the chloride has a definite fluxing effect on the sulphate, the mixture melting at around 700°C. Similarly to chloride alone, the sulphate produced no detectable corrosion on preoxidised specimens, although electron probe microanalysis again confirmed a high concentration of contaminant in the gap between the inner adherent scale and the outer bulk scale. The sulphur distribution is

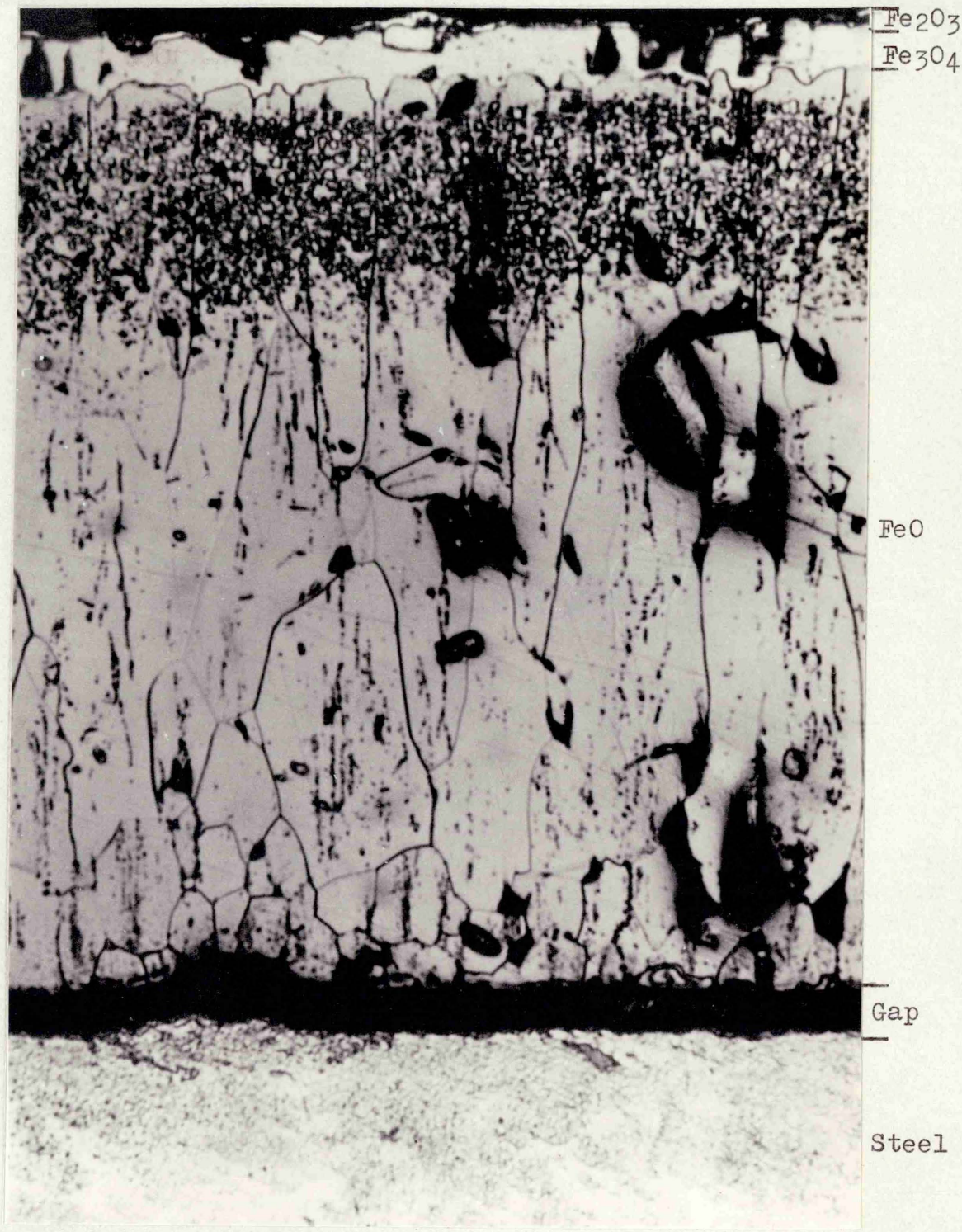

Fig. 4.6. Micrograph of mild steel after salt attack at 700°C on preoxidised specimen (Mag. x 350)

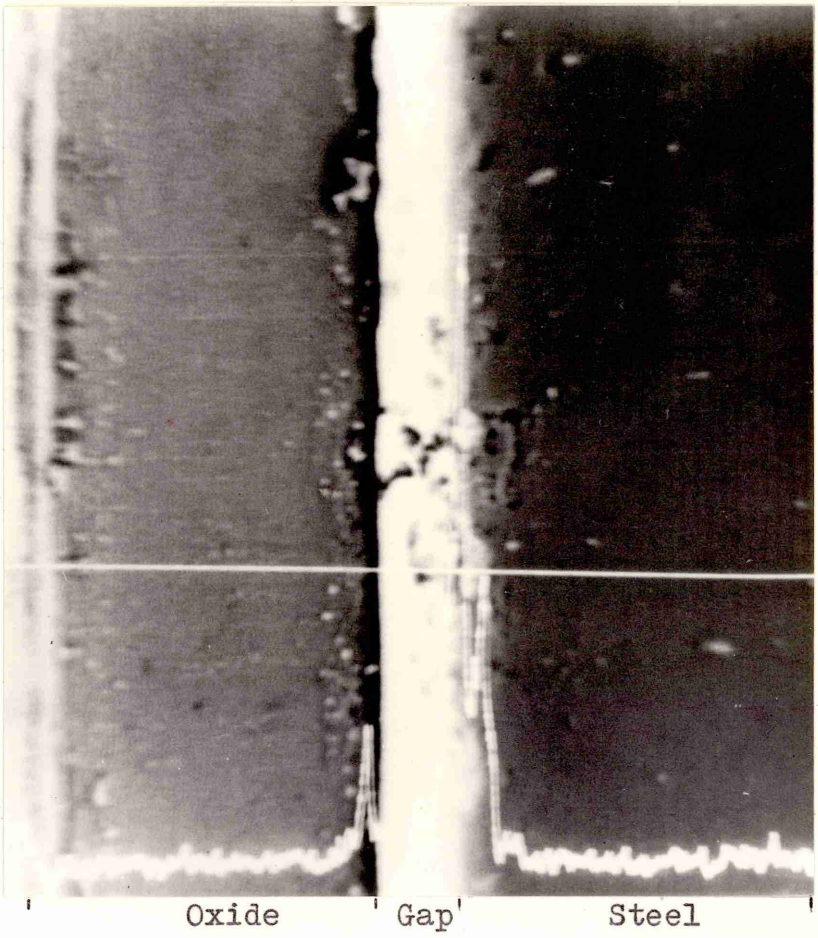

Fig. 4.7. Electron probe microanalysis trace of chlorine across oxide on mild steel corroded at 700°C (Mag. x 400)

Fig. 4.8. Hot stage photograph at room temperature after sodium sulphate corrosion at 900°C (Mag. x 11)

Fig. 4.9. Hot stage photograph at room temperature after sodium chloride plus sodium sulphate corrosion at 900°C (Mag. x 15)

shown in Fig. 4.10. together with the relevant electron image.

Metallographic examination of a longitudinal section in the specimen, through the point on the surface where the contaminant grains were placed, showed that the metal surface was apparently unattacked for both sodium chloride or sulphate, Fig. 4.11. This shows the presence of the thin inner oxide layer of the order of six microns, adherent to the metal surface, and this layer was not observed on the mild steel, Fig. 4.6.. Stereoscan photographs showing this inner adherent layer are shown in Fig. 4.12., and Fig. 4.13..

The gap between the bulk scale and the thin adherent scale in the EN2 specimen could have been produced during preoxidation or during cooling due to stress relief by detachment of the bulk scale. However, metallographic examination across the scale after preoxidation revealed this gap, but no magnetite layer on either side. This shows that the bulk scale became detached during cooling after preoxidation, and subsequent reheating for the corrosion test resulted in further oxidation of the FeO around the gap, producing magnetite as shown in Fig. 4.11..

This distribution of chloride across the scale after salt attack was again determined using electron probe microanalysis and the electron image is shown in Fig. 4.14., together with the chlorine distribution. It can be seen that a high concentration of chloride is present in the gap between the adherent oxide layer and the bulk scale. This shows that the chloride passed through the porous outer scale, but could not penetrate the inner, adherent compact layer. The distribution of contaminant was also verified by an X ray diffraction technique which analysed the surface of a previously preoxidised specimen after exposure to salt at 700°C. Layers of oxide were systematically removed and the only diffraction lines of a compound containing a chloride radical which were detected were those pertaining to sodium chloride. These results show that sodium chloride penetrated the outer scale but was prevented from reacting with the base metal by the inner adherent layer.

For enhanced corrosion resistance this layer must be maintained throughout service life. The ability of the layer to remain protective by withstanding strains such as those induced by thermal shock, is therefore of considerable importance. Failure of the inner adherent layer on cooling from the preoxidation temperature was not observed metallographically, and was also confirmed by the thermal shock experiment detailed in Chapter 2. Moreover, no further corrosion was observed whether salt crystals were added to the surface oxide at room temperature, and the specimen reheated, or when added at the test temperature. The addition of salt at room

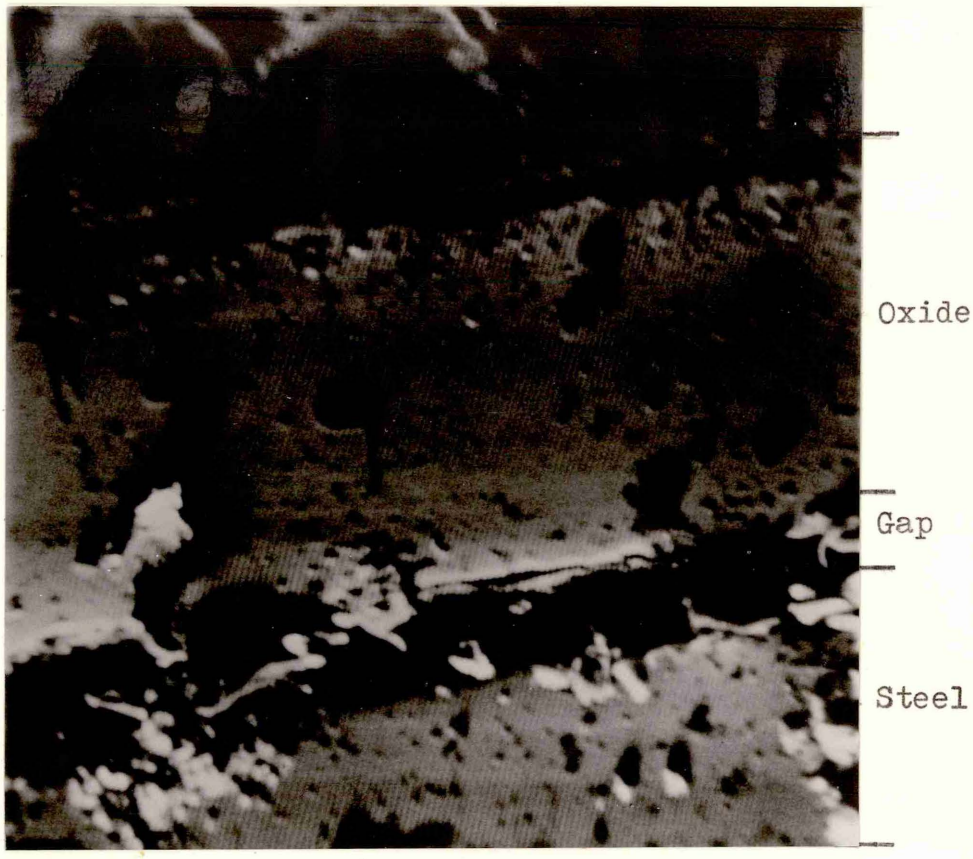

Electron image (Mag. x 350)

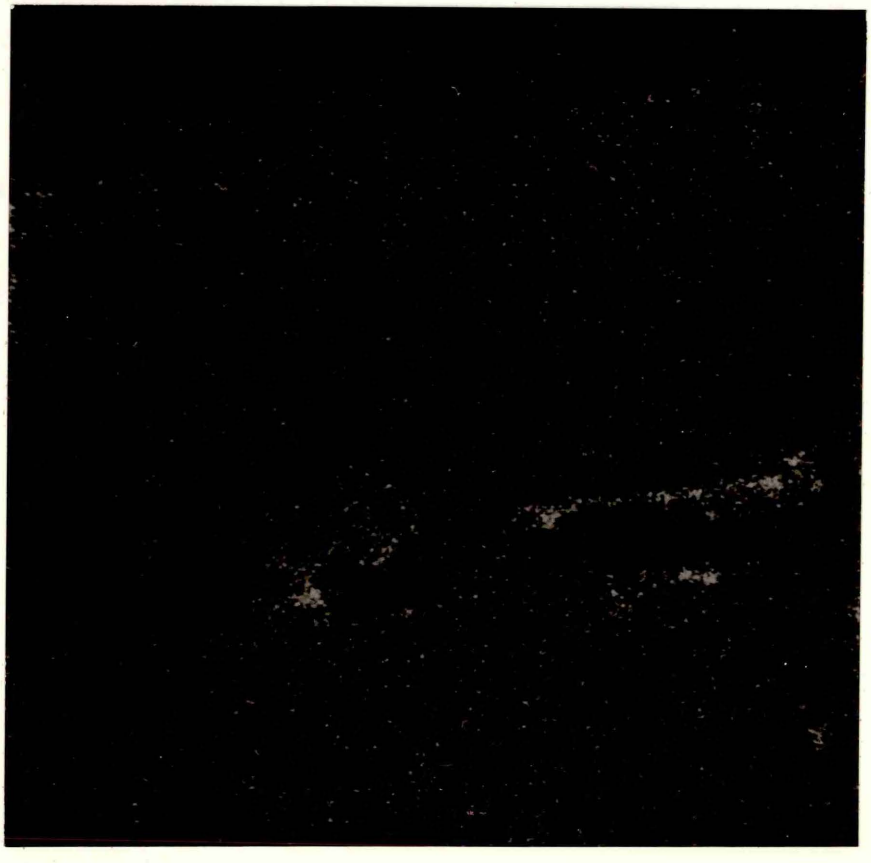

Fig. 4.10. Sulphur distribution in EN2 steel treated with sodium sulphate at 800°C

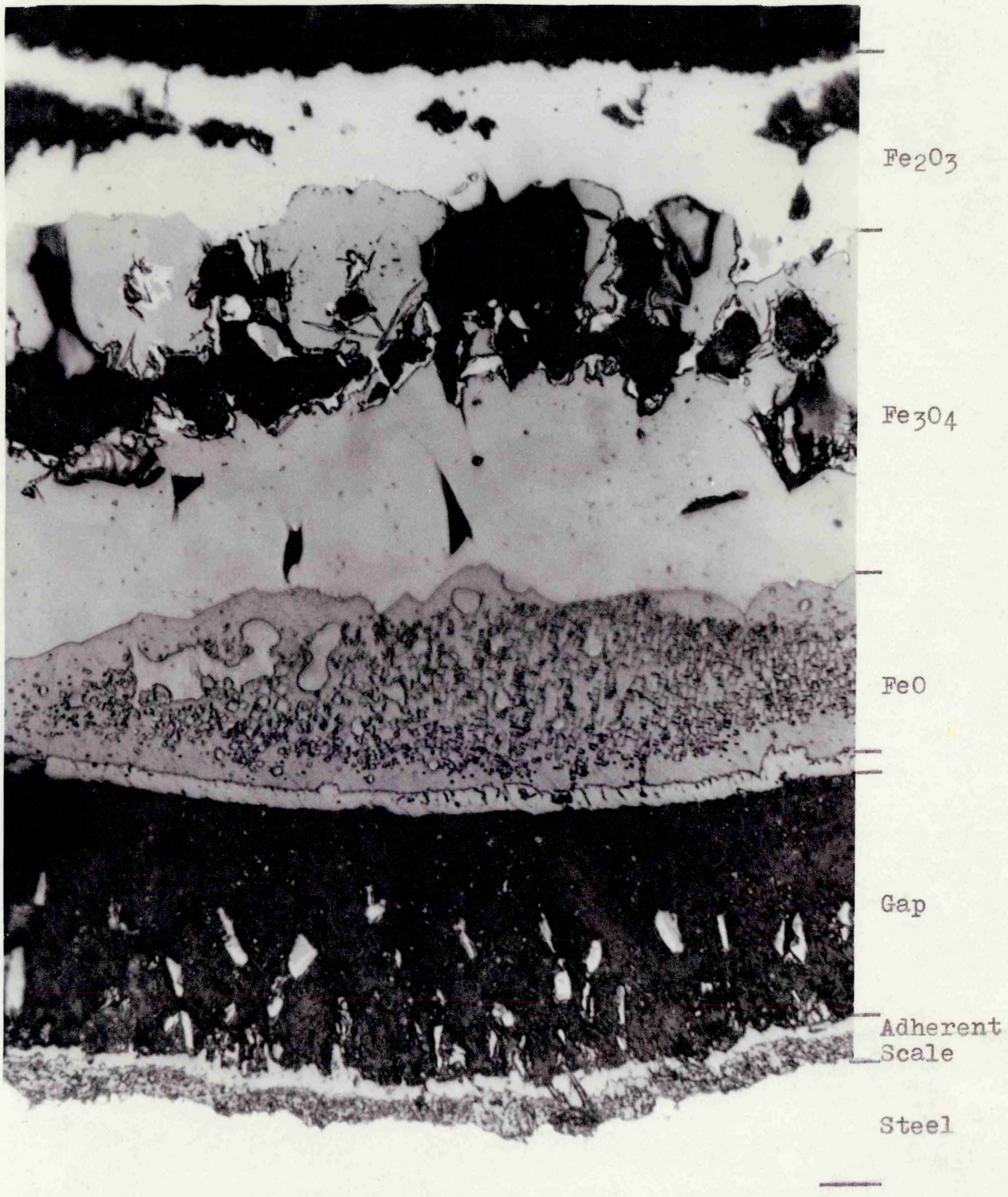

Fig. 4.11. Longitudinal section of preoxidised EN2 steel after salt exposure at 700°C (Mag. x 350)

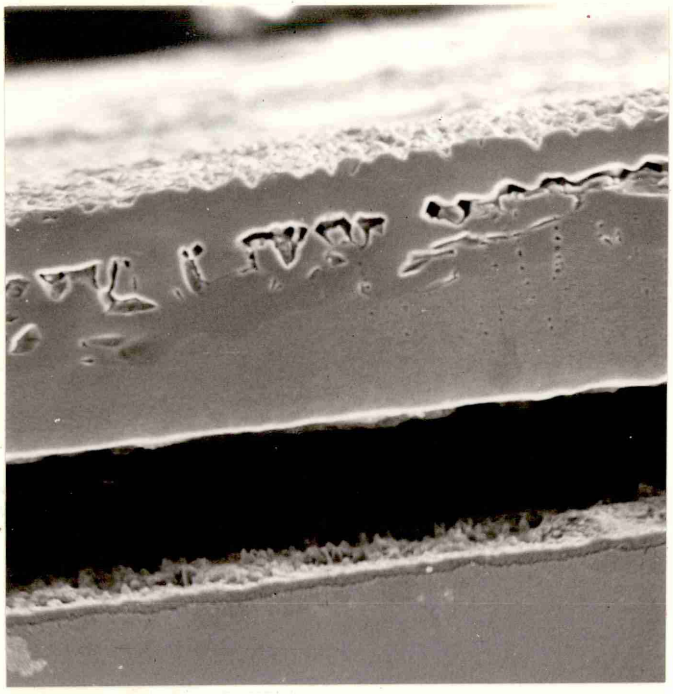

Fig. 4.12. Stereoscan of oxide on EN2 steel oxidised at 800°C (Mag. x 272)

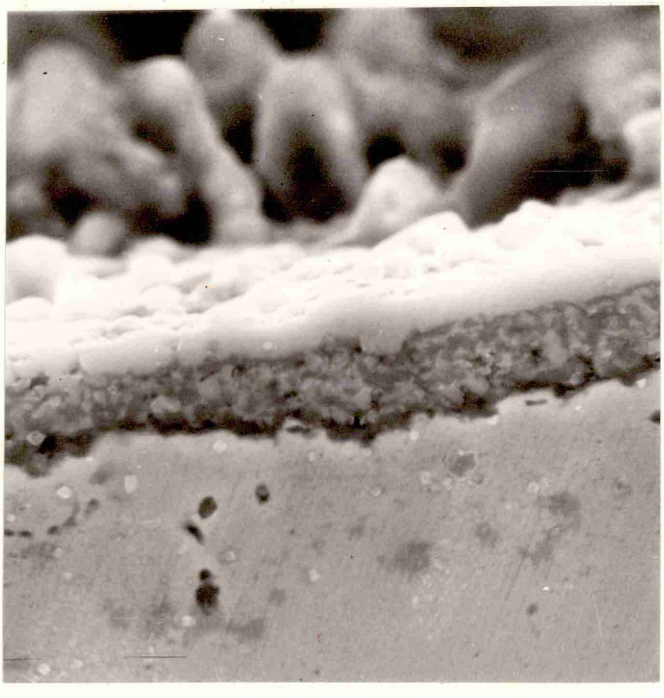

Fig. 4.13. Stereoscan of inner adherent layer on EN2 steel (Mag. x 2720)

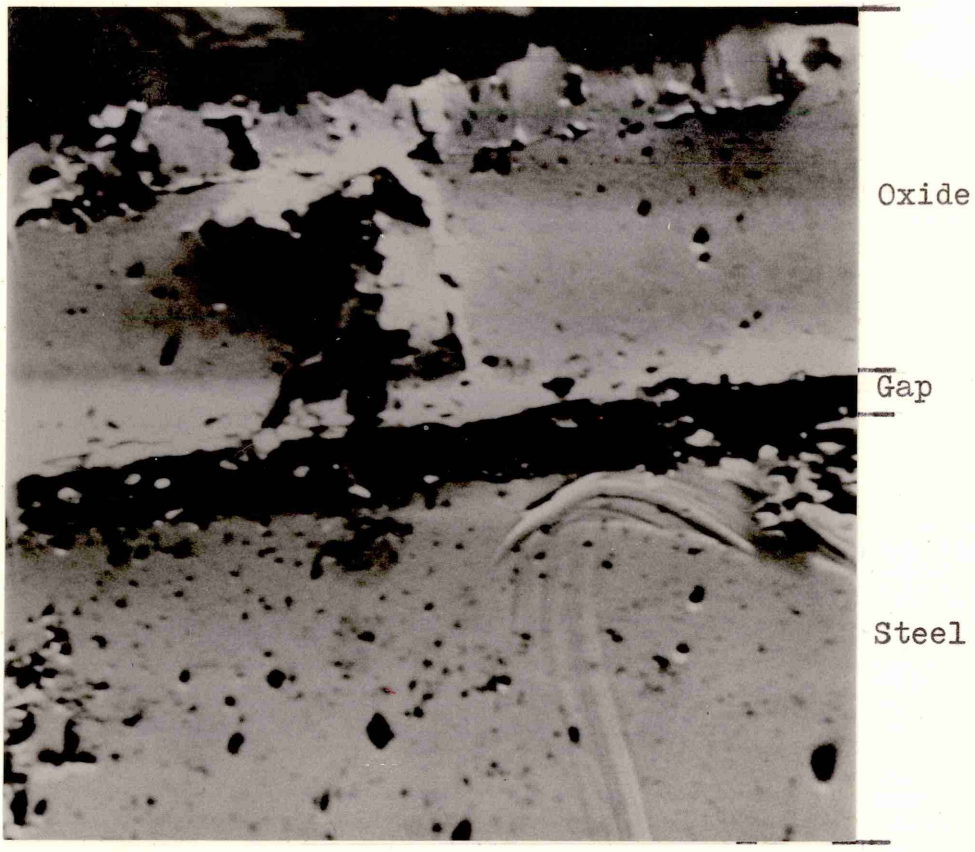

Electron image (Mag. x 350)

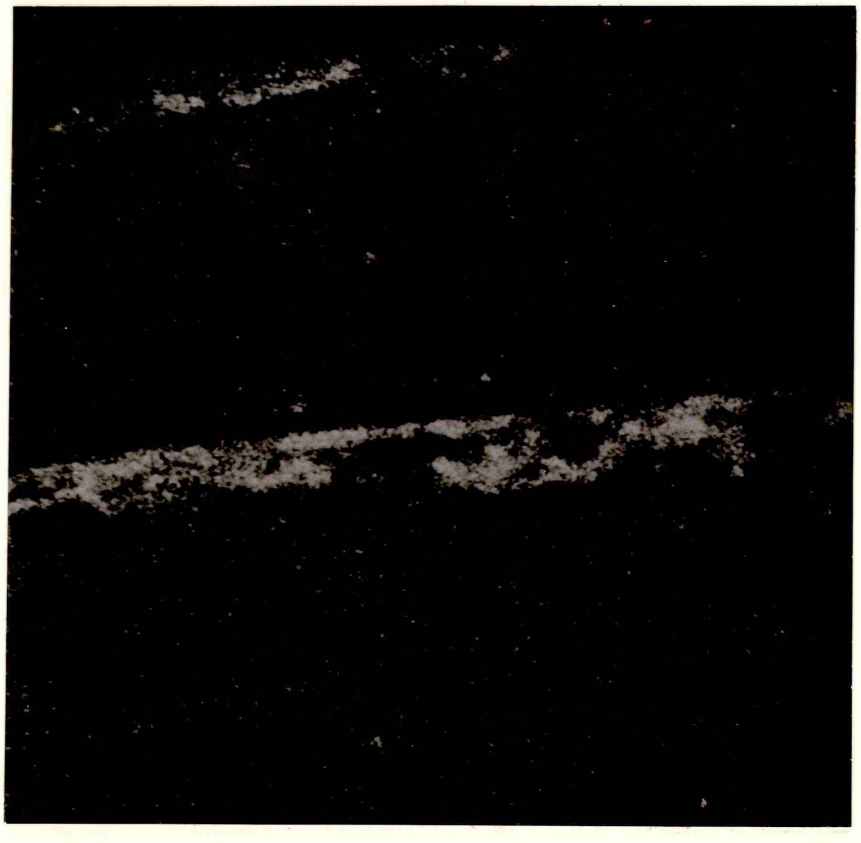

Fig. 4.14. Chlorine distribution in EN2 steel treated with sodium chloride at 800°C

temperature would be expected to reveal the presence of cooling cracks if they were present, by causing increased corrosion on reheating, but this was not found with EN2 specimens.

Electron probe microanalysis indicated that the inner adherent oxide layer contained a larger concentration of nickel and silicon than the base steel. The silicon distribution was not uniform along the adherent scale, but was concentrated in discrete areas with the remainder of the scale having a silicon content of about the same as the steel. The nickel enrichment was uniform along the length of the inner oxide layer and a typical microprobe trace of nickel concentration across the inner scale layer is shown in Fig. 4.15..

Other investigators (75)(102) have noted a nickel rich inner scale, but usually on steels containing greater than 1% nickel. Indeed, it is well known that nickel promotes mill scale adherence which results in problems associated with scale removal during processing. Although the EN2 steel used in the present work contained very small amounts of nickel, the work of Peters and Engell (84) has suggested that less than 0·4 wt.% of other elements can have a marked effect on the adherence of scales on iron. It may also be noted that Peters and Engell showed that 0·16% silicon produced a reduction in metal/oxide adherence. Hence, although it has not been possible in the present work to differentiate conclusively between the effects of nickel and silicon, the distribution of these two elements in the inner scale together with evidence from other researchers, suggests that the presence of nickel is the more probable explanation for enhanced adhesion of the inner layer.

Small concentrations of nickel in the adherent layer may enhance thermal shock resistance, by three different mechanisms. Firstly, it may increase adherence by producing nickel rich filaments at the steel/scale interface (75)(102). Secondly. it may improve the scale plasticity thereby inhibiting crack propagation and enhancing resistance to spalling. In fact, increased scale plasticity has been suggested (53) as a possible reason for the improvement in thermal shock characteristics of the oxides on Fe/Cr alloys when nickel is present (103). Finally it may improve the spalling resistance of the interface during thermal shock. This arises from disparity in the coefficients of thermal expansion of the metal and the oxide, and the thermal expansion coefficients of nickel ($17{\cdot}6 \times 10^{-6}/^{o}C$) and nickel oxide ($17{\cdot}1 \times 10^{-6}/^{o}C$) are greater than that for FeO ($12{\cdot}2 \times 10^{-6}/^{o}C$ (59). Hence the presence of nickel or nickel oxide in the scale near the scale/metal interface may result in an increase in the effective coefficient of expansion of the adherent scale layer

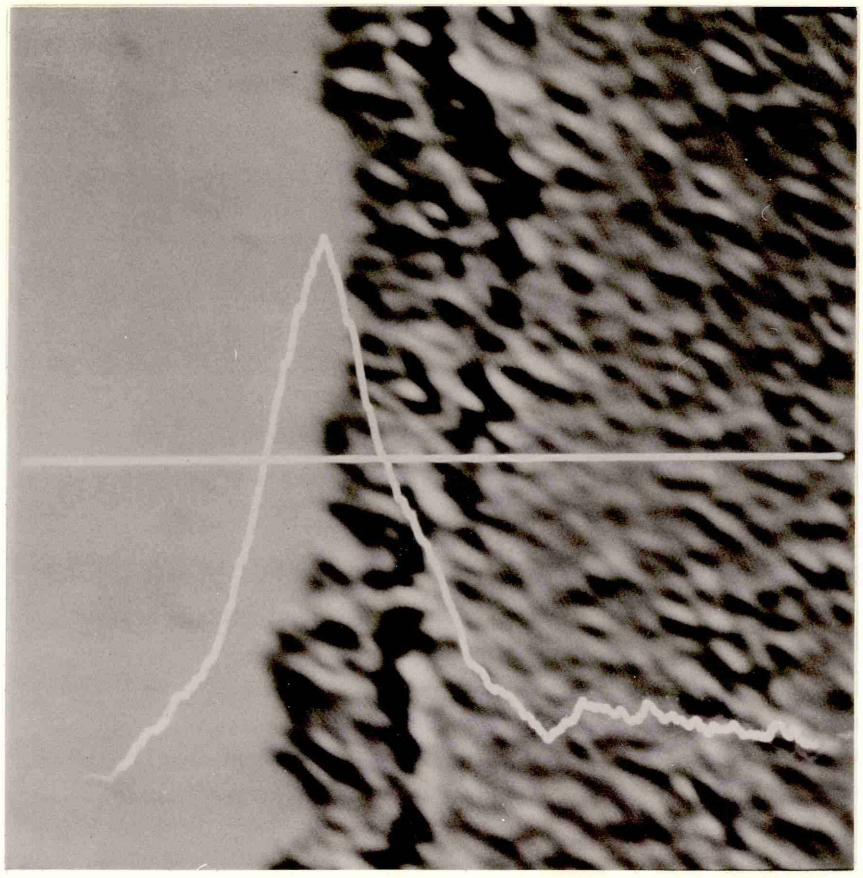

Fig. 4.15. Electron probe microanalysis trace of nickel across inner adherent scale on EN2 steel (Mag. x 1200)

towards that of Fe which is 15 x $10^{-6}/^{o}C$, and the consequent interfacial strain could be reduced.

4.3. Corrosion of vibration specimens

The hot stage microscopy tests yield valuable qualitative evidence of the difference in corrosion behaviour exhibited by steels of similar composition. The vibration technique was expected to yield further evidence of the disparity between the oxides on the two steels by examining their mechanical properties and adhesion.

The change in resonant frequency Δf, of a cylindrical specimen was followed during oxidation and, once a trend had been established, usually after three or four hours, a combustion boat containing sodium chloride was inserted into the furnace directly beneath the specimen. In the investigation of the corrosion resistance of Armco iron (97), this introduction of salt caused an immediate large fall in frequency at temperatures in the range 600° - 780°C. The authors showed that such discontinuity in frequency response could only occur if the mechanical properties of the oxidised specimen suddenly changed by some disruption of the oxide. Hot stage microscopy revealed that disruption was usually by failure of the scale/metal interface, resulting in blistering.

Using the present EN2 steel, no change in frequency was observed either, instantaneously, on the introduction of salt or, subsequently in terms of change in the rate of scaling. A total of 20 tests were carried out over the temperature range 650° to 900°C at times up to 75 hours including repeated salt insertions and some representative results shown in Fig. 4.16. confirm the hot stage observations in that mechanical disruption of the scale by the salt was not detected. As mechanical failure of the oxide is usually by blistering and decohesion, the vibration results again indicate the effectiveness of the inner adherent oxide layer in restricting access of the salt to the metal surface even though it is capable of passing through the porous bulk scale.

As a comparison, Johnson Matthey "Specpure" iron specimens and mild steel specimens were also tested using the vibration technique. Following admission of the salt, the natural resonant frequency of the pure iron specimen fell significantly, producing a marked discontinuity in the isothermal frequency response which is indicative of oxide damage. A typical example of the frequency/time trace is also shown in Fig. 4.16..Similar results were obtained using sulphate instead of chloride as the contaminant.

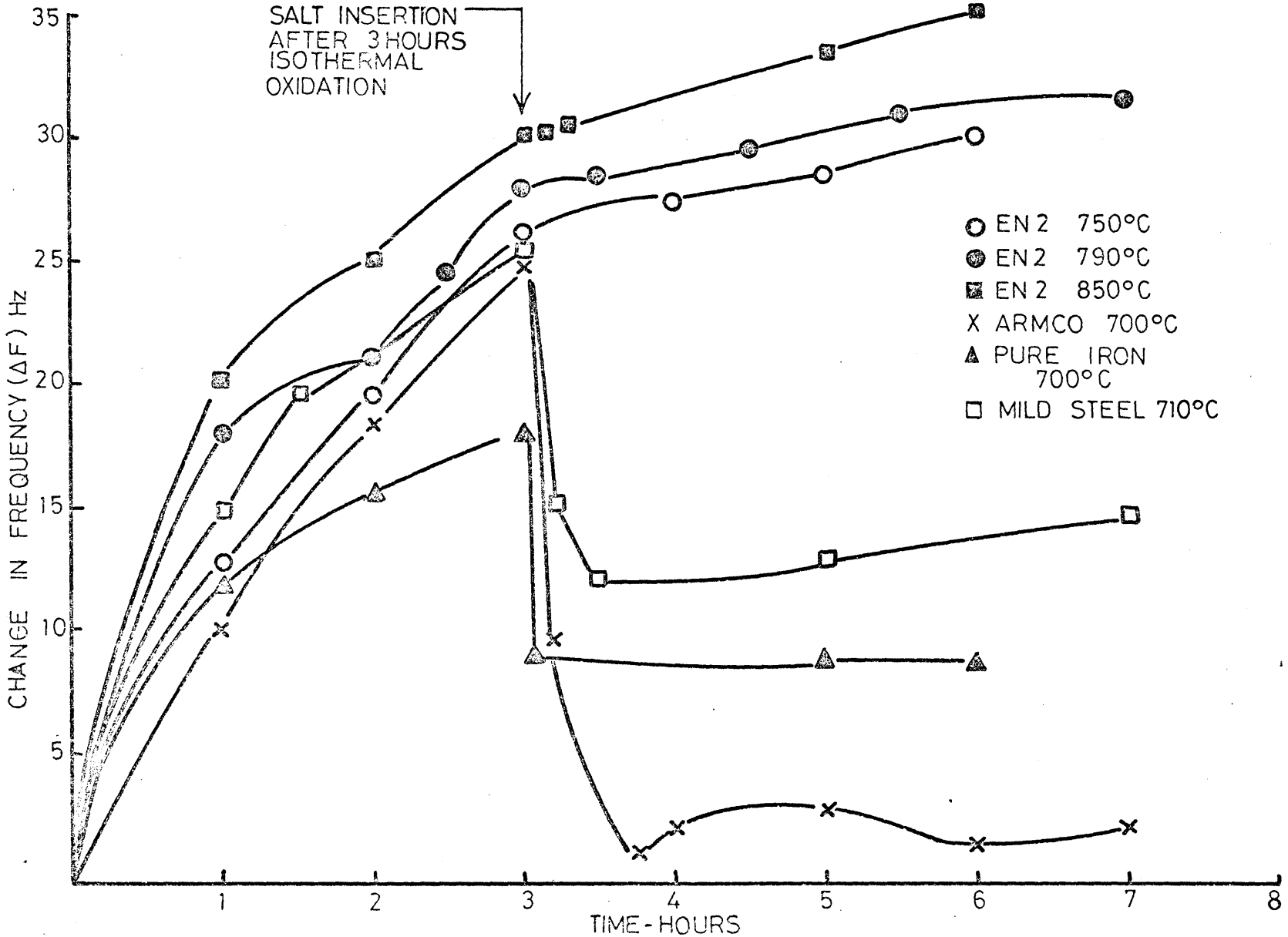

FIG.4·16 THE EFFECT OF SALT CONTAMINATION ON THE NATURAL RESONANT FREQUENCY OF IRON AND STEEL DURING OXIDATION

4.4. Salt vapour exposure tests

The previous tests determined the cause of enhanced corrosion resistance of EN2 steel in terms of the adherence of a thin, mechanically sound scale layer at the metal surface. A quantitative assessment of the degree of protection against sodium chloride, offered by the scale on the EN2 steel, was accomplished by means of simple exposure tests.

Weighed specimens of pure iron and the EN2 steel were preoxidised for the same times at temperatures of 600°, 700° and 800°C and subjected either to further oxidation or to sodium chloride vapour corrosion. The specimen weight losses were determined, after descaling, at the end of each test, and the average of results from a minimum of three identical tests are shown in Figs. 4.17. to 4.21.. The specimen weight losses after preoxidation were computed from weight gain using factors obtained from separate descaling tests. It may be seen in Fig. 4.21. that protection at 900°C is not complete, because at this temperature metallography shows that the inner adherent layer has become partly undermined by void formation. However, even at this temperature, this figure shows more protection relative to the pure iron is afforded by preoxidation of the EN2. Thus the behaviour of the EN2 steel at all temperatures up to 900°C is in direct contrast to the behaviour of pure iron, under identical conditions, which showed an accelerated rate of attack when exposed to the sodium chloride vapour.

The influence of preoxidation on resistance to corrosion was emphatically confirmed by inserting non-preoxidised specimens into the chloride vapour. The weight losses of the non-preoxidised EN2 specimens, determined after descaling, were greater than those for specimens which had been oxidised and then corroded, even though the total exposure time was less (Figs. 4.17. to 4.21.). The same tests on pure iron specimens reveal that preoxidised specimens offer little or no, advantage over non-preoxidised specimens in resisting sodium chloride attack. No reaction was detected when samples of iron oxide were heated for long periods in molten sodium chloride and/or sodium sulphate.

Some further work was carried out using apparatus developed by Johnson (104) on this EN2 steel, in which polished specimens were coated with a thin layer of either sodium chloride or sodium sulphate, and heated for one hour in either oxygen-free argon or air. It was found that again preoxidising for two hours at 900°C was effective in preventing corrosive attack, and the only effect noted was some spalling of the scale after exposure to sulphate in an argon atmosphere. Of the non-preoxidised samples the most severe attack was produced by sulphate in an argon atmosphere, which attacked in a uniform pitting manner beneath a deep black voluminous

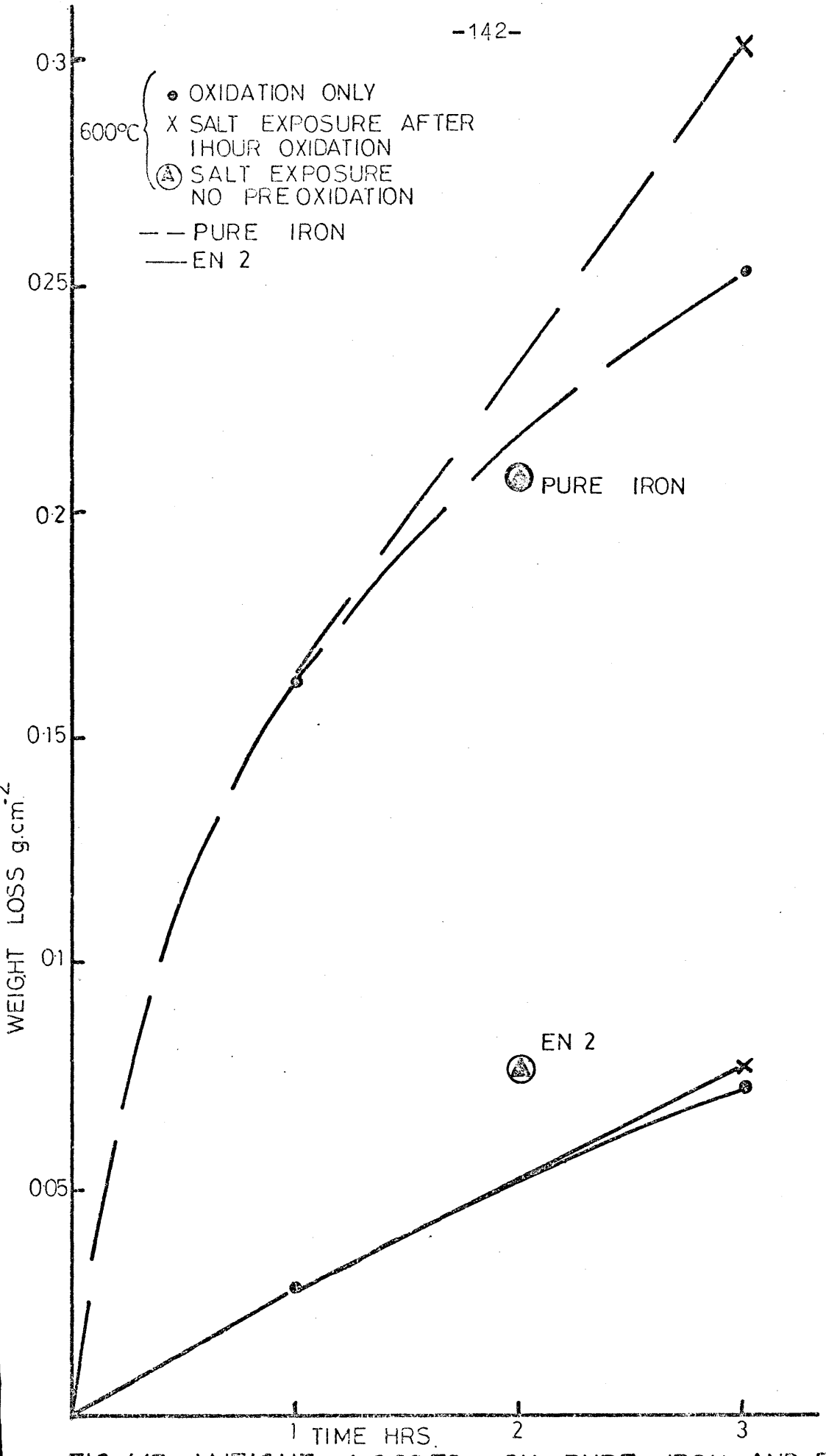

FIG.4·17 WEIGHT LOSSES ON PURE IRON AND EN2 STEEL DURING ISOTHERMAL OXIDATION AND/OR CORROSION AT 600°C FOR 3 HOURS.

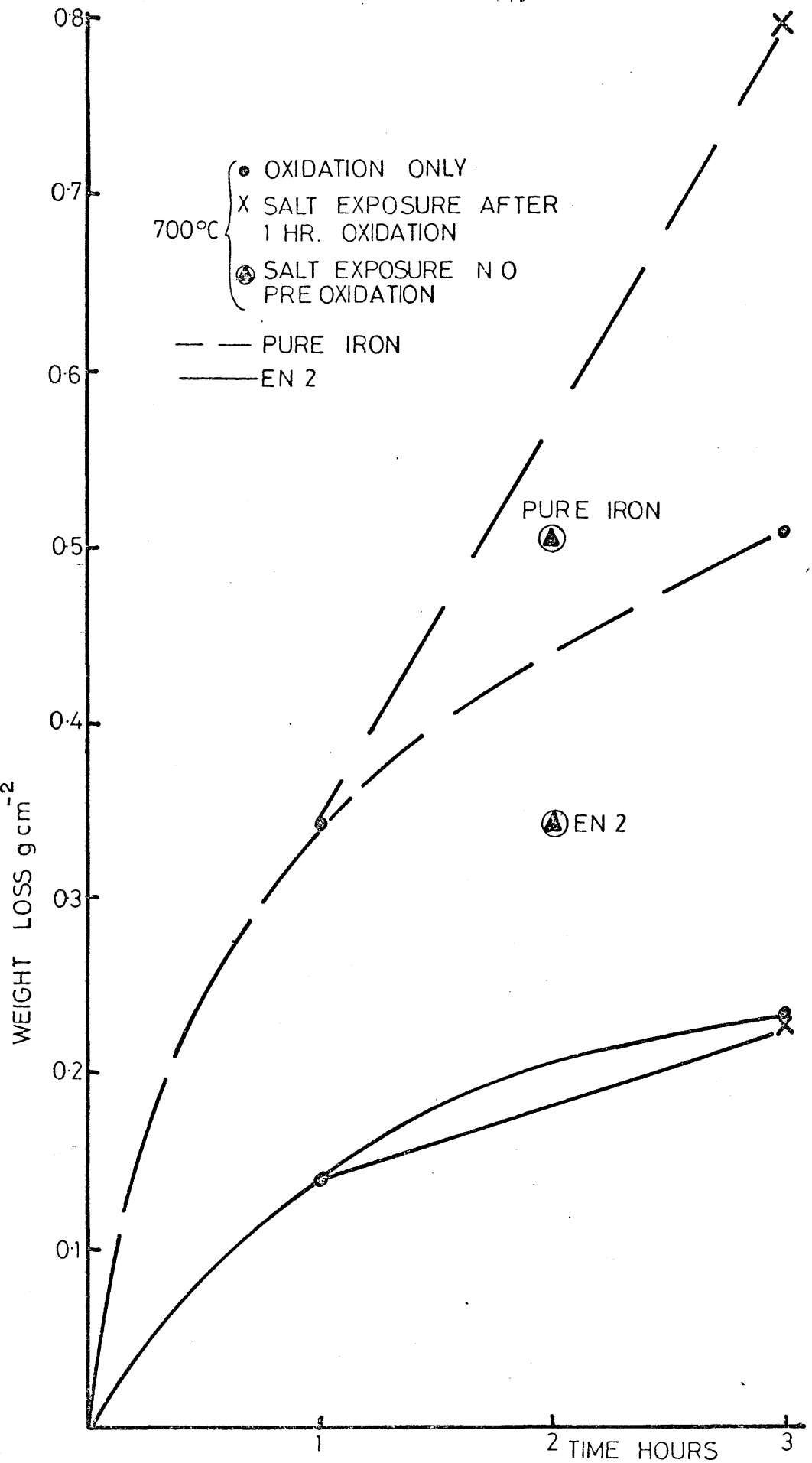

FIG.4·18 WEIGHT LOSSES ON PURE IRON AND EN 2 STEEL DURING ISOTHERMAL OXIDATION AND/OR CORROSION AT 700°C FOR 3 HOURS

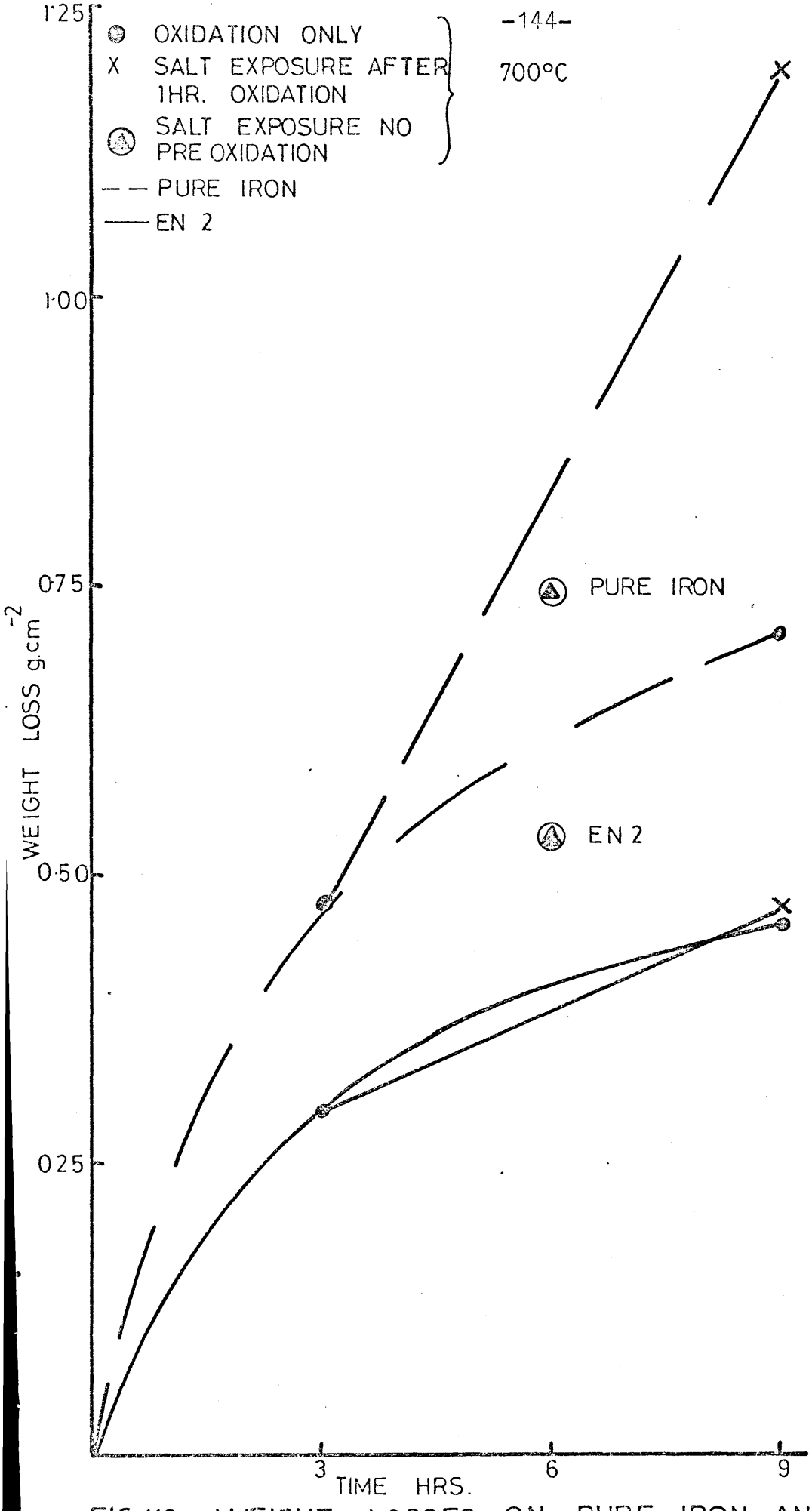

FIG 419 WEIGHT LOSSES ON PURE IRON AND EN2 STEEL DURING ISOTHERMAL OXIDATION AND/OR CORROSION AT 700°C FOR 9 HOURS

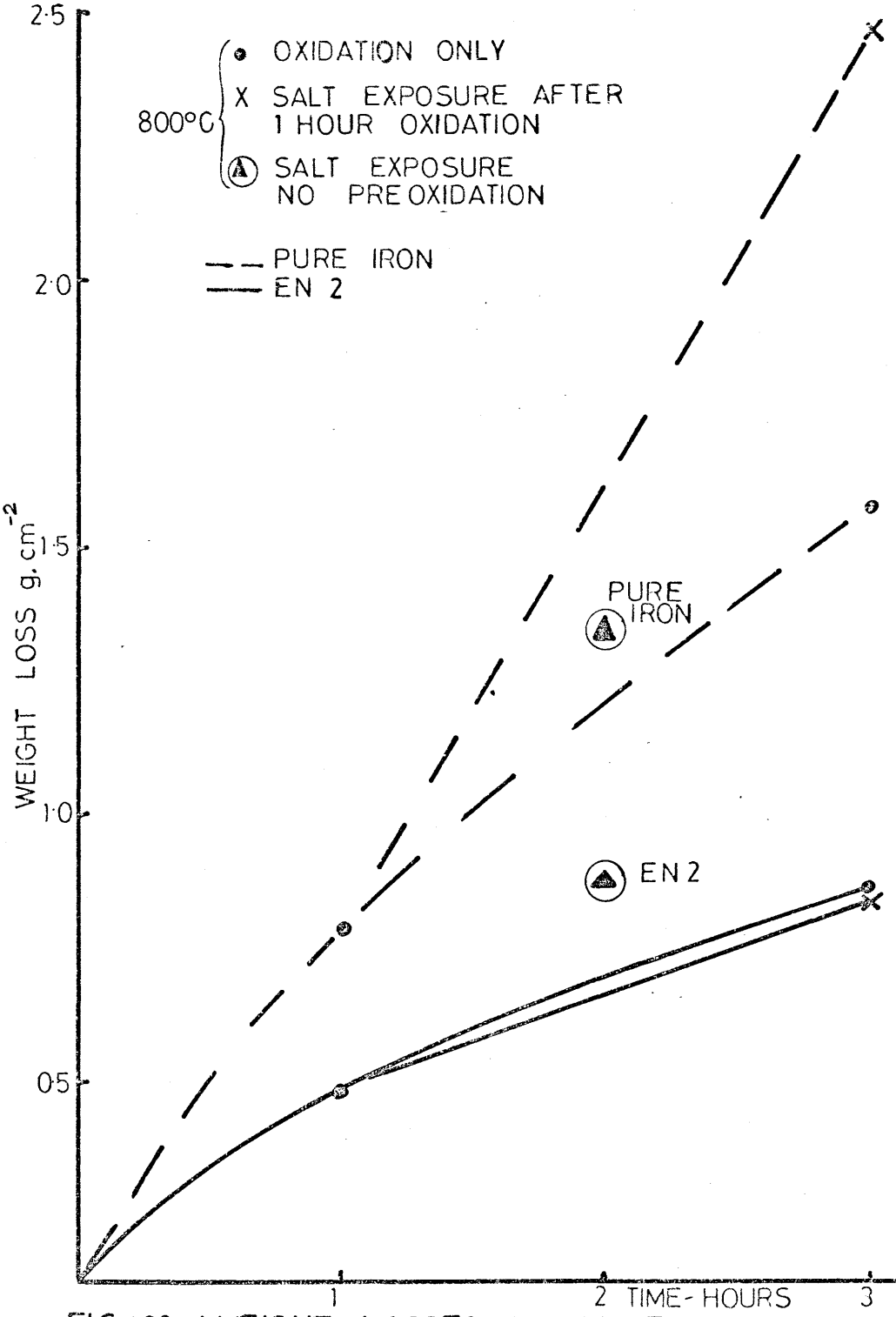

FIG 4·20 WEIGHT LOSSES ON PURE IRON AND EN2 STEEL DURING ISOTHERMAL OXIDATION AND/OR CORROSION AT 800°C FOR 3 HOURS

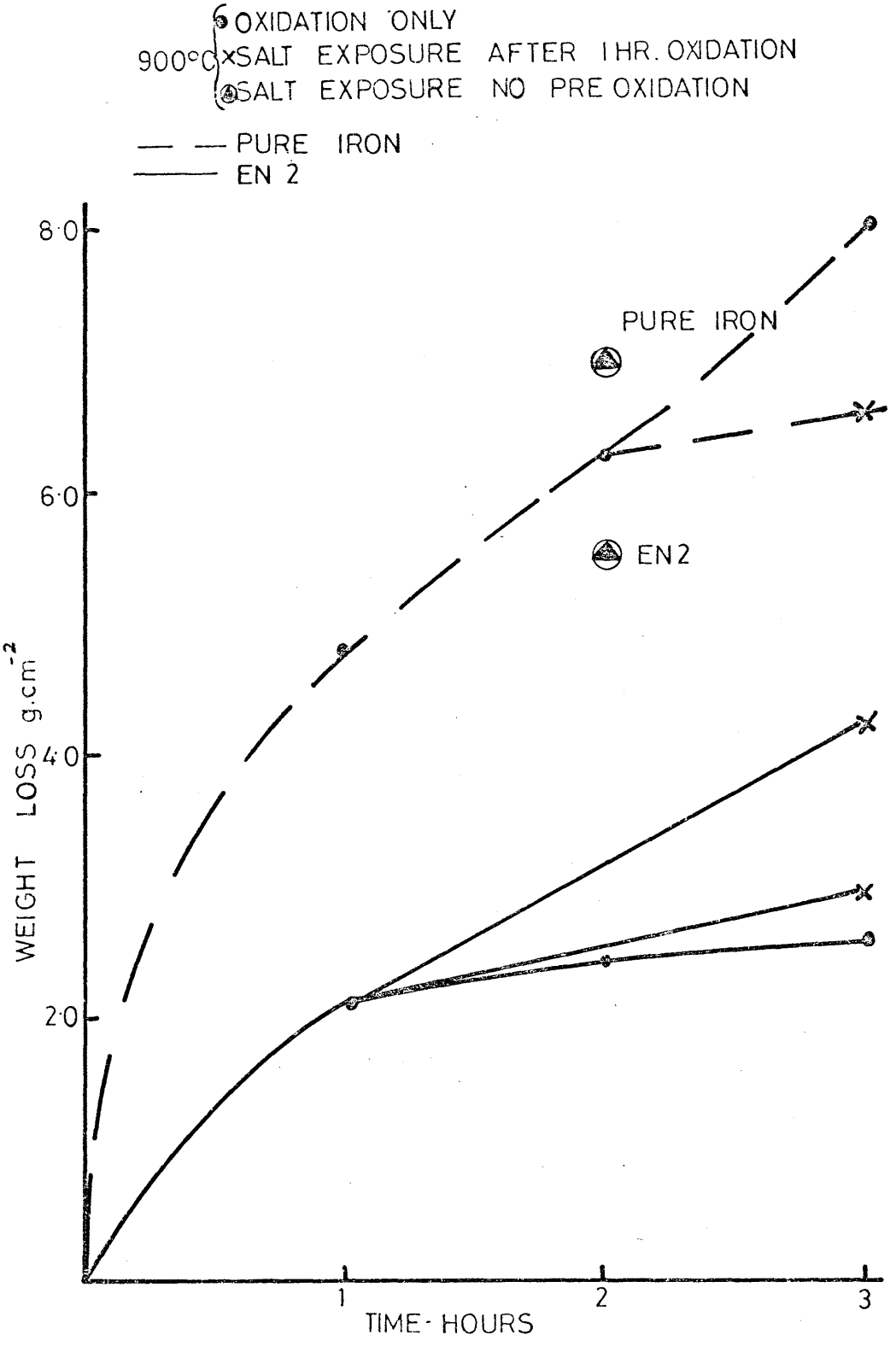

FIG 4·21 WEIGHT LOSS ON PURE IRON AND EN 2 STEEL DURING ISOTHERMAL OXIDATION AND/OR CORROSION AT 900°C FOR 3 HOURS

corrosion product. X ray analysis of this product was only able to determine FeO plus a trace of another substance which was unidentifiable. The specimen treated with sodium chloride in an argon atmosphere showed strong evidence of a brown volatile corrosion product. Metallography of these non-preoxidised samples indicated a general surface attack with no intergranular penetration. The chloride coated specimens heated in air were very similar in appearence to the sulphate coated samples, and in both cases were less attacked than the argon heated ones.

4.5. Summary and conclusions

Contamination with sodium chloride and sodium sulphate has been found effective in increasing the rate of oxidation of the materials examined, only when the contaminant was able to come into contact with the metal surface. The ensuing reaction has been observed even at the contaminant vapour pressures produced at the low test temperatures.

The corrosion mechanism that seems best able to explain the phenomena observed is that sodium chloride in contact with the steel surface produces a volatile chloride compound rather than an oxychloride, since such a volatile product is formed even in an oxygen-free atmosphere. The attack produced by sodium sulphate is somewhat more difficult to explain in that most researchers agree that the presence of SO_3 is necessary for corrosion to occur. If this is so it seems likely that it must be produced by decomposition of some of the sodium sulphate. The ensuing reaction could then be triggered by locally reducing conditions, perhaps involving the metal surface as a reducing agent, which would explain why attack is more severe in argon where reducing conditions would be more easily obtainable. No evidence has been obtained as to whether the total corrosion reaction proceeds through a pyrosulphate or an alkali iron trisulphate mechanism.

The enhanced corrosion produced when chlorine is added to the sulphate could be produced in three ways:-
(a) The chloride may assist in the initial reaction triggering process.
(b) The volatile chloride compound is able to mechanically disrupt the oxide scale forming on the surface, allowing the sulphate access to the steel surface.
(c) The noted fluxing effect of chloride on the sulphate producing a liquid phase at a lower temperature than in the pure compound.

A sufficiently adherent oxide may act as a physical barrier to the passage of contaminant to the metal surface and thereby prevent corrosive attack. Such an adherent oxide has been observed on the EN2 steel which was found to resist chloride and sulphate corrosion isothermally,

whereas, on pure iron, Armco iron, and mild steel, which do not form barrier layers, severe blistering occured. Even under thermal shock conditions the inner scale layer on EN2 steel remained adherent, and impervious to contaminant penetration. The adherence of this inner layer has been attributed to the presence of a relatively small quantity of nickel (0·2%) in the steel which becomes concentrated in the scale at the scale/metal interface.

CHAPTER 5

5. DISCUSSION AND CONCLUSIONS

5.1. Discussion and summary

The vibration technique originated by Bruce and Hancock (54) has been fitted with more sensitive electronic equipment, and has been used to study several aspects of the oxidation and corrosion of irons and steels. The technique has been found suitable for the determination of the dynamic modulus of surface oxides, and very sensitive to any phenomena that disrupt the mechanical integrity or adhesive properties of the oxide. There are, however, several areas connected with this technique that could usefully be further investigated. Firstly, there is the presence of more than one resonant frequency peak in some of the experiments. Whilst the problems of these spurious frequencies may be largely overcome, for example, by assymetric loading and vibrator insulation, it would be advantageous to have a clear definition of their source and means of elimination. Secondly, although the application of thermobalance results to provide the kinetic data required for the dynamic modulus analysis is satisfactory, an improvement would be if the measurement of the oxidation kinetics could be incorporated directly into the vibration apparatus. This would improve the accuracy and reproducibility of the method, particularly when examining metals, like steels, whose oxides form in an irregular, discontinuous manner. A likely possibility should be to incorporate some form of manometer device whereby the consumption of oxygen could be monitored and related to the rate of oxide formation.

The discontinuous change of resonant frequency during the isothermal oxidation of mild steels, reported by Bruce and Hancock (54), has been confirmed in this investigation. Whilst it is difficult to obtain definitive evidence of the cause of these discontinuities, all of the circumstantial evidence points to the cause being detachment of the oxide either at the metal/oxide interface, or fracture within the oxide, depending on the alloying elements present. Metallography has clearly shown detachment of the oxide from the metal or from the inner adherent oxide layer, with large areas of the detached scale transformed to the higher iron oxides. This indicates that the detachment had occured at temperature, rather than during cooling. The stresses induced during cooling obviously assist in the propogation of these longitudinal faults, leading to virtually complete oxide detachment at room temperature. Once the oxide has become detached, either isothermally or during cooling, cracking of the oxide may result. Of

the two methods used for studying the response of the surface oxides to thermal shocks, the vibration technique has been found to be much more sensitive than the thermobalance and, for example, has indicated the important role played by the stresses produced by FeO decomposition on the incidence of oxide damage. This is because the vibration technique is now able to detect oxide damage during cooling and does not have to rely on an accelerated rate of oxidation upon reheating as in the previous apparatus (54), and as is the case with the thermobalance.

The presence of the defective oxide scale, produced by growth, cooling, geometry or applied stresses, has several important consequences. Since the oxide dynamic modulus is dependant on the density and composition of the surface oxide it is greatly affected by the presence of cracks, porosity and any oxide detachment. The result is that the modulus measured using this technique is an effective modulus, which is variable and has a lower value than would be expected for a compact oxide. It also means that the surface oxide makes a smaller contribution to the total stiffness of the metal/oxide composite than would otherwise be the case. The presence of defects in the oxide scale is one reason why the room temperature dynamic modulus predicted by this determination is much lower than that quoted for solid oxide. For example Doraiswanie (100) determined the room temperature dynamic modulus of naturally occuring magnetite crystals as 38×10^6 psi, compared with a value of $26{\cdot}5 \times 10^6$ psi predicted from the results obtained here. The other reason for this discrepancy is that the surface oxide is a composite of all three iron oxides, compared with the pure Fe_3O_4 examined by Doraiswanie (100). At all temperatures up to 900°C the effective oxide modulus is less than that of the underlying steel.

The formation of a porous defective oxide also has a large influence on the kinetics of oxidation in that the classical theory of oxidation assumes diffusion, by cation or anion, through the oxide scale with transfer at the metal/scale or scale/atmosphere interfaces. Defects in the scale may influence this process either by limiting the area of contact between scale and the metal if detachment occurs, and/or, by providing "short circuit" paths for the oxygen in the case of cracks perpendicular to the interface.

Cracking of the oxide may also permit ready access of the contaminants to the metal surface, and severely limit any protection afforded by an otherwise compact oxide layer. This was found to be the case with pure iron and a mild steel studied in this investigation. Electron probe microanalysis indicated a concentration of chlorine, from sodium chloride on the oxide surface,

in the gap between steel and oxide, with no evidence of any diffusion gradient through the scale. The increase in corrosion resistance imparted by a compact adherent oxide acting as a physical barrier to the ingress of corrodents was clearly emphasised by the behaviour of the EN2 type steel investigated. During oxidation this steel was found to form a compact, very adherent oxide layer on the metal surface. Oxide detachment isothermally or during cooling occured at the interface between this inner scale and the bulk scale layer. The inner scale was found to be virtually undamaged by thermal shock or applied tensile loading, and to be completely resistant to the passage of sodium chloride and sodium sulphate contaminants in the temperature and time range investigated. The particularly good adhesion of the inner scale was attributed to the presence of a higher than the average (0·20%) concentration of nickel in this region. Several possibilities exist for the mechanism by which such a nickel concentration might enhance adhesion. It may either form nickel rich filaments at the interface, although electron probe microanalysis did not discern their presence, or it might increase the plasticity of the scale thereby inhibiting crack propagation. The third possibility is by altering the coefficient of thermal expansion of the oxide, thereby reducing the disparity between the coefficients of the metal and the oxide. This mechanism would only be effective in limiting stresses due to cooling and should not affect isothermal properties e.g. during isothermal tensile loading. Thus, of the three possibilities considered, the most likely explanation seems to be that of the presence of nickel in the inner scale improving the plasticity of the oxide, which would be effective in reducing damage from any source of stress as is observed.

All of the irons and steels investigated were attacked by sodium chloride and/or sodium sulphate, unless protected by an inner adherent scale. It has been suggested (39) that the active radical in such corrosion is the cation, but the evidence from this investigation is that it is actually the anion that is reactive, for example, evidenced by the behaviour of sodium nitrate and potassium chloride. It is also clear that under the conditions used in these tests reaction between the contaminant and the oxide scale did not play an important part in the overall corrosive attack. For serious corrosion to occur the corrodent must be able to reach the metal surface, and this is normally accomplished through cracks and defects in the scale layer.

The experiments carried out into the effects of applied stress on oxide cracking were of an exploratory nature, but they have shown some important points. The

vibration technique is admirably suited as an oxide crack detection system when coupled to the load application method used. The accuracy of the strains to oxide failure results obtained would obviously be increased if suitable extensometry were fitted. The probable form of extensometry required would be such that true specimen extension could be measured for the range of loads and temperatures required using extensometers attached directly to the specimen. This data could then be used as a calibration of the system to determine strains of a specimen without attached extensometers, i.e. while still able to monitor the natural resonant frequency which would not be possible with permanently fitted exensometers.

The form of oxide failure produced by the tensile loading was, as might be expected, that of cracks in the oxide perpendicular to the oxide/metal interface. The number of cracks produced was largely dependant on the level of applied stress, which is in agreement with the type of analysis of elastic cracking devised by Grosskreutz and McNeil (71). The majority of the cracks were found to penetrate right through the oxide scale thickness, but did not extend through the inner scale layer on the EN2 steel. The strains accomodated by the oxide before cracking were found to increase with incraesing temperature, indicating the higher oxide plasticity at higher temperatures which agrees with the trend repofted by Bruce and Hancock (54). The strains to oxide fracture, determined whilst the steel specimen was subject to elastic deformation, were found to vary from 0•015% at 600°C to about 0•023% at 900°C. These strains compare with the strain of 0•18% determined by the thermobalance method, on one of the isolated occasions when a thermal shock produced an enhanced oxidation rate upon reheating. In the thermal shock experiment the increased oxidation rate must mean that the inner scale must have been damaged, and there was no such damage detected in the applied load experiments. The vibration cooling curves indicated failure of the bulk oxide around 570°C when slowly cooled from 700°C which is equivalent to a strain of 0•04% due to the difference in metal and oxide thermal expansion coefficients. In this case though, the FeO transformation is exerting an added stress factor which is difficult to quantify.

If we use the data of Tylecote (59) for the wholly elastic strains to U.T.S., it means that of the 0•015% total strain to fracture at 600°C approximately 0•01% strain would be plastic. This is not really a very valid method though, since materials and method of testing are so different. It does however, further indicate that the strains calculated in this work are of the same order as determined by other researchers. Further work using this type of hot deformation system coupled with the

vibration technique should yield more useful data concerning the elastic and plastic properties of surface oxides during growth.

5.2. Conclusions

Some conclusions that may be drawn from the work desribed in this thesis are:-

(a) During isothermal oxidation of the mild steels examined, oxide damage occured intermittently, largely in the form of detachment of the oxide at the scale/metal interface. This detachment was readily detected using the vibration technique described.

(b) The vibration technique was also able to determine the effective dynamic modulus of the surface oxide at various temperatures, and it was found to be lower than might be expected for bulk oxide. This was attributed to the presence of a high proportion of porosity and cracking in the oxide scale (up to 60%).

(c) All of the irons and steels investigated were found to be attacked by sodium chloride and/or sodium sulphate at temperatures higher than about 350°C, only if the corrodents were able to contact the steel surface. Preoxidation was found to be ineffective in limiting such corrosive attack, except in the case of an EN2 type steel investigated.

(d) The EN2 type steel was found to form a thin inner adherent layer on the metal surface. This layer was found to be nickel rich, and to provide an effective barrier against chloride and sulphate corrosion. The inner layer was also very resistant to damage by thermal shock or applied tensile stress.

(e) A method of applying a tensile stress to an oxidising vibration specimen has been successfully attempted, using the change in specimen resonant frequency as a means of oxide crack detection. The cracks produced by the application of a tensile load were found to be perpendicular to the applied load, and to be equally spaced along the specimen. The crack spacing was found to depend on the applied stress level, with the majority of cracks extending right through the bulk scale thickness.

(f) The strains required to produce oxide damage were found to increase with increased temperature from 0·015% at 600°C to 0·023% at 900°C. Once the steel became plastically deformed the maximum strains withstood by the oxide was calculated at 1·03%, and strain in the steel plastic region did not appear to be temperature dependant.

(g) A threshold stress of 5000 - 6000 psi was required before extensive oxide cracking occured.

ACKNOWLEDGEMENTS

I wish to thank all members of the academic and technical staff, and fellow students of the Department of Materials, for their practical assistance and helpful discussions. I especially acknowledge the assistance given by my supervisor, Dr. R.C.Hurst, Professor P.Hancock, and D.Timpson, technician for the High Temperature Corrosion Group.

Finally, I wish to thank Mrs.J.Cunliffe for the preparation of the line diagrams in this thesis, and my wife for her understanding durin the experimental work and the thesis typing.

REFERENCES

19 (1) DAVIES,M.H. SIMNAD,M.T. BIRCHENALL,C.E. — On the mechanisms and kinetics of scaling of iron. J Metals, Vol.3, 10, Oct.1951, pp.889-896.

20 (2) LAUKONIS,J.V. — Fifth International Congress for electron microscopy. Academic Press, New York, Vol. 1, C - 911961.

21 (3) GULBRANSEN,E.A. HICKMAN,J.W. — An electron diffraction study of oxide films formed on Fe, Co, Ni, Cr, and Cu at high temperatures. Trans. of the A.I.M.E., Vol. 171, Oct., pp.306-343.

22 (4) STANLEY,J.K. van HOENE,J. HUNTOON,R.T. — The oxidation of pure iron. Trans. A.S.M., Vol.43, 1951, pp.426-453.

(5) PHLANIKAR,C.A. BALDWIN,W.A. — Ibid. p.48.

(6) BERNARD,J. COQUELLE,O. — Nouvelle recherches sur l'oxydation du fer aux temperatures elevees par la methode micrographique. Rev. Met. Mem., Vol.43, 4, April.1946, pp.113-124.

23 (7) WAGNER,C. — Theorie der geordneten Mischphasen. Zeit. fur Phys. Chem. B22, 1931, pp.177-186.

24 (8) WAGNER,C. — Beitrag zur theorie des Anlaufrorgangs. 1 Zeit. fur Phys. Chem. B21, 1933, pp.25-41.

25 (9) WAGNER,C. — Beitrag zur theorie des Anlaufrorgangs. 2 Zeit. fur Phys. Chem. B32, 1936, pp.447-462.

26 (10) PAIDASSI,J. — The kinetics of air oxidation of iron in the range 700° - 1250°C. Acta. Met., Vol.6, 1958, pp.184-194.

27 (11) HOLMES,D.R. — New corrosion resistant high temperature heat exchanger materials. Corrosion Sci., Vol.8, 1968, pp.603-622.

28 (12) BERNARD,J. — The oxidation of metals and alloys. Met. Reviews, Vol.9, 36, 1964, pp.473-503.

29 (13) LAWLESS,K.R. — The oxidation of metals. Energetics in metallurgical phenomena. Vol.1, University of Denver, 1962.

(14) GERMAN,P.A. MAXWELL,D. — Some observations on dilute iron alloys. Werkstoffe und Korrosion, Vol.22. 1971, pp.382-355.

(15) HANCOCK,P. — Corrosion of alloys at high temperatures in atmospheres consisting of fuel combustion products and associated impuities. H.M.S.O., London, 1968.

(16) WICKERT,K. — Forms of corrosion and the behaviour of metals and additions in firing installations. D.A.C.H.E.M.A., Conference, Frankfurt, April, 1965.

(17) FITZER,E. SCHWAB,J. — Berg u Hullen Monats, Vol.98, 1, 1953. Quoted in Ref.(16).

(18) ALEXANDER,P.A. MARSDEN,R.A. — Corrosion of superheater materials by residual oil ash. The mechanism of corrosion by fuel impurities. Butterworths, London, 1963, pp.542-555.

(19) SMALL,N.J. STRAWSON,H. LEWIS,A. — Recent advances in the chemistry of fuel oil ash. Ibid. pp.238-253.

(20) JOHNSON,L.B. — Oxygen transport and steel corrosion by Sodium/Vanadium oxides. Ind.Eng.Chem., Vol.8, p.55 et.seq.

(21) PANTHONY,K. — Reported in Ref. (15).

(22) FAIRMAN,L. — Mechanism of accelerated oxidation by Vanadium. Corrosion Science, Vol.2, Pergammon Press,London,1962, pp.293-296.

(23) REID,W.T. — External corrosion and deposits. Elsevier, New York,1971.

(24) ROSS,T.K. — The distribution of sulphur in corrosion products formed by sulphur dioxide on mild steel. Corrosion Scienxe, Vol.5, 1965, pp.327-330.

(25) PREECE,A. — The desirability of removing sulphur from gaseous fuels for heating ferrous metal. J.I.S.I., Vol.147, 1943, pp.43-50.

(26) EDSTROM,J.E. — Scaling of 18-8 stainless steel in reheating furnace atmospheres. J.I.S.I., Vol.185, 1957, pp.523-533.

(27) FLATLEY,T.
BIRKS,N.
Oxidation of iron in atmospheres containing sulphur dioxide.
J.I.S.I., Vol.209, July 1971, pp.523-533

(28) COREY,R.C.
CROSS,B.J.
REID,W.T.
External corrosion of furnace wall tubes.
Trans.A.S.M.E.,Vol.67, 1945, pp.279-302.

(29) ALEXANDER,P.A.
Effects of sulphates and chlorides on the oxidation of superheater alloys.
The mechanism of corrosion by fuel impurities. Butterworths, London, 1963, pp.571-582.

(30) SIMONS,E.L.
BROWNING,G.V.
LIEBHAFSKY,H.A.
Sodium sulphate in gas turbines.
Corrosion, Vol.11, Dec. 1955, pp.505-514.

(31) DRAVNIEKS,A.
In discussion, Ref. (30).

(32) SYKES,C.
SHIRLEY,H.T.
High temerature steels and alloys for gas turbines.
I.S.I. Special Report No.43, July, 1952.

(33) RAHMEL,A.
Influence of calcium and magnesium sulphates on the high temperature oxidation of Cr/Ni steels in the presence of alkali sulphates and SO_3.
The mechanism of corrosion by fuel impurities. Butterworths, London, 1963, pp.556-570.

(34) CAIN,C.
NELSON,W.
Corrosion of superheaters and reheaters of pulverised-coal-fired boilers. Part 2.
Trans.A.S.M.E. Series A, Vol.83, 1961, pp.468-473.

(35) ADAMS,A.M.
RAASK,E.
Complex sulphates in coal-fired boiler deposits.
The mechanism of corrosion by fuel impurities. Butterworths, London, 1963, pp.496-507.

(36) BOLL,R.H.
PATEL,H.C.
The role of chemical thermodynamics in analysing gas side problems in boilers.
A.S.M.E. Paper No.60-WA-182, 1961, pp.1-17.

(37) CAIN,C.
NELSON,W.
Corrosion of superheaters and reheaters of pulverised coal-fired boilers. Part 1.
Trans.A.S.M.E.,Series A, Vol.82, 1960, pp.194-204.

(38) STRINGER,J.
Hot corrosion in gas turbines.
M.C.I.C. Report No.72-08, Batelle-Columbus, June, 1972.

(39) GOEBEL,J.A.
PETTIT,F.S.
GOWARD,G.W.
Hot corrosion mechanisms in stationary gas turbines.
C.E.G.B. Conference on Deposition and Corrosion in gas turbines. London, Dec., 1972.

(40) SHEWMON,P.G.
Material problems in breeder reactors.
Metal Science J.,Vol.7, 1973, pp.36-40.

(41) HARLOW,W.F.
Causes of high dewpoint temperatures in boiler flue gases.
Proc.Inst.Mech.Eng.,Vol.151, 1944, pp.293-298.

(42) CROSSLEY,H.E.
External fouling and corrosion of boiler plant: A commentary.
J.Inst.of Fuel, Vol.40, Aug.,1967, pp.342-347.

(43) EDWARDS,A.M.
JACKSON,P.J.
HOWES,L.S.
Operational trial of superheater steels in a pulverised-fuel-fired boiler burning east midland coal.
J.Inst.of Fuel, Vol.35, 1962, pp.16-28.

(44) GREENERT,W.J.
High temperature slag corrosion of metallic materials.
Corrosion, Vol.18, 1962, pp.57t-67t, pp.91t-95t.

(45) PICKERING,W.H.
BECK,F.H.
FONTANA,M.G.
Rapid intergranular oxidation of 18-8 stainless steels by oxygen and dry sodium chloride at elevated temperatures.
Trans.A.S.M.,Vol.53, 1961, pp.793-803.

(46) TOFT,L.H.
MARSDEN,R.H.
Metallurgical aspects of the fire side corrosion of superheater tube materials.
The mechanism of corrosion by fuel impurities. Butterworths, London, 1963, pp.591-603.

(47) MARSDEN,R.H.
Discussion. Ibid. p.634.

(48) DeCRESCENTE,M.A.
BORNSTEIN,N.S.
Formation and reactivity thermodynamics of sodium sulphate with gas turbine alloys.
Corrosion, Vol.24, 5, May, 1968, pp.127-133.

(49) TSCHINKEL,J.G.
Reported in Ref. (38).

(50) CUTLER,A.J.B.
HALSTEAD,W.D.
LAXTON,J.W.
The role of chloride in the corrosion caused by flue gases and their deposits.
Trans.A.S.M.E.,Vol.93, Series A, 1971, p.307.

(51) CUTLER,A.J.B.
GRANT,C.J.
Electrochemical measurements of corrosion rates for gas turbines.
C.E.G.B. Conference on Deposition and Corrosion in gas turbines.
London, Dec.,1972.

39 (52) STRINGER,J.
Stress generation and relief in growing oxide films.
Corrosion Science, Vol.10, 1970, pp.513-543.

37 (53) HANCOCK,P.
HURST,R.C.
The mechanical properties and breakdown of surface oxide films at elevated temperatures.
To be published in Advances in Corrosion Science and Technology, 1973.

(54) BRUCE,D.
HANCOCK,P.
Influence of mechanical properties of surface oxide films on oxidation mechanisms.
J.Inst.of Metals, Vol.97, 1969, pp.140-155.

38 (55) JAENICKE,W.
LEISTIKOW,S.
STADLER,A.
Mechanical stresses during the oxidation of copper, and their influence on oxidation kinetics.
J.Electrochem. Soc.,Vol.111, 1964, pp.1031-1037.

40 (56) HOWES,V.R.
RICHARDSON,C.N.
The initial stresses developed during oxidation of Fe-Cr alloys.
Corrosion Science, Vol.9, 1969, pp.385-394.

(57) DOUGLASS,D.L.
The role of oxide plasticity on the oxidation behaviour of metals. A review.
Oxidation of Metals, Vol.1, No.1, 1969, pp.127-142.

42 (58) CATHCART,J.V.
PETERSEN,G.F.
SPARKS,C.J.
Oxidation rate and oxide structural defects.
Surfaces and Interfaces, 1- Chemical and Physical characteristics. Syracuse University Press, 1967,pp.333-346.

(59) TYLECOTE,R.F.
Factors influencing the adherence of oxides on metals.
J.I.S.I.,Vol.196, 1960, pp.135-141.

(60) DOUGLASS,D.L.
Exfoliation and the mechanical behaviour of scales.
A.S.M. Seminar "Oxidation of metals and alloys",Oct.,1970, Cleveland,Ohio.

(61) BIRCHENALL,C.E.
The role of spinel oxides in the oxidation of iron and its alloys.
Z.Electrochem. Vol.63, 1958, pp.790-793.

(62) STRINGER,J.
The effects of alloying on oxidation:Quantitative treatments.
Met. Reviews,No.107, Vol.11, 1966, pp.113-128.

(63) CLAUER,A.H.
SELTZER,M.S.
WILCOX,B.A.
The effect of non-stoichiometry on creep of oxides.
Mat.Sci.Research, Vol.5, 1971, pp.361-384.

(64) ILSCHNER,B.
REPPICH,B.
RIECKE,E.
High temperature steady state creep and atomic disorder in iron oxide.
Faraday Soc.Disc.,Vol.38, 1964, pp.243-250.

(65) VAGNARD,G.
Etude de la deformation plastique du protoxyde de fer.
Thesis, Faculte des Sciences de L'Universite de Paris, 1965.

(66) MACKENZIE,J.D.
BIRCHENALL,C.E.
Plastic flow of iron oxides and the oxidation of iron.
Corrosion, Vol.13, 12, Dec., 1957, pp.783-785.

(67) APPLEBY,W.K.
TYLECOTE,R.F.
Stresses during the gaseous oxidation of metals.
Corr.Sci.,Vol.10, 1970, pp.325-341.

(68) HULLEY,J.M.
ROLLS,R.
High temperature cohesion and adhesion of oxide scales on mild steel.
J.I.S.I.,Vol.196, Nov.,1970, pp.1029-1030.

(69) HOLMES,D.R.
PASCOE,R.T.
Strain/oxide interactions in steels and model alloys.
Werkstoffe u Korrosion, Vol.23, 10, Oct.,1972, pp.859-870

(70) WARD,G.
HOCKENHULL,B.S.
HANCOCK,P.
The effect of cyclic stressing on the oxidation a low carbon steel.
To be published in Trans.A.S.M., 1973.

(71) GROSSKREUTZ,J.C.
McNEIL,M.B.
The fracture of surface coatings on a strained substrate.
J.App.Phys.,Vol.40,1, 1969, pp.355-359.

(72) TYLECOTE,R.F.
The adherence of oxide films on metals.
J.I.S.I.,Vol.195, Aug.,1960, pp.380-385.

(73) PAIDASSI,J.
Sur l'oxydation du fer dans l'air dans l'intervalle 400° - 700°C.
Acta.Met.,Vol.4, 1956, pp.227-229.

(74) ENGELL,H.
WEVER,F.
Some basic problems of the formation and adherence of scale on iron.
Acta.Met.,Vol.5, 1957, pp.695-702.

(75) TUCK,C.W.
BARLOW,J.
The effect of reheating furnace atmospheres on the adhesion of scale to metal.
Iron and Steel, Feb.,1972, pp.31-38.

(76) JUENKER,D.W.
MEUSSNER,R.A.
BIRCHENALL,C.E.
Cavity formation in iron oxide.
Corrosion, Vol.14, Jan.,1958, pp.57-64.

(77) PFEIL,L.B.
The oxidation of iron and steel at high temperature.
J.I.S.I.,Vol.119, 1929, pp.501-560.

(78) GRIFFITHS,R.
The blistering of iron oxide scales and the conditions for the formation of a non-adherent scale.
J.I.S.I.,Vol.130, 1934, pp.377-384.

(79) TUCK,W.
ODGERS,M.
SACHS,K.
Oxidation of Fe at 950°C in oxygen/water vapour mixtures.
Corrosion Science, Vol.9, 1969, pp.271-285.

(80) DUNNINGTON,D.W.
BECK,F.H.
FONTANA,M.G.
The mechanism of scale formation on iron at high temperatures.
Corrosion, Vol.8, Jan., 1952, pp.2-13.

(81) TYLECOTE,R.F.
MITCHELL,T.E.
Marker movements in the oxidation of iron and some other metals. J.I.S.I.,Vol.196, Dec., 1960, pp.445-453.

(82) BRUCE,D.
HANCOCK,P.
Influence of specimen geometry on the growth and mechanical stability of surface oxides on iron and steel in the temperature range 570° - 800°C. J.I.S.I.,Vol.196, Nov.,1970, pp.1021-1024.

(83) ROMANSKI,J.
Geometrical factors in studies of the kinetics of oxidation of metals at high temperatures. Corrosion Science, Vol.8, 1968, pp.67-102.

(84) PETERS,F.K.
ENGELL,H.K.
Die haftfestigteit von zunderschichten auf stahl. Archiv. fur Eisenhuttenwessen, Vol.30, 1959, pp.275-283.

(85) WRIGHT,I.G.
Oxidation of iron-,nickel-,and cobalt- based alloys. M.C.I.C.,Report 72-07, Batelle-Columbus, June, 1972.

(86) TEDMON,C.S.
The high temperature oxidation of Fe-Cr alloys in the composition range of 25% -95% Cr. J.Electrochem.Soc.,Vol.114, 1967, pp.788-795.

(87) CAPLAN,D.
COHEN,M.
Scaling of Fe-26Cr alloys at 870° - 1200°C. J.Electrochem.Soc.,Vol.112,5, 1965, pp.471-477.

(88) TIEN,J.K.
RAND,W.H.
The effect of active element additions on void formation during oxidation. Scripta.Met.,Vol.6, 1972, pp.55-58.

(89) BATEMAN,G.J.
ROLLS,R.
Structure and adhesion of oxide scales on iron-aluminium alloys. Br.Corrosion J.Vol.5, May,1970, pp.123-127.

(90) ARNOLD,F.
ROLLS,R.
The structure and adhesion of oxide scales on iron/nickel/molbdenum, and iron/chromium/molybdenum alloys. Werkstoffeu.Korrosio,Vol.23, 10, Oct.,1972, pp.886-893.

(91) NICHOLSON,A.
Quoted in Ref.(92).

(92) WOOTON,M.R. — An assessment of the methods available for measuring scale-metal adhesion and the mechanical properties of oxides. C.E.G.B.Report from Berkely Nuclear Labs.,RB/D/N2116,Nov.1971.

(93) LORD RAYLEIGH — Theory of sound. Vol.1, 2nd Edition 1894/1896, London, Macmillam.

(94) BRUCE,D. — Examination of the physical properties and mode of growth of thermally formed oxides by a vibrational technique. Ph.D. Thesis, Glasgow, 1967.

(95) HURST,R.C. HANCOCK,P. — Measurement of the mechanical properties of growing surface films in oxidising environments. Werkstoffe u Korrosion, Vol.23,9, Sept.,1972, pp.773-776.

(96) HURST,R.C. JOHNSON,J.B. DAVIES,M. HANCOCK,P. — Sulphate attack of nickel-based alloys and mild steel. C.E.G.B. Conference on Deposition and Corrosion in gas turbines, London, Dec.,1972.

(97) NOWICK,A.S. — Internal friction in metals. Progress in Metal Physics,Vol.4,1, p.53.

(98) LEAK,G.M. — Grain Boundary damping. 1:Pure iron

(99) WACHTMAN,Jr.J.B. TEFFT,W.E. — Effect of suspension position on apparent values of internal friction determined by Forsters' method. The review of Scientific Instruments, Vol.29,6, June,1958, pp.517-520.

(100) DORAISWANIE,M.S. — Elastic constants ofMagnetite, Pyrite and Chromite. Proc,Ind.Acad.of Sci.,Vol.25, A5, 1947, pp.413-416.

(101) HANCOCK,P. HURST,R.C. SOLLARS,A.R. — Paper presented to the ISMC Conference, July,1971, Sheffield- To be published in J.I.S.I.

(102) SACHS,K. — Oxidation of steels containing nickel. J.I.S.I.,Vol.187,1957, pp.93-104.

(103) EISELSTEIN,H.L. SKINNER,E.N. — The effect of composition on the scaling of iron-chromium-nickel alloys subjected to cyclic temperature conditions. A.S.T.M. S.T.P.,Vol.165,1954,pp.162-172.

(104) JOHNSON,J.B. — Ph.D. Thesis,Cranfield Inst. of Tech. 1973.